A TWO MICRON ALL SKY SURVEY VIEW OF THE SAGITTARIUS DWARF GALAXY. I. MORPHOLOGY OF THE SAGITTARIUS CORE AND TIDAL ARMS

Steven R. Majewski,[1] M. F. Skrutskie,[1] Martin D. Weinberg,[2] and James C. Ostheimer[1]

ABSTRACT

We present the first all-sky view of the Sagittarius (Sgr) dwarf galaxy mapped by M-giant star tracers detected in the complete Two Micron All Sky Survey (2MASS). Near-infrared photometry of Sgr's prominent M-giant population permits an unprecedentedly clear view of the center of Sgr. The main body is fitted with a King profile of limiting major-axis radius 30°—substantially larger than previously found or assumed—beyond which is a prominent break in the density profile from stars in the Sgr tidal tails; thus the Sgr radial profile resembles that of Galactic dwarf speroidal (dSph) satellites. Adopting traditional methods for analyzing dSph light profiles, we determine the brightness of the main body of Sgr to be $M_V = -13.27$ (the brightest of the known Galactic dSph galaxies) and the total Sgr mass-to-light ratio to be 25 in solar units. However, we regard the latter result with suspicion and argue that much of the observed structure beyond the King-fit core radius (224′) may be outside the actual Sgr tidal radius as the former dwarf spiral/irregular satellite undergoes catastrophic disruption during its last orbits. The M-giant distribution of Sgr exhibits a central density cusp at the same location as, but not due to, the old stars constituting the globular cluster M54. A striking trailing tidal tail is found to extend from the Sgr center and arc across the south Galactic hemisphere with approximately constant density and mean distance varying from ∼20 to 40 kpc. A prominent leading debris arm extends from the Sgr center northward of the Galactic plane to an apogalacticon ∼45 kpc from the Sun and then turns toward the north Galactic cap (NGC), from where it descends back toward the Galactic plane, becomes foreshortened, and, at brighter magnitudes, covers the NGC. The leading and trailing Sgr tails lie along a well-defined orbital plane about the Galactic center. The Sun lies within a kiloparsec of that plane and near the path of leading Sgr debris; thus, it is possible that former Sgr stars are near or in the solar neighborhood. We discuss the implications of this new view of the Sgr galaxy and its entrails for the character of the Sgr orbit, mass, mass-loss rate, and contribution of stars to the Milky Way halo. The minimal precession displayed by the Sgr tidal debris along its inclined orbit supports the notion of a nearly spherical Galactic potential. The number of M giants in the Sgr tails is at least 15% that contained within the King limiting radius of the main Sgr body. The fact that M giants, presumably formed within the past few gigayears in the Sgr nucleus, are nevertheless so widespread along the Sgr tidal arms not only places limits on the dynamical age of these arms but also poses a timing problem that bears on the recent binding energy of the Sgr core and that is most naturally explained by recent and catastrophic mass loss. Sgr appears to contribute more than 75% of the high-latitude, halo M giants, despite substantial reservoirs of M giants in the Magellanic Clouds. No evidence of extended M-giant tidal debris from the Magellanic Clouds is found. Generally good correspondence is found between the M-giant, all-sky map of the Sgr system and all previously published detections of potential Sgr debris, with the exception of Sgr carbon stars, which must be subluminous compared with counterparts in other Galactic satellites in order to resolve the discrepancy.

Subject headings: galaxies: individual (Sagittarius Dwarf) — galaxies: stellar content — Galaxy: halo — Galaxy: kinematics and dynamics — Galaxy: structure — Local Group

1. INTRODUCTION

The Sagittarius (Sgr) dwarf galaxy is a striking example of the process of satellite disruption and assimilation long presumed responsible for populating the Galactic halo (e.g., Searle & Zinn 1978). Alternatively, viewed as test particles, a sufficiently complete spatial and kinematical sample of Sgr stars can reveal underlying gravitational potentials, tracing the total mass of luminous and dark matter in both Sgr and the Milky Way (Sackett et al. 1994; Johnston et al. 1999c; Ibata et al. 2001b). Since the discovery of Sgr (Ibata

et al. 1994) there have followed a number of observations (reviewed below and in § 8) to characterize the distribution and motion of the tidal debris and which have aided models of the disruption of the satellite in the Milky Way's potential. Early observations were largely restricted to small fields of view but nevertheless painted the general picture of a substantially tidally disrupted satellite distributed across a sizeable portion of the celestial sphere.

However, many issues remain controversial and intertwined, particularly the following:

1. The dark matter content in the bound Sgr system, which is integrally tied to the long-term integrity and mass-loss rate of the satellite (e.g., Ibata & Lewis 1998; Gómez-Flechoso 1998; Gómez-Flechoso, Fux, & Martinet 1999).

2. The survivability of the Sgr system in its present orbit, which, even if it contains substantial dark matter, should not last a Hubble time (Velázquez & White 1995; Johnston,

[1] Department of Astronomy, University of Virginia, Charlottesville, VA 22903-0818; srm4n@virginia.edu, mfs4n@virginia.edu, jco9w@virginia.edu.

[2] Department of Astronomy, University of Massachusetts, 719 North Pleasant Street, Amherst, MA 01003-9305; weinberg@astro.umass.edu.

Spergel, & Hernquist 1995). Solutions to this dilemma range from a fine-tuning of the dark matter configuration within the satellite (Ibata & Lewis 1998), to an evolving orbit for the satellite (Zhao 1998; Gómez-Flechoso et al. 1999), or to the creation of Sgr at later times as the daughter product of another, more major merger (Gómez-Flechoso 1999).

3. The original mass of the Sgr satellite, which today is smaller by an amount depending on the mass density (dark matter content) and orbital history of the system.

4. The fractional contribution of Sgr stars (e.g., Ibata et al. 2001b; Vivas et al. 2001; Newberg et al. 2002) and clusters (e.g., Irwin 1999; Dinescu et al. 2000, 2001; Palma et al. 2002; Bellazzini et al. 2002a, 2003) to the Galactic halo, which must also satisfy limits imposed by the distribution of properties for Galactic halo field stars (e.g., Unavane, Wyse, & Gilmore 1996; but see Majewski et al. 2002b).

5. The shape and size of the Galactic halo. Tidal tails are extremely sensitive to the amount and distribution of mass in the Galaxy (e.g., Johnston et al. 1999c; Murali & Dubinski 1999). At least one study of the Sgr orbit (Ibata et al. 2001b) suggests the Milky Way dark halo to be nearly spherical, which places the Milky Way at an extreme of the wide range of dark halo flattenings (e.g., Sackett & Pogge 1995; Olling 1997; Peñarrubia et al. 2000; Sparke 2002). This result is at odds with (a) star count studies, which typically find $c/a \sim 0.6$–0.8 (e.g., Robin, Reylé, & Crézé 2000; Siegel et al. 2002; Reid & Majewski 1993 and references therein); (b) dynamical studies of halo tracers (Binney, May, & Ostriker 1987; Amendt & Cuddeford 1994; see also van der Marel 1991) and of H i layers (see summary by Merrifield 2002); (c) Galactic microlensing studies, which imply a flattened halo (Samurovic, Cirkovic, & Milosevic-Zdjelar 1999); and (d) expectations for very triaxial halos in models of structure formation in the presence of cold dark matter (CDM; e.g., Frenk et al. 1988; Dubinski & Carlberg 1991; Warren et al. 1992) and especially models that include gas dissipation (e.g., Dubinski 1994; Steinmetz & Muller 1995).

6. The degree of visible substructure in the halo, which is directly related to the Galactic accretion history (Tremaine 1993; Bullock, Kravtsov, & Weinberg 2001). For luminous halo stellar populations, some mixture of Eggen, Lynden-Bell, & Sandage (1962) and Searle & Zinn (1978) formation pictures is typically postulated (e.g., see review by Majewski 1993), but evidence is increasing that the stellar halo is only weakly phase-mixed and highly substructured (Majewski, Munn, & Hawley 1996; Vivas et al. 2001; Gilmore, Wyse, & Norris 2002; Majewski 2003). The contribution of Sgr to this substructure is not well established. Recent evidence suggests that Sgr contributes of order 5% of the halo M giants in a correlated stream (Ibata et al. 2002a; but see § 7.2).

7. The degree of invisible substructure in the halo. CDM models for the formation of galaxy halos predict the persistence of long-lived "subhalos" (e.g., Navarro, Frenk, & White 1996, 1997) at a number greatly exceeding the number of luminous Galactic satellites (Klypin et al. 1999; Moore et al. 1999). The degree of coherence of tidal debris streams provide a powerful constraint on the lumpiness of the Galactic halo potential (Font et al. 2001; Johnston et al. 2002b; Ibata et al. 2001b; Mayer et al. 2001).

Models for the interaction of Sgr with the Milky Way under different assumptions of orbit, Galactic potential, and Sgr dark matter content make distinct and testable predictions for the appearance of the satellite and its debris today (e.g., Velázquez & White 1995; Johnston et al. 1995; Edelshohn & Elmegreen 1997; Ibata et al. 1997; Ibata & Lewis 1998; Gómez-Flechoso, Fux, & Martinet 1999; Johnston et al. 1999a; Jiang & Binney 2000; Helmi & White 2001). Thus, improved observational constraints—e.g., on the detailed distribution (e.g., Gómez-Flechoso et al. 1999; Jiang & Binney 2000) and degree of coherence of the Sgr debris (Ibata et al. 2002b; Johnston, Spergel, & Haydn 2002b)—can greatly increase our understanding of both the Milky Way and Sgr systems.

Previous studies of Sgr include a patchwork of approaches and directions of the sky, but, aided by the advent of large-area surveys, including the Sloan Digital Sky Survey (SDSS) and Quasar Equatorial Survey Team (QUEST) RR Lyrae survey, a more global picture of the Sgr dwarf and its remains has begun to emerge. For example, a survey locating 75 high-latitude, halo carbon stars by Ibata et al. (2001b) finds more than half to lie along a great circle consistent with the likely Sgr orbit. Confirmation of this great circle comes from the location of coherent clumps of A-type (Yanny et al. 2000), RR Lyrae (Ivezić et al. 2000; Vivas et al. 2001), red clump (Mateo, Olszewski, & Morrison 1998; Majewski et al. 1999a), and main-sequence turnoff stars (Martínez-Delgado et al. 2001b, 2001c, 2002; Newberg et al. 2002) in surveys that intersect this great circle at various points. Other studies have suggested an even more complex multiply wrapped Sgr configuration around the Galaxy (Johnston et al. 1999a; Dinescu et al. 2000; Dohm-Palmer et al. 2001; Kundu et al. 2002). In some cases, detections of Sgr debris far-flung from the Sgr center are supplemented with dynamical information (e.g., Majewski et al. 1999a; Ibata et al. 2001b; Dinescu et al. 2000, 2002; Kundu et al. 2002) useful for constraining the system dynamics.

However, to date, no single, unbiased, global, empirical characterization of Sgr exists. The Two Micron All Sky Survey (2MASS) remedies this situation by offering homogeneous photometry in bandpasses less sensitive to the effects of reddening and with complete sky coverage. Studies of the high-density, inner regions of the Sgr galaxy from early release 2MASS data are already in hand and delineate the bulk photometric characteristics of Sgr stars in the 2MASS bandpasses (Alard 2001; Cole 2001): Sgr apparently contains stars with a metal abundance of $[Fe/H] = -0.5$ or more (see also Bonifacio et al. 1999), and, as a result, contains a substantial number of M giants. The combination of J, H, and K_s passbands permits color-based discrimination of M-giant stars from (foreground) M dwarfs, a fact that was exploited, for example, by Ibata et al. (2002a) to detect an excess of halo giants defining a great circle with a pole consistent with that extracted from the analysis of halo carbon stars.

Here we use the complete all-sky 2MASS source extractions to characterize the distribution of the Sgr M-giant population as projected on the sky, as well as in three dimensions. This analysis reveals a King profile, dSph-like appearance of the central region and extensive, well-defined, trailing and leading Sgr tidal tails in the south and north Galactic hemispheres. Among the remarkable aspects of the Sgr tidal debris stream are its coherence and nearly constant density over $360°$ of orbital longitude and that tidal debris from Sgr very likely rains down from the north Galactic pole (NGP) onto the solar neighborhood.

2. 2MASS SELECTION OF SGR M-GIANT CANDIDATES

Near-IR (NIR) colors of giant and dwarf stars are degenerate for early spectral types ($<$K7 or $J-K_s \lesssim 0.55$) but become distinct in two-color diagrams for the latest spectral types because of opacity effects (primarily a minimum in the H^- opacity at 1.6 μm with modulation by H_2^-) that have a large effect in the H band. The color divergence begins for sources with $J-K \gtrsim 0.85$ (Lee 1970; Glass 1975; Mould 1976; Bessell & Brett 1988). A preliminary selection of candidates with $J-K_s > 0.85$ was made from the 2MASS (final processing) working survey point-source database covering more than 99.9% of the sky. Sgr tidal features were evident in celestial sphere projections of color/magnitude cuts even in this preliminary selection.

Subsequent reddening correction eliminates intrinsically blue objects that do not satisfy our color selection criteria (below). To account for differential reddening around the Galaxy we have interpolated $E(B-V)$ for each of the selected stars with algorithms and reddening data provided by Schlegel et al. (1998), who give $E(B-V)$ values derived from IRAS 100 μm emission all-sky maps. Each source was then dereddened after adopting the following selective and total extinction laws:

$$E(J - K_s) = 0.54E(B - V) ,$$
$$E(J - H) = 0.34E(B - V) ,$$
$$A(K_s) = 0.28E(B - V) . \qquad (1)$$

For the remainder of our analysis, sources with $E(B-V) > 0.555$, corresponding to $E(J-K_s) = 0.30$, were excluded to avoid potential contamination from excessively reddened sources.

Noise in stellar colors smears the distinction between dwarfs and giants. 2MASS aperture magnitudes are more precise than the point-spread function fitted magnitudes for the brighter ($K_s \lesssim 12.5$, $J < 14$) stars.[3] The photometry used here is exclusively aperture photometry where the quoted photometric uncertainty was less than 0.06 mag in all three bands. This strong constraint on photometric accuracy imposes a completeness limit on the 2MASS selection used here of approximately $K_s < 13.5$, substantially brighter than the 99% survey completeness requirement of $K_s < 14.3$.

Evaluation of the ($J-H$, $J-K_s$) color-color diagram of the center of Sgr permits further refinement of the color selection criteria for Sgr M giants. Figure 1 shows the $(J-K_s, K_s)_0$ color-magnitude and color-color diagrams for 2MASS point sources in 3×3 deg^2 areas centered on the center of Sgr and in a control field centered on a point reflected across the Galactic $l = 0$ axis at the same Galactic latitude. To make the Sgr red giant branch even more clear, we include (Fig. 1c) the results of a statistical subtraction in color-magnitude space of the control field from the Sgr center field using the same method as Layden & Sarajedini (2000) with their aspect ratio parameter $\alpha = 5$. Significant small-scale variations in reddening and population densities mean that the subtraction is not perfect, but the position of

the Sgr red giant branch (RGB) in both Figures 1c and 1f are obvious.[4] Features related to the Milky Way bulge (e.g., a ghostly RGB and horizontal branch red clump) are visible in the color-magnitude diagram (CMD) several magnitudes brighter than the Sgr RGB.

The initial selection for M giants is conservative, balancing a desire for a large statistical sample of M giants but with minimal contamination by other stars (improperly dereddened dwarfs and stars with large photometric errors; see Fig. 2a), and satisfies (Fig. 2)

$$J - K_s > 0.85 ,$$
$$J - H < 0.561(J - K_s) + 0.36 ,$$
$$J - H > 0.561(J - K_s) + 0.22 , \qquad (2)$$

where all magnitudes are in the intrinsic, dereddened 2MASS system.

From a partial survey of the central regions of Sgr, Whitelock et al. (1999) estimate that the Sgr dwarf galaxy contains of order 100 N-type carbon stars (a slight underestimate; see discussion of Fig. 20 below). Carbon stars, because they have extreme, easily identifiable NIR colors, make them a potentially useful tracer of the Sgr debris stream (e.g., Ibata et al. 2001b). However, Sgr carbons have a large spread in luminosity, and a number are long-period variable (see Fig. 19 below), which yields large uncertainties in estimated photometric parallaxes relative to the better defined M-giant color-magnitude relation. Thus, in this paper we rely predominantly on the much more populous M giants to trace the Sgr tidal streams, but we include a discussion of the carbon stars in § 8.3.

3. SALIENT FEATURES OF ALL-SKY MAPS OF 2MASS M-GIANT CANDIDATES

The center of Sgr is a readily apparent feature of all-sky images of the 2MASS point-source catalog already in the public domain.[5] Various aspects of Sgr's debris stream also become readily apparent in color-magnitude windows of the point-source catalog that highlight Sgr M giants at specific distances. Figure 3 shows two such windows.

Several large-scale features are evident in Figure 3. Some are artifacts of heavy and patchy differential reddening near the Galactic plane. Reddening can shift early-type stellar colors into the giant star two-color locus (Fig. 2). Several prominent extensions from the disk correspond to high-latitude dust in the Galaxy also seen in IRAS 100 μm maps.

Figure 3 shows Sgr debris at varying distances in a great circle around the entire celestial sphere. The most prominent M-giant features, apart from the Galactic center and plane, are the Magellanic Clouds and the Sgr center at $(\alpha, \delta) = (284°, -30°)$ (discussed in § 4). Stretching from the Sgr center itself, southward for a short span and then

---

[3] See R. Cutri et al. 2003, Explanatory Supplement to the 2MASS All Sky Data Release, at http://www.ipac.caltech.edu/2mass/releases/allsky/doc.

[4] We show in § 4 that the semimajor axis of Sgr is about 30° and the ellipticity $(1 - b/a)$ is about 0.65, which means that the control field here, although near the minor axis of Sgr, is still within a radius that contains a measurable Sgr density. However, the Sgr density in the field at this radius is about 1% that of the center, so the presence of some Sgr stars in the control field does not effect our interpretation of the CMD here or our analysis of the Sgr luminosity function in Fig. 21.
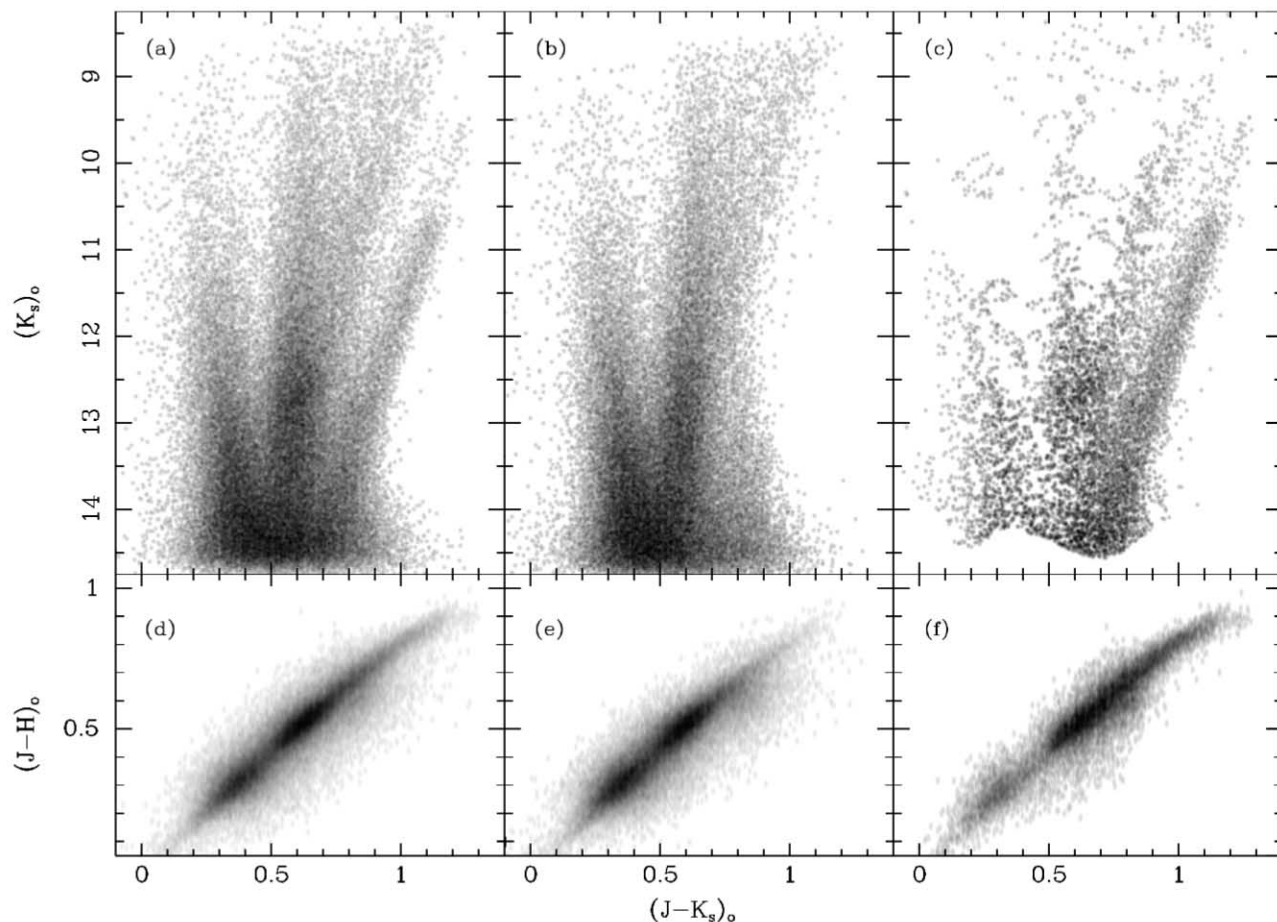
[5] See, e.g., http://www.ipac.caltech.edu/2mass/gallery/showcase/allsky/index.html.

Fig. 1.—Near-infrared ($J-K_s$, K_s) CMDs of (*a*) the Sgr center, (*b*) a control field of identical area and Galactic coordinates reflected about $l = 0°$, and (*c*) a star by star subtraction of (*b*) from (*a*). Panels (*d*)–(*f*) show the corresponding ($J-K_s$, $J-H$) two-color diagrams for the samples shown in (*a*)–(*c*). All sources are dereddened using the Schlegel et al. (1998) maps.

northward, is a " southern arc." In § 6 we explore the distance distribution of the arc and show that it extends physically from the main body of Sgr. The distance modulus of the southern arc is more or less constant for more than

$100°$ from the Sgr center toward the Galactic anticenter. The arc may, in fact, cross the Galactic plane at the anticenter and cross into the northern Galactic hemisphere, albeit at very low surface density in M giants.
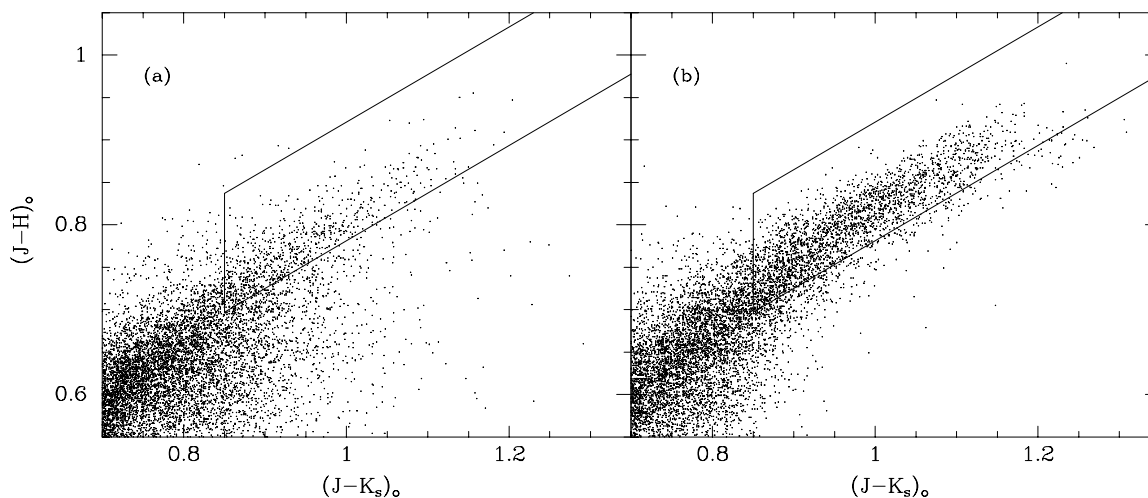

Fig. 2.—Solid lines indicate the color-color selection criteria adopted to find M giants for most of this paper. (*a*) The distribution of stars in the control field, from Fig. 1*e*. (*b*) The distribution of stars from the statistically subtracted sample in Fig. 1*f*. Note that the control field, selected to be a Galactic longitude match to the Sgr center field, still contains about a 1% contribution from the Sgr dwarf itself.
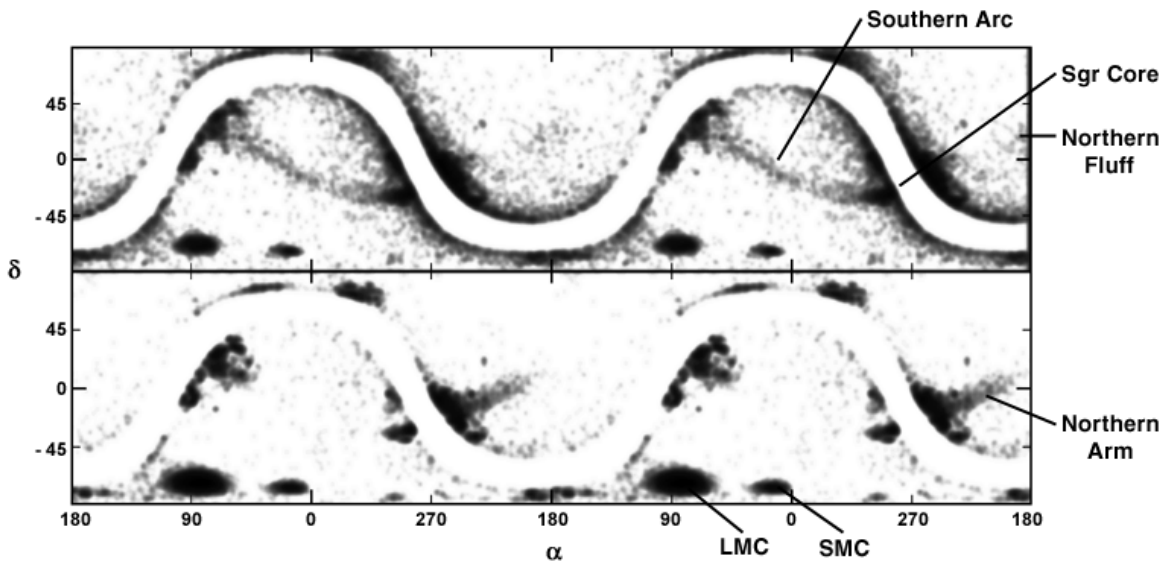
FIG. 3.—Smoothed maps of the sky in equatorial coordinates for two color-magnitude windows of the (nondereddened) 2MASS point-source catalog filtered optimally to show the southern arc (*top*) and the northern arm (*bottom*): $11 \leq K_s \leq 12$ and $1.00 < J-K_s < 1.05$ (*top*), and $12 \leq K_s \leq 13$ and $1.05 < J-K_s < 1.15$ (*bottom*). We show two cycles around the sky to demonstrate the continuity of features.

More than a magnitude fainter than the arc is a spike of M giants extending prominently northward from the Galactic center direction. This " northern arm " has a longitudinal gradient in median K_s magnitude, which indicates a growing distance with increasing Galactic latitude until reaching the north Galactic cap. The brighter magnitude slice in Figure 3 shows a subtle, more extended, "fluffy" distribution of M-giant candidates situated near the termination point of the northern arm. The fluffy concentration spans several tens of degrees, obviously wider than either the northern arm or southern arc, but with less surface density. As we show in § 6, the bright northern fluff represents a severely foreshortened extension of the northern arm. Indeed, in even brighter magnitude windows, this "north fluff" is still present, but is spread out over steradians. At the brightest 2MASS magnitudes it encompasses nearly all of the northern Galactic hemisphere, as would be expected for a large structure very near the Sun (§ 6.4).

4. ANALYSIS OF THE SAGITTARIUS CENTER

The extended, low surface brightness, central regions of Sgr lie nearly behind the Galactic center, which leads to significant contamination by foreground Milky Way bulge and disk stars and obscuration by patchy foreground dust. Early star-count analyses by Ibata, Gilmore, & Irwin (1995) and Ibata et al. (1997) explored the center and southward (Mateo et al. 1998). More recently, studies of RR Lyrae stars examined the more obscured regions north of the center (Cseresnjes, Alard, & Guibert 2000; see also Alard 1996; Alcock et al. 1997). However, the integrated structure of the central part of Sgr remains uncertain. For example, while roughly agreeing on the derived Sgr major-axis scale length-of-fit exponential profiles, Mateo et al. (1998) identify a break in the southern profile of Sgr at a radius of $20°$, while Cseresnjes et al. (2000) identify one at a substantially different density in the northern profile at only $6°$.

Despite its rather irregular appearance in optical maps, Sgr is most often assumed to be a dwarf spheroidal (dSph) type galaxy, because (1) it lacks significant H I (Koribalski, Johnston, & Otrupcek 1994; Burton & Lockman 1999), (2) it contains both old stars and has experienced extended star formation epochs (e.g., Mateo et al. 1995; Layden & Sarajedini 2000) but is not presently forming stars (Bellazzini et al. 1999b), and (3) like other dSph galaxies, Sgr appears to have a rather large M/L (Ibata et al. 1997). Alternatively, it is often postulated (Bassino & Muzzio 1995; Sarajedini & Layden 1995; Layden & Sarajedini 2000; see also discussion by Da Costa & Armandroff 1995) that because the center of Sgr appears to coincide with the globular cluster M54 (Ibata et al. 1995, 1997), the M54+Sgr combination may represent a *nucleated dwarf elliptical* galaxy (Zinnecker et al. 1988; Freeman 1993). Because Sgr exhibits an apparent metallicity gradient with overall higher metallicity in the center (Bellazzini et al. 1999a, 1999b; Alard 2001; but see Cseresnjes 2001) along with rather young, ~0.5 to ~3 Gyr stellar populations there (e.g., Bellazzini et al. 1999b; Layden & Sarajedini 2000), Alard (2001) postulates a third scenario—that Sgr may be more like an LMC-type galaxy with an inner disk, or perhaps a recently disrupted disk. While other dSph galaxies have been shown to have metallicity gradients (e.g., Light 1988; Da Costa et al. 1996; Hurley-Keller, Mateo, & Grebel 1999; Majewski et al. 1999b; Harbeck et al. 2001), Sgr has among the most young and metal-rich constituent populations for dSph's in the Local Group. Weinberg (2000) showed that the stellar disk of a dwarf spiral without a massive dark matter halo, such as the LMC, will be heated by a combination of resonant tidal forcing and precession to form a spheroidal in several gigayears. Recent simulations by Mayer et al. (2001) confirm this result. We believe that a consistent and natural interpretation of the disparate facts that follow is that (1) because Sgr was recently undergoing significant star formation, it must have formerly been a dwarf spiral or irregular galaxy, and (2) a combination of

mass loss from tidal encounters and star formation activity has transformed Sgr into a dSph and brought it to a point of critical stability.

The 2MASS database presents the first opportunity for a large-scale, uniform study of the extended central parts of Sgr at NIR wavelengths where the effects of reddening are diminished. These data clarify a number of the above issues regarding the nature of the Sgr galaxy.

4.1. Radial Profile Fits to the Sgr Center

Figure 4 illustrates the distribution of candidate M giants around the nominal Sgr center and selected with $E(B-V) < 0.555$, $0.95 < (J-K_s)_0 < 1.10$, and $10.5 < (K_s)_0 < 12.0$. This magnitude range excludes strong foreground contamination from brighter Galactic bulge/disk stars and a smaller number of likely disk stars at fainter magnitudes (see discussion of Fig. 8 below). The NIR appearance of Sgr is far smoother than that seen in optical star-count analyses (e.g., Ibata, Gilmore, & Irwin 1995; Ibata et al. 1997): at NIR wavelengths the central body of the Sgr system closely resembles a dSph galaxy.

To show quantitatively its similarity to the appearance of dSph galaxies, we fit the least reddened M-giant data for the Sgr center—that with $b < -10°$ (Fig. 4)—with two functional forms using the Bayesian methods and analytical forms described by Ostheimer (2003): a King (1962) profile and a power law+core (PLC) model. Table 1 and Figure 5 summarize these results. Proceeding with such fits to the center of the Sgr system requires careful consideration of the density contribution by the long Sgr tidal arms (Fig. 3). A simple King profile fit to star counts at all positions angles (Fig. 5a) does not properly account for the unbound tidal debris in these arms manifested as a " break " from a nominal King shape at a major-axis radius of about 1300′ (even more visible in Figs. 5c and 12 below). A model fit primarily along the Sgr minor axis minimizes the influence of these tidal arm stars (situated mainly along the major axis at large radii) and yields a King parameterization that fits the observed density well to an equivalent major-axis radius of 1500′ (Fig. 5b). This King parameterization is given in Table 1. Transferring this King profile, derived primarily
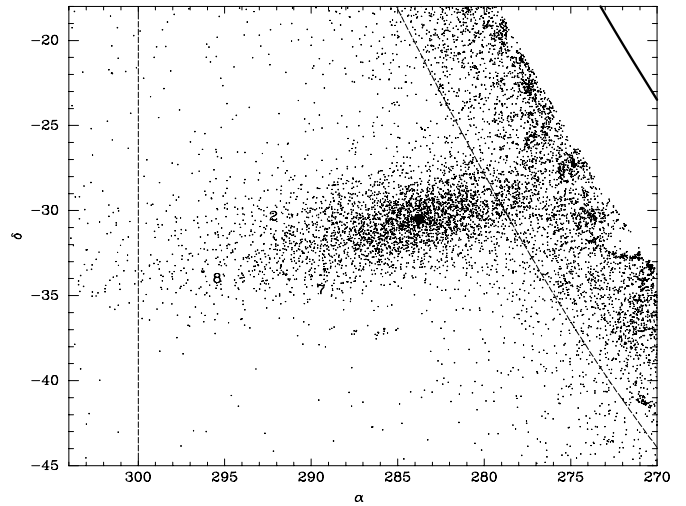

Fig. 4.—View of the central parts of Sgr near where it crosses the Galactic midplane (*upper right, thick line*). Sources up to $b = -5°$ are shown; the results of very patchy reddening can be seen for $b > -10°$ (*angled dashed line*). The symbols mark the locations of globular clusters as follows: " 2 " is Arp 2, " 7 " is Terzan 7, " 8 " is Terzan 8, and the filled circle is the location of the cluster M54. The region to the left of the angled dashed line was used in the King profile fit and the power law+core fits to the central region shown in Figs. 5a and 5d, respectively. The region delimited by both dashed lines was used in the King profile fits to the Sgr center shown in Fig. 5b and given in Table 1.

from Sgr stars along the minor axis, back to the average radial profile from stars at all azimuthal angles (i.e., all Fig. 4 data with $b < -10°$) reveals more clearly the transition from the central Sgr configuration to stars in the southern arc, which have a more or less constant surface density along their extent (see Fig. 13 below), but which present a power-law decline when included in the azimuthal profile average (Fig. 5c). Despite the major improvement in the fit of the King profile at interior radii, the position angle (100°.5 vs. 104°.3), the ellipticity ($\epsilon = 1 - b/a = 0.62$ vs. 0.65), and the declination of the core ($\Delta\delta = 3′$) change only slightly with this fit to the major-axis–truncated data.

TABLE 1
PROFILE FITS TO THE SGR MAIN BODY

Parameter	King Profile Fit	Power Law+Core Fit
$\alpha_{\rm center}$ (deg)	283.7467 ± 0.0133	283.8313 ± 0.0034
$\delta_{\rm center}$ (deg)	-30.4606 ± 0.0256	-30.5454 ± 0.0114
$\alpha_{\rm center}$ (J2000.0)	$18^{\rm h}54^{\rm m}59\overset{\rm s}{.}2 \pm 00^{\rm h}00^{\rm m}03\overset{\rm s}{.}2$	$18^{\rm h}55^{\rm m}19\overset{\rm s}{.}5 \pm 00^{\rm h}00^{\rm m}00\overset{\rm s}{.}8$
$\delta_{\rm center}$ (J2000.0)	$-30°27′38″ \pm 00°01′32″$	$-30°32′43″ \pm 00°00′41″$
l (deg)	5.6193	5.5690
b (deg)	-14.0660	-14.1665
Background (stars arcmin^{-2})	1.422 ± 0.075	$2.016 \pm 0.623 \times 10^{-6}$
Position angle (deg)	104.3 ± 0.6	100.2 ± 0.6
Ellipticity	0.65 ± 0.01	0.62 ± 0.01
Core radius (arcmin)	224 ± 12	234 ± 10
King limiting radius (arcmin)	1801 ± 112	. . .
Power-law index, ν	. . .	1.44 ± 0.03

NOTES.—The power law+core fit is to the data in Fig. 4 trimmed only by $b < -10°$. The King parameterization is fitted to the Fig. 4 data trimmed both by $\alpha < 300°$ (J2000.0) and $b < -10°$. This King parameterization is shown in Figs. 5b and 5c. The fit is robust to varying the right ascension cutoff to more conservatively exclude tidal features along the major axis. The errors for all parameters given have been derived using a Metropolis Markov Chain algorithm (see Ostheimer et al. 2003).
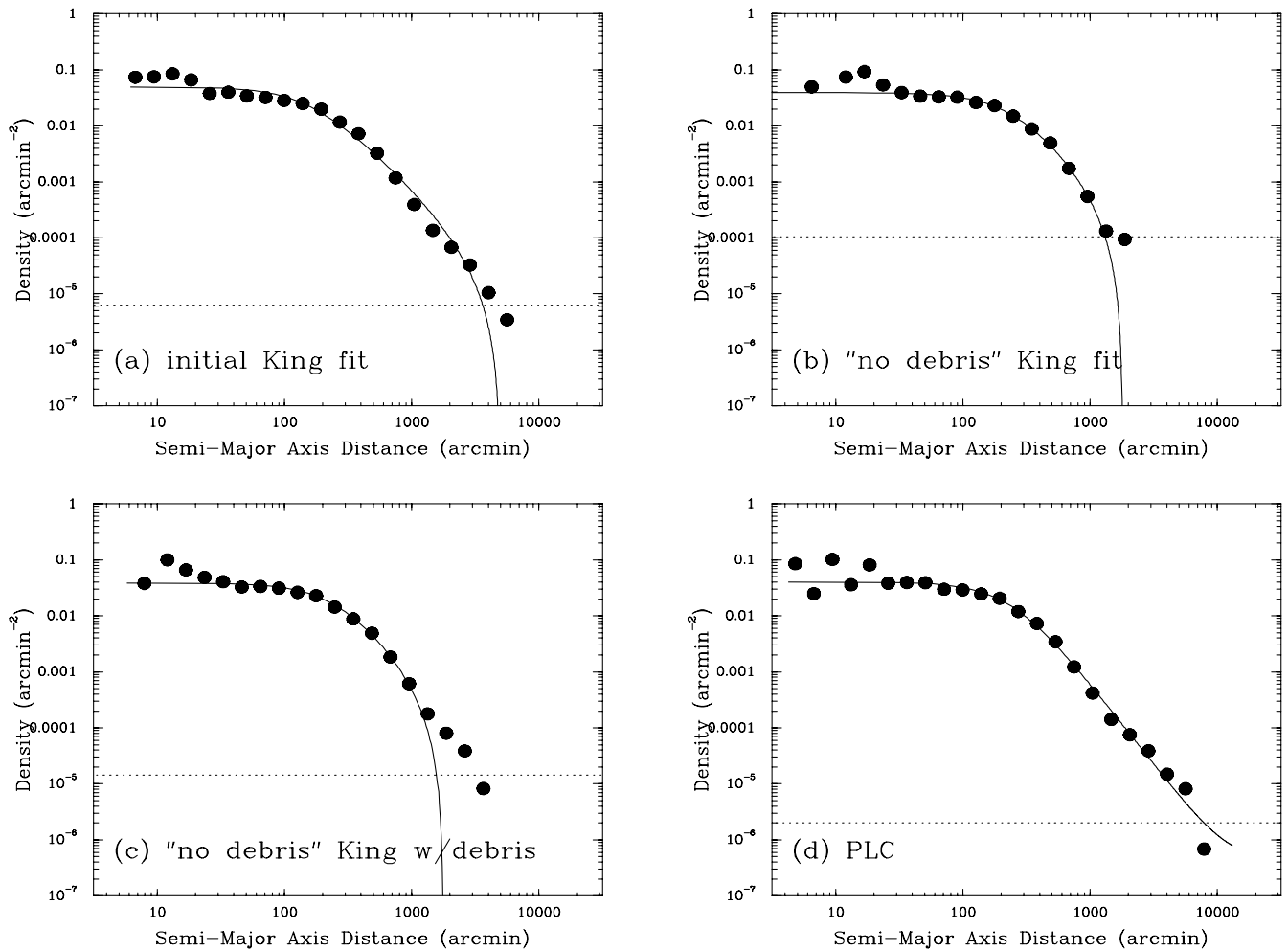
Fig. 5.—Model fits to the radial profile of the Sgr main body. (*a*) Fit to the entire area shown in Fig. 4, but with $b < -10°$. (*b*) Fit to data with an additional restriction to Fig. 4 of $\alpha < 300°$ (J2000.0) to minimize the influence of unbound stars forming the start of the trailing tidal arm along the major axis. This fit is given in Table 1. (*c*) The derived fit from panel (*b*), but with the full data set from (*a*). All parameters from the (*b*) fit are utilized, except the background level, which has been refitted because of variations in the background level when different Galactic latitude ranges are considered. (*d*) Power law+core fit to the same data as used in (*a*). In all cases, the dotted lines are the derived level of the background, which has been subtracted from the data and the fit curves. Note that the data points in each panel change position because of rebinning that reflects different ellipticities and position angles derived from the fits.

A single power-law fit to the full azimuthally averaged radial density profile can only accommodate the general character of the density decline (Fig. 5*d*), but not the detailed shape of the radial profile; for example, it "averages over" the kink in the density profile discussed above. The mean power-law fit (with $\nu = 1.44$; see Ostheimer 2003 for the precise function of the model) corresponds at large radii to an $r^{-\gamma}$ decline with $\gamma \sim 2.88$, which is overly steep beyond the break near 1300′, where the data appear to decline more like $\gamma \sim 2$. This $\gamma \sim 2$ decline is similar to that observed beyond the King limiting radius of the Carina dSph (Majewski et al. 2000).

The Table 1 King and PLC model fits yield Sgr position angles in the range of those found by previous analyses: Mateo et al. (1998) obtained a position angle of $104°.8 \pm 1°.2$, while Cseresnjes, Alard, & Guibert (2000) obtained a position angle of $108°.4$. Not surprisingly, both of our model fits find the center of the Sgr system to be of high ellipticity, $\epsilon = 0.62$–0.65, although not quite as high as the $\epsilon = 0.80 \pm 0.15$ previously reported (Mateo 1998). Fits to the centers of several other Local Group dSph galaxies yield

similar ellipticities, e.g., in And III (Caldwell et al. 1992; Ostheimer 2003) and Ursa Minor (Irwin & Hatzidimitriou 1995; Kleyna et al. 1998; Bellazzini et al. 2002b; Palma et al. 2003). Indeed, the structure of Sgr bears similarity to Ursa Minor (Martínez-Delgado et al. 2001a; Palma et al. 2003) and Carina (Majewski et al. 2000), for which significant tidal disruption has been proposed. Extreme ellipticities compared to the standard for dwarf galaxies (e.g., Sung et al. 1998) already suggests that we are observing systems in a disrupting, transient state.

4.2. *Departures from a King Profile*

4.2.1. *Nucleus*

Two differences of the observed versus fitted radial profiles are noteworthy: the presence of a break population (§ 4.2.2) and the appearance of a "nucleus" within about 20′–25′ that is elevated above the density trend immediately exterior to this radius. The centers of the King and PLC fits lie within a few arcminutes of the center of the massive globular cluster NGC 6715 (M54) at $(\alpha, \delta) = (18^h 55^m 03\overset{s}{.}3,$

$-30°28'42$) (J2000.0). The excess 2MASS star counts over the flat core of the King profile fit might be attributed to the cluster itself; however, (1) the core, half-light, and tidal radii of M54 have been derived (Trager, King, & Djorgovski 1995) as $0.''11$, $0.''46$, and $7.''5$—too small to account for the extent of the excess observed, and (2) the metallicity of M54 is [Fe/H] $= -1.7$ and its age is 14–16 Gyr (Layden & Sarajedini 2000), so it should not contain stars as red as the M giants used for the fits (and shown in Fig. 4) and is thus "invisible" to our survey [the tip of the corresponding RGB is at $(J-K_s)_{2MASS} = 0.724$; Bertelli et al. 1994]. The 2MASS results demonstrate that there is a nuclear condensation in the Sgr system that is independent of the presence of the metal-poor population typically identified with the M54 globular cluster, whether or not M54 is a stellar system distinct from Sgr.

Layden & Sarajedini (2000) have recently shown that all metallicity Sgr populations are clumped around M54, with the most metal-rich ([Fe/H] ~ -0.5) and young (1 and 2.5–3 Gyr) stellar populations particularly so (see also Sarajedini & Layden 1995; Marconi et al. 1998; Bellazzini et al. 1999a). Our finding of a cuspy distribution in the center of the Sgr profile is similar to the findings of Cseresnjes et al. (2000), who with their various fits also faced problems with the peaked central density of RR Lyrae stars. That our highest Sgr density is coincident with the position of M54 is consistent with the findings of other large-area studies of the Sgr center (Ibata et al. 1995, 1997; Bellazzini et al. 1999a). Whether M54 represents the actual nucleus of Sgr or just happens to reside at the bottom of the Sgr potential well remains uncertain, and M54's relation to, and potential role in creating, the much more metal-rich populations condensed around it are matters unsettled. These and related issues are explored in more detail by Da Costa & Armandroff (1995) and Layden & Sarajedini (2000).

Although the overall radial profile of Sgr resembles that of other dSphs (and even includes the presence of a "break population" at large radii; see below), the presence of a nucleated center is a distinguishing feature of the Sgr system.

4.2.2. King Profile Break

The azimuthally averaged 2MASS Sgr radial profile shows a "break" from a King model near a semimajor axis of about 1300' (Fig. 5). This "King+break" profile looks just like those expected for tidally disrupted dwarf galaxies (Johnston et al. 1999b). Moreover, the Sgr radial profile resembles those of other Galactic dSphs found to have breaks from a King profile at large radii (see Irwin & Hatzidimitiou 1995)—for example Carina (Kuhn, Smith, & Hawley 1996; Majewski et al. 2000), Ursa Minor (Kocevski & Kuhn 2000; Martínez-Delgado et al. 2001a; Palma et al. 2003), Sculptor (Westfall et al. 2000, and in preparation; Walcher et al. 2003), and Leo I (Sohn et al. 2003, in preparation)—although we note that the Sgr major-axis, King limiting radius, $r_l \sim 12.6$ kpc, is more than twice that of any of the other Milky Way dSph galaxies (see below). If Sgr is a member of this homologous, Galactic dSph family, it presents at least one case where the break population is bona fide tidal debris and lends support to claims that break populations in other dwarfs may similarly imply tidal disruption (see discussion in Majewski et al. 2002a, for example).

Earlier, in a star-count analysis of fields along the major axis, Mateo et al. (1998) observed a "kink" at $\sim 20°$ radius[6] and speculated that it might arise from a transition from a distinct Sgr dwarf to tidal stream debris. On the other hand, Johnston et al. (1999a) suggested that this kink in the surface density actually demarcates a transition from debris released on the most recent perigalactic passage and older debris (a possibility also mentioned by Mateo et al. 1998). More recently, Helmi & White (2001) asserted that this feature in the surface density demarcates the approximate projected radius between still-bound material and stars lost by Sgr in the last perigalacticon passage. While it is universally accepted that the stars beyond the kink represent unbound, tidal debris, the interpretation of the stars *inside* this radius—bound or unbound—clearly has great bearing on what one derives for the mass and mass-to-light ratio of the present bound center of the Sgr system.

4.3. Sgr Mass-to-Light Ratio Revisited
4.3.1. Previous Work

The dark matter content of the Sgr dwarf remains controversial (Ibata & Lewis 1998; Gómez-Flechoso 1999). The mass density of the satellite determines its long-term integrity. Early investigations (Ibata et al. 1997) postulated that "Sgr is being tidally distorted and is tidally limited, but is not disrupted as yet," and derived a Sgr model with a central mass-to-light ratio of $(M/L_V) \sim 50$ (in the present discussion, all mass-to-light ratios are in solar units, $M_\odot/L_{\odot,V}$). This dark matter–dominated, prolate but tidally limited model, where mass does not follow light, was motivated by the apparent delicacy and short-livedness of low-mass King models when placed in the most likely Sgr orbits (Velázquez & White 1995; Johnston et al. 1995). It was further suggested that Sgr could not have been significantly larger than observed today; otherwise "we would expect to find its 'missing mass' as a substantial population of Sagittarius dwarf debris—globular clusters and stars—along its dispersion orbit" (Ibata et al. 1997). Subsequently, with the observed extent of the Sgr system growing and the clear indication of mass loss into tidal debris tails, the picture of Sgr changed dramatically, with the dwarf recognized to be "in the process of being tidally disrupted and assimilated into the Milky Way" (Ibata 1999). But an apparent conundrum remained: even were Sgr to contain substantial dark matter—sufficient to account for the observed large central velocity dispersion and suggesting a global M/L_V at the level of the most extreme cases among the Galactic dSph population—it would not be enough to solve the puzzle of how the dwarf could have survived as long as it has in its present orbit.

Fine-tuning of the dark matter configuration within the satellite provides one possible solution (Ibata & Lewis 1998). Such models with rigid, very extended dark matter haloes yield concomitantly high $M/L \sim 100$, yet still cannot match some characteristics of the observed Sgr system, and the suggested form of the dark halo is difficult to interpret with conventional forms of dark matter, as pointed out by Helmi & White (2001).

---

[6] Mateo et al.'s (1998) "one-dimensional" Sgr profile matches well the representation of 2MASS density with longitude along the major axis (see discussion of Fig. 13). Both analyses show this "kink" at about the same location.

More prosaic alternatives, albeit ones requiring their own dynamical fine-tuning, have been put forward to address the dilemma of a fragile Sgr surviving a Hubble time. For example, Zhao (1998) proposed that Sgr has not always been in its present orbit but rather was deflected from a "safer" orbit by an encounter with the Magellanic Clouds several gigayears ago. Gómez-Flechoso et al. (1999) suggested that as long as the full Galactic tidal field is experienced slowly (e.g., through a prolonged decay of an orbit via dynamical friction), even a satellite that is not dark-matter–dominated could survive many orbits (see also Jiang & Binney 2000). Dynamical friction models require substantial mass loss in the satellite over the course of the orbit transition. Alternatively, Gómez-Flechoso et al. (1999) propose that Sgr may have formed in the tidal tail of a larger parent undergoing a major merger.

Recently, Helmi & White (2001) claim to find two self-consistent Sgr models, one purely stellar ("model I," with initial mass $4.66 \times 10^8\ M_\odot$ and $M/L \sim 2.25$) and the other with an extended dark halo ("model II," with initial mass $1.7 \times 10^9\ M_\odot$ and $M/L \sim 15.1$) that, when evolved in the Sgr orbit for nearly a Hubble time, reproduce all data then available. The tidal radius in their model II, 10.4 kpc, is similar to the Sgr major-axis King limiting radius found above ($r_l = 12.6$ kpc). From being able to identify two viable structural models, Helmi & White conclude that a long-lived Sgr is not "in any way anomalous." However, it should be noted that their models succeed by using a lighter Milky Way (asymptotic circular velocity for the flat rotation curve of only 186 km s^{-1} and mass interior to present Sgr location of $7.87 \times 10^{10}\ M_\odot$) and more benign Sgr orbit (larger, 70 kpc apocenter and longer, ~ 1 Gyr period) than typically used by previous models.

4.3.2. *Standard M/L Derivation*

The derived mass and mass-to-light ratio of Sgr obviously depend on interpretation of the observed central structure. In the discussion that follows, we distinguish between the true tidal radius, $r_{\rm tid}$, of the system—that distance from the center of Sgr where stars become unbound—and the empirically found radius, r_l, where the best-fit King function plunges to zero.[7] For a dwarf galaxy or globular cluster in near-equilibrium in a tidal field, we expect $r_{\rm tid} \gtrsim r_l$. Although we have ample reason to expect that the Sgr dwarf is disrupting rapidly (see below), for simplicity we take $r_{\rm tid} = r_l$ and use the 2MASS structural parameters to rederive Sgr's M/L according to the standard King (1966) prescription widely applied to spheroidal systems. We do so with the caveat that the results of such an analysis do not apply for other ratios $f = r_{\rm tid}/r_l$, as, for example, in the two extreme cases already mentioned: (1) an extended dark matter halo (a constant M/L is an implicit assumption of the King method) or (2) where the majority of the observed central Sgr structure represents unbound stars.

Therefore, using the King profile parameters in Table 1 to represent the *bound* part of the Sgr system, we convert the integrated light profile to a total brightness by matching the M-giant density at a specific radius to the equivalent surface

---

[7] We note that what we call r_l here is what King (1962) calls the empirical tidal radius, r_t, whereas he discusses a limiting radius, $r_{\rm lim}$, in a manner similar to our discussion of the true tidal radius in § 4.3.3.

brightness measured at the same radius. The Table 1 King profile fit does not track the elevated density cusp in the center of Sgr, so the peak surface brightness of Sgr is unrepresentative of the inner King brightness. Fortunately, Mateo et al. (1995) have measured the surface brightness of Sgr outside the central condensation, while Mateo et al. (1998) have estimated the "central" surface brightness as part of an extrapolation of a fit to the brightness profile that also ignores the cusp; both methods obtain $\Sigma_{0,V} = 25.2 \pm 0.3$ mag arcsec^{-2}. With the latter value for the flat part of our density profile, an integration of the King profile yields a total apparent magnitude for Sgr of $V_0 = 3.63$, which is virtually identical to one of the results obtained by Mateo et al. (1998, their $V_{\rm tot,1}$), even though Mateo et al. integrate a two-component exponential profile fit to their one-dimensional cross-sectional profile of Sgr and their integration *includes* the tidal debris profile, whereas we fit and integrate a King profile fit to the full two-dimensional shape of Sgr and include only the supposedly *bound* stars in the integration. The two methods coincide because the Mateo et al. adoption of a 3 : 1 axis ratio for the inner shape of Sgr (Ibata et al. 1997) matches well our findings for the Sgr ellipticity, and, moreover, the tidal debris contribution in the area they surveyed makes a relatively minor contribution to the total luminosity. Ignoring the central cusp likely underestimates the total Sgr luminosity by less than 5%.

A Sgr distance modulus of $(m - M)_0 = 16.90 \pm 0.15$ (Ibata et al. 1997), implies an absolute magnitude of $M_V = -13.27$ for the bound part of the galaxy. Thus, the Sgr dSph is apparently the most luminous of the Milky Way family. Ignoring the effects of stellar evolution and a variable star formation history, we find that adding the central cusp and the M-giant debris trails (§ 7.1) increases the minimum luminosity of the Sgr *progenitor* by several tenths of a magnitude over the present Sgr brightness. That Sgr and the Fornax dSph (which has $M_V = -13.2$; Mateo 1998) are of comparable luminosity is consistent with the currently established globular cluster specific frequency of the two systems: Fornax has six clusters, and Sgr almost certainly has five (see § 8 below), and possibly several more (Palma et al. 2002; Bellazzini et al. 2002a, 2003).

To estimate the bound mass of Sgr, we use the formalism of King (1966) as outlined by Richstone & Tremaine (1986). Thus, the mass of Sgr is given by

$$M_{\rm tot} = 166.5 r_c \mu / \beta , \qquad (3)$$

where the scaling parameter μ is given by King (1966) as ~ 9.38 for on object with the observed concentration of Sgr, i.e., $\log(r_t/r_c) = 0.905$ (Table 1). The velocity parameter β is related to the observed velocity dispersion, most commonly taken as the 11.4 km s^{-1} value in Ibata et al.'s (1997) field "f7" in the Sgr core. This dispersion yields $\beta \sim 0.8^2/\sigma^2$ (Binney & Tremaine 1987, see their Fig. 4.11), $M_{\rm tot} = 4.9 \times 10^8\ M_\odot$, and $M_{\rm tot}/L_{\rm tot} = 25$ in solar units (where we adopt the total V-band luminosity from above as $2 \times 10^7\ L_\odot$). That there appears to be a nuclear concentration of stars (and therefore mass) that encompasses Ibata et al.'s field f7 raises concern that the velocity dispersion there may be enhanced. Ibata et al.'s next field out from the Sgr center, at several core radii, is "f5," for which the velocity dispersion is only 9.2 km s^{-1}. Adopting this dispersion, however,

leads to little difference: $\beta \sim 0.6^2/\sigma^2$, $M_{\rm tot} = 5.8 \times 10^8\,M_\odot$, and $M_{\rm tot}/L_{\rm tot} = 29$.

These $(M/L)_{\rm tot}$ values are 2–4 times smaller than suggested by earlier studies, except that of Mateo et al. (1998). But it is important to point out that the Table 1 *structural parameters* are also significantly different than those that have been adopted in previous studies and models of the Sgr system. For example, while the stellar distributions in Helmi & White's (2001) Sgr models have similar concentrations, $c = \log_{10}(r_t/r_c)$, to the $c = 0.90$ here, the actual scale of their *initial* Sgr stellar systems are more than a factor of 3 smaller than found here, and one expects the tidal radius to *decrease* with time. The models by Ibata & Lewis (1998) and Gómez-Flechoso et al. (1999) are similarly spatially compressed. Indeed, no model in the Ibata & Lewis (1998) library has a tidal radius anywhere near the r_l derived here (their model K9, with a tidal radius two-thirds our r_l but a similar mass and approximately similar $[\Psi/\sigma^2]$ parameter is probably the closest match to the observed 2MASS M-giant parameters). Most of these models have been influenced by the original structural parameters derived for the Sgr dwarf by Ibata et al. (1997), which yielded a half-light radius that is almost exactly 3 times smaller than derived here. The large difference in the derived core radius is likely because we have fitted (Fig. 5) a King profile to the entire system *and that fit is generally insensitive to the localized central cusp of Sgr*, whereas Ibata et al. use the cusp to define the central surface brightness, from which they search for a half-light decrement. In effect, the Table 1 profile fits to the Sgr dSph result in a satellite that has an overall structure that is much more distended than typically assumed; however, as we now show, this extended size begs the question of whether it can actually represent the limits of the *bound* Sgr core.

4.3.3. *Whither the Tidal Radius?*

Interpretations of the central parts of the Sgr system range from those where the bulk of Sgr within the ~ 9 kpc " break " radius is still bound, to models (Velázquez & White 1995; Johnston et al. 1999a; Law et al. 2003 and a fuller paper in preparation), where the bulk of the extent of the King profile is constituted by unbound stars. Indeed, recent models by Johnston, Choi, & Guhathakurta (2002a) have shown that breaklike features in the radial profiles of tidally disrupting satellites can appear at several times the analytically estimated tidal radius, especially for satellites near pericenter.

Based on simple dynamical arguments, we argue that a bound radius with $f = r_{\rm tid}/r_l$ as high as unity seems unlikely. Although only a rough guide, especially in the case of a highly elliptical satellite on a noncircular orbit, the Roche tidal limit (e.g., eq. [3] in King 1962) can be used to derive a relationship between the tidal radius and enclosed satellite mass. In this case we assume a Milky Way mass interior to Sgr's present position of $1.8 \times 10^{11}\,M_\odot$ (e.g., Burkert 1997) and normalize to the semimajor axis $r_l = 12.6$ kpc to obtain the approximate mass of Sgr within the tidal radius as

$$m_{\rm Sgr} = 1.6 \times 10^{11}\,M_\odot f^3 \,. \qquad (4)$$

Clearly, under the presumption that $f = 1$ we obtain an extraordinarily heavy Sgr. Instead, to be conservative, we acknowledge that the Sgr core is extremely tidally distorted and presume the *semiminor* axis to be a better representation of $r_{\rm tid}$, so that $f = 0.35$; thus we obtain $m_{\rm Sgr} \sim 6.9 \times 10^9\,M_\odot$

and a total $M/L_V \sim 343$. While a comparably high M/L has recently been claimed for the Draco dSph on the basis of internal velocity dispersion measures (Kleyna et al. 2002), it is hard to understand how Sgr could be so obviously losing mass into long tidal tails under these conditions (whereas, in contrast, several studies claim *no* detection of tidal tails around Draco; Odenkirchen et al. 2001b; Aparicio et al. 2001). Moreover, even this mass estimate is likely to be low since, as argued by, e.g., von Hoerner (1957) and King (1962), the effective tidal radius should be calculated at the perigalacticon of the orbit. In any case, that these tidal approximation estimates are substantially at odds with that obtained from the King (1966) methodology in § 4.3.2 indicates that f cannot be near unity and casts doubt on *both* analyses dependent on this assumption.

On the other hand, analysis of the spatial and kinematical dispersion of the Sgr tidal tail M giants presented in this paper by Law et al. (2003) suggests that the present bound mass of Sgr is approximately $3 \times 10^8\,M_\odot$. If we adopt this more modest mass for Sgr (although a mass still at the high end among members of the Milky Way dSph family), then the Roche limit predicts an instantaneous Sgr $r_{\rm tid}$ more like 1.5 kpc, which is of order the measured King *core* radius (Table 1). Such a physical configuration will be greatly susceptible to tides (Pryor 1996; Burkert 1997), and, as found in the Johnston et al. (1999a) and Law et al. (2003) Sgr models—which have been shown to match the observed (e.g., Fig. 13 below) Sgr surface brightness profile well—the majority of the observed light profile consists of debris recently detached from the satellite in a major, destructive mass-loss event. While perhaps uncomfortable to anthropic sensibilities, " . . .it must clearly be possible. Any satellite must suffer final catastrophic disruption on some pericentric passage, and in the case of Sagittarius we are seeing a system where this event occurred only after a series of previous less damaging encounters had reduced its mass and binding energy to the point of critical stability " (Velázquez & White 1995).

With the suggestion by Hayashi et al. (2003) that such tidal limit approximations tend to overestimate the bound mass in tidally disrupting systems, it becomes possible to contemplate that the even more centrally defined nuclear " cusp " might represent the *bound* Sgr core embedded in an extensive cocoon of unbound stars. In so doing, we return the length scales of the problem to of order those utilized in the model studies that have queued their Sgr structural parameters from the half-light decrements measured from the central surface brightness of the *cusp*.

4.3.4. *The M-Giant Conundrum*

Reducing the actual tidal radius and binding energy of the satellite also helps resolve a timing problem posed by the presence of stars as young as the Sgr M giants in extended, comparably aged tidal tails. As we show in § 6.6, the bulk of the M giants explored in this paper are likely formed relatively recently—within the past several gigayears but no more than about 5 Gyr ago (Layden & Sarajedini 2000). These stars are found in tidal tails of a length that requires about several gigayears to form (§ 6; Law et al. 2003), thereby leaving relatively little time between when the M giants were created and when they escaped the bound Sgr system. The problem is exacerbated if the size scale of the bound Sgr galaxy is much larger than the expected,

hundreds of parsecs radius for the star formation region—as, for example, in the type of Sgr contemplated in § 4.3.2—because no secular diffusive mechanism can lead to the acceleration of stars in a dSph galaxy on the required timescales.

On the other hand, escape of stars formed several giga-years ago in a central starburst would have been far easier if, in the course of critical disruption, the Sgr tidal radius became of order the size of that starburst region; thus a present true tidal radius of order a kiloparsec in size or smaller is far more likely than one of order r_l, or even $0.35r_l$. M-giant escape would be enhanced were the most recent starburst spread out over a rotating disk rather than in a nuclear concentration.[8] It is also possible that the starburst itself may have contributed to the destruction of Sgr. Starburst-driven galactic winds have been evoked to explain a number of properties of dwarf galaxies, including typically low metallicities as a result of the loss of enriched gas. Clearly, wholesale blowout of gas has not been a character-istic of the star-forming processes in Sgr, given its multiple populations and age-metallicity relation (Layden & Saraje-dini 2000; see Table 3 below), but even fractional loss of gas in supernova winds would have contributed to drops in the Sgr binding energy after each starburst. This mass loss allows the bound part of Sgr, including the starburst region, to expand and makes it possible for young stars to reach the true tidal radius. While outside the scope of the present investigation, the formation of *M-giant* tidal tails (§§ 5 and 6) would seem to provide a rather powerful constraint on full chemodynamical evolutionary models of the Sgr system.

Until the actual extent of the bound Sgr system is defini-tively established, it will be difficult to establish its true M/L and dark matter content. Obviously, the standard methodol-ogy of § 4.3.2 will be an increasingly poor approximation as r_{tid} departs from r_l, although exactly how M/L changes as f decreases is not obvious (it depends on a proper accounting of both the enclosed light and the actual distribution of bound mass). One might also wonder whether the similarity of the Sgr radial profile to those of other dSph galaxies trans-lates to a similarity of *physical state* in these other systems. Problems with the typical values of M/L inferred from cen-tral velocity dispersions for *other* dSph systems that may not be in virial equilibrium have been discussed by, e.g., Kuhn & Miller (1989), Kroupa (1997), Gómez-Flechoso (1998), Klessen & Kroupa (1998), Majewski et al. (2002a), and Gómez-Flechoso & Martínez-Delgado (2003).

5. GREAT CIRCLE M-GIANT STREAMS, THE SGR ORBITAL PLANE, AND A SGR COORDINATE SYSTEM

5.1. Great Circle Cell Counts of M Giants

To study the Sgr system over its full extent, we first define a coordinate system natural to the tidal debris system and in which projection effects are minimized. Because Sgr and its debris lie close to one great circle defined by its orbit (Fig. 3), we adopt the method of great circle cell counts ("GC3"; Johnston, Hernquist, & Bolte 1996) to derive an initial

approximation to the orientation of the Sgr orbital plane. A similar approach was adopted by Ibata et al. (2002a) on the 2MASS Second Incremental Data Release; in their analysis of 26.4% of the sky, Ibata et al. identified a peak in the M-giant candidate source counts corresponding to a Sgr plane with pole at $(l, b) = (95°, 13°)$. Ibata et al. (2001b) have also explored carbon star counts in great circle cells and found a peak at $(l, b) = (90°, 13°)$ identified with Sgr.

To establish the Sgr orbital geometry we select M-giant candidates with $0.95 < (J-K_s)_0 < 1.10$ and $E(B-V) < 0.555$. The sample is further limited to M-giant candidates with projected photometric parallax distances from 13 to 65 kpc—the primary distance range for the majority of mate-rial in the southern arc and northern arm. While limiting the volume of our GC3 assessment of tidal streams, the above photometric parallax limit also reduces the contribution of "false positive" detections at the faint end of the survey magnitude range (see discussion in § 6.6). GC3 runs with a variety of Galactic latitude limitations were made, both including and excluding the main body of Sgr. By excluding the high-density central part of Sgr we give more weight to the tidal debris in the derivation of the best-fit plane, but the results of the analysis were rather robust to these variations, as well as in variations in the angular width of the cells and in the step size of the poles: for runs with various cell sizes and exclusion zones the peak in GC3 counts yielded poles within a degree of $(l, b) = (273°, -13°)$.[9]

Figure 6a shows the GC3 pole count analysis for a sample limited to $|b| > 30°$ and excluding the Large and Small Magellanic Clouds.[10] A great circle cell width of 5° is used. The pole from this particular figure is $(l, b) = (272°, -12°)$. By a quirk of nature, the Sgr debris plane is similar to that of the ecliptic [which has a pole $(l, b) = (276°, -30°)$].

5.2. Best-Fitting Sagittarius Plane

5.2.1. Fit in Galactic Cartesian Coordinates

The GC3 methodology assumes that the debris under study is sufficiently far away that the effects of Galacto-centric parallax are negligible; i.e., strictly speaking, nonpre-cessing debris streams will follow great circles across the sky only when viewed from the Galactic center. However, parts of the Sgr debris stream come sufficiently close to the Sun and the Galactic center that several effects of perspective come into play (Fig. 7). That (1) the Sun is not directly in the orbital plane of Sgr and (2) the southern arc and northern arm stars are at rather different distances from us means that different GC3 poles are derived by analysis of the two tidal tails independently: we obtain GC3 poles of $(279°, -18°)$ and $(271°.5, -11°.5)$ when we divide the data set into northern and the southern Galactic hemispheres, respectively (Figs. 6b and 6c).

To remove these Galactocentric parallax effects, we next search for the best-fitting Sgr orbital plane in the Cartesian Galactic coordinate system. To place the survey into these coordinates, a photometric parallax is calculated for each

---

[8] The present Sgr system appears to show no minor-axis rotation; how-ever, the signal of any major-axis rotation has yet to be separated from other longitudinal velocity variations (Ibata et al. 1997).
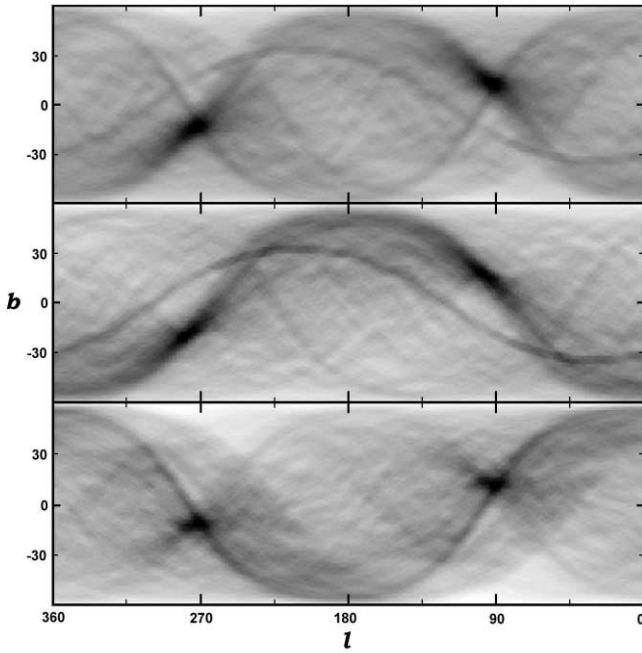
[9] Any great circle distribution on the sky produces two antipodal peaks in the cell counts. Contrasting with Ibata et al. (2002a), we elect to identify Sgr with the peak in the south Galactic hemisphere because this corre-sponds to the *angular momentum pole* of the satellite itself (see also Palma et al. 2002).

[10] The Magellanic Clouds were removed by excluding the zone $260° < l < 320°$ and $-53° < b < -25°$.

Fig. 6.—Great circle cell counts for M-giant candidates in the projected distance range 13–65 kpc and $|b| > 30°$. The plots are in sky-right, Galactic coordinates, from $360° > l > 0°$ and $-60° < b < 60°$. The top panel shows the results for both hemispheres together, the middle panel is for inclusion of only northern hemisphere data, and the bottom panel is for inclusion of only southern hemisphere data. From all panels we have removed the Magellenic Clouds from the sample to remove the rather strong great circle pole families they contribute. The darkest patches correspond to the pole of the Sgr tidal debris stream at approximately $(l, b) = (272°, -13°)$ and its corresponding antipode. No other strong peaks occur in this particular stellar sample of M giants. Arclike features in the GC3 distributions result from various localized density peaks in the sky distribution.

star using an absolute magnitude-color relation derived from the RGB color-magnitude data shown in Figure 1c. The fit was restricted to the 1675 stars in the restricted range $0.9 \le (J-K_s)_0 \le 1.10$, the primary M-giant color range explored in this paper. With $2.5\,\sigma$ iterative rejection of 158 stars, the following fit is obtained with an rms of 0.36 mag:

$$K_s = -8.650(J - K_s)_0 + 20.374 . \quad (5)$$

The resultant distance scale (after assuming a Sgr distance modulus of 16.90; Mateo 1998) is approximately 13% smaller at $(J-K_s)_0 = 1.0$ than one obtained from adopting the primary locus for an $[Fe/H] \approx -0.45$ population identified by Cole (2001) as a good match to 2MASS observations of the Sgr center:

$$M_{K_s,\mathrm{CIT}} = -9.43(J - K_s)_{0,\mathrm{CIT}} + 3.623 , \quad (6)$$

which translates to

$$K_s = -8.930(J - K_s)_0 + 20.383 \quad (7)$$

after transforming the Elias et al. (1982) Caltech/CTIO (CIT) system into the natural 2MASS filter system using the equations given by Carpenter (2001). Use of the color-magnitude calibration from Figure 1c is preferred because (1) it is derived from a fit specific to the restricted color range explored in this paper, (2) the new relation is derived from a background-subtracted CMD of the Sgr center, (3) it was

fitted in the natural 2MASS photometric system and so is free of transformation equation uncertainties, and (4) it derives from a catalog of the center of Sgr almost 10 times larger than Cole used.

Adopting this mean RGB color-magnitude relation implicitly translates the astrophysical scatter within the Sgr RGB into an imposed artificial scatter about calculated mean photometric parallaxes for Sgr features. The intrinsic vertical width of the Sgr RGB in Figure 1c for the $0.9 \le (J-K_s)_0 \le 1.1$ color range determined above $[\sigma(K_s) \sim 0.36\ \mathrm{mag}]$ is likely only slightly underestimated by excision of the weak tail to brighter M_{K_s}, more metal-poor Sgr RGB stars (other possible systematic effects related to the relative numbers of metal-weak populations are addressed in § 6.6). For sources with $J-K_s \sim 1$, this intrinsic "standard candle" scatter dominates the contribution from 2MASS color errors until $K_s \sim 11$. Combining both the astrophysical scatter and the determined (see footnote 3) 2MASS aperture photometry uncertainties, we estimate the imposed fractional distance spread to be approximately $\sigma_d/d = 0.20$ for most stars in the survey, rising to $\sigma_d/d \sim 0.25$ for sources with $K_s \sim 13.5$. We also note the possibility of systematic errors in the M-giant distance scale that are linear with errors in the adopted distance of the Sgr core; Mateo (1998) suggests that the error on the distance to Sgr is about 8%.

To fit the Sgr orbital plane, we first winnow the M-giant sample to those within 15 kpc of the plane defined by the GC3 pole from § 5.1. Technically, this plane includes the Sun and not the Galactic center; however, because the Sun is almost in the Sgr orbital plane (see below), the 15 kpc limit is more than generous enough to include all of the Sgr tidal debris. A restrictive color selection of $1.0 \le (J-K_s)_0 < 1.1$ removes a large amount of contamination by photometric errors in the distance range of concern for Sgr debris (see § 6.6 and discussion of Figs. 14 and 15) and also lessens the effects of systematic photometric parallax errors by color. To remove any remaining photometric error contaminants of this color-restricted sample, and with some foreknowledge of the position of the Sgr debris streams (§ 6), we remove stars with $Z_{\mathrm{GC}} \ge 50$ kpc and $Z_{\mathrm{GC}} \le -30$ kpc. Finally, stars from the disk and bulge are removed with a requirement that $|Z_{\mathrm{GC}}| > 11$ kpc; this also removes stars from the center of Sgr and prevents them from biasing the fit (in the end, this has only a minor effect on the results).[11]

From this sample we determine a least-squares best-fitting plane by iteratively removing $2\,\sigma$ outliers, redrawing the sample to those stars within 15 kpc of the new plane (and with the other limits above) and repeating the fit. From a final sample of 1161 stars, from which 695 lie within $2\,\sigma$ (and where the rms is 1.78 kpc), we find the best-fitting plane in Galactic coordinates (defined where the Sun is at $X_{\mathrm{GC}} = 0$ and this axis is positive toward the Galactic

---

[11] S-shaped structures have been seen in the case of, e.g., the globular cluster Palomar 5 (Odenkirchen et al. 2001a, 2003; Rockosi et al. 2002) and the Ursa Minor dSph (Palma et al. 2003)—both systems for which our perspective is nearly edge-on to the orbital plane. An "isophotal twisting" that resembles part of an S-shape is also apparent in Figs. 4, 7e, and 7f. Because the northern limb of the bound part of the Sgr system lies in the Galactic midplane, both ends of the S-shape twisting of the central parts of Sgr are not evenly sampled in our data. Thus, including the heavy statistical weight of the unequally sampled inner parts of the Sgr system in our analysis would result in a slight biasing to the best-fitting plane.
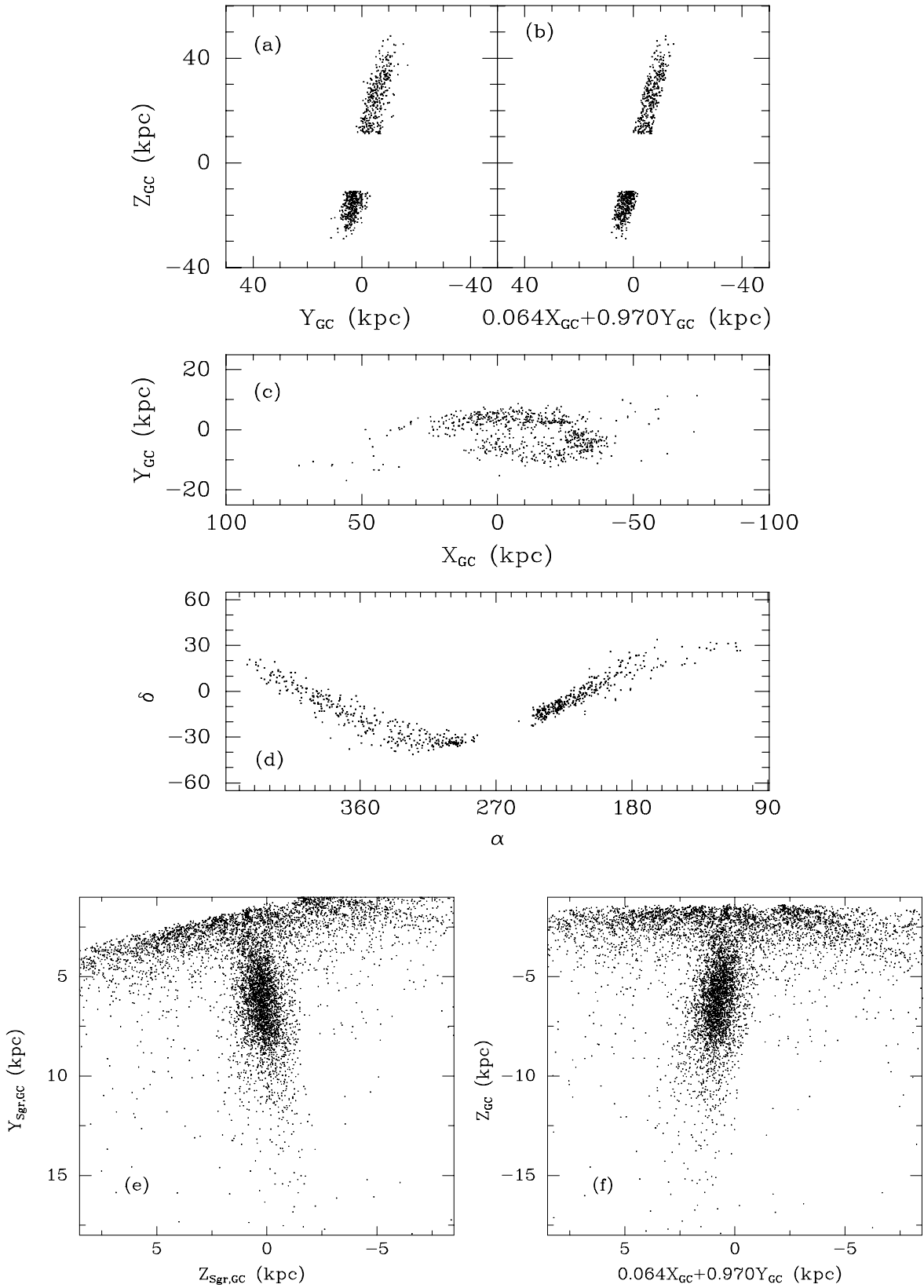
FIG. 7.—In (*a*)–(*d*) the points used to define the Sgr orbital plane are used to show various projection effects. (*a*) The Galactic Y_{GC}-Z_{GC} plane. (*b*) The plane shown in (*a*), but rotated by 3°.8. This projected plane is perpendicular to the derived best-fitting plane. By definition, the width of the material is narrower in Fig. 7*b* than in Fig. 7*a*. (*c*) A projection parallel to the Galactic plane. (*d*) The projection on the sky in celestial coordinates, showing the foreshortening effects of varying proximity to the Sun. In (*e*) and (*f*) edge-on views of the best-fitting Sgr plane for all stars with $(J-K_s)_0 > 1.0$ and $E(B-V) < 0.555$ are shown, restricted to stars on the far side of the Galactic center [$R_{GC} \cos(\Lambda_{GC} + 21°.60) > 7$ kpc] to highlight the Sgr center. Both figures are edge-on to both the Galactic plane and to the Sgr plane, but the coordinate system in (*e*) has the best-fitting Sgr plane ($Z_{Sgr,GC} = 0$) vertical, while (*f*) is rotated so that the Galactic plane is ($Z_{GC} = 0$) is horizontal. Canting of the Sgr main body with respect to both these planes is evident.

anticenter, analogous to the left-handed system described in Mihalas & Binney, their § 6.1) to be

$$0.064X_{GC} + 0.970Y_{GC} + 0.233Z_{GC} + 0.776 \text{ kpc} = 0 . \quad (8)$$

The derived errors on the coefficients are (0.002, 0.008, 0.002, 0.038), respectively. This plane corresponds to a Galactocentric orbital pole of $(l_{GC}, b_{GC}) = (273\overset{\circ}{.}8, -13\overset{\circ}{.}5)$, only slightly different from that obtained with the GC3 analysis. The pole derived here is independent of any distance scale errors—such errors affect only the distance to the plane from the Sun (the fourth constant in the equation, 0.776 kpc) and from the Galactic center. Note that the best-fitting plane was not constrained to include the Galactic center; if we assume the Galactic center to lie at $(X_{GC}, Y_{GC}, Z_{GC}) = (-8.5, 0, 0)$ kpc, this point lies 0.23 kpc from the plane. Had this plane been more inclined to the X_{GC} axis, defining it would have given a new estimate of the distance to the Galactic center, which presumably lies in the Sgr orbital plane; unfortunately very little leverage on this is offered in the present configuration. However, this technique may be applicable to other extended halo tidal streams orbiting the Galactic center found in the future.

5.2.2. *The Flatness and Proximity of the Sgr Plane*

Our proximity to the Sgr plane is a rare coincidence. If we adopt the solar position as $3\overset{\circ}{.}8$ from the Sgr-Galactic plane line of nodes, we are closer to the Sgr orbital plane during less than 4% of our own orbit around the Galaxy. This number drops to 2% when we consider that it is only on this side of the Galactic center that the Sgr leading debris arm (as traced by M giants) apparently gets near the solar circle (see §§ 6.4 and 9). Our 0.78 kpc distance from the Sgr plane is less than half the rms spread in Sgr debris about the plane fit above, so that if Sgr debris passes within a few kpc of the solar circle, we are very likely to be amidst that debris. Sections 6.4 and 9 address the implications of this unusual time in solar system history.

That the Sun is not *precisely* in the orbital plane leads to perspective effects shown in Figure 7. Only those stars used in the derivation of the best-fitting plane and lying within 2 σ are shown.[12] Figures 7a and 7b compare the slightly different perspectives offered by a projection on the X_{GC}-Z_{GC} plane and the plane obtained by rotation of $3\overset{\circ}{.}8$, which allows a direct edge-on view of Sgr. Because of the variation in distance of Sgr tidal debris from the Sun, a slight " bowing " of the apparent Sgr orbital plane is removed when viewed more edge-on. This bowing (seen more obviously in Fig. 16 below) explains the differences in derived GC3 poles for northern and southern hemisphere GC3 analyses in § 5.1.

The coherence of the Sgr debris tightly to one plane highlights how little precession the Sgr system experiences for the 1–2 Gyr of orbit traced by the observable debris—no more than a few degrees total (Law et al. 2003). Orbital precession in tidal tails is acutely sensitive to the shape of the halo potential (see Johnston, Sackett, & Bullock 2001; Mayer et al. 2002), and the flatness of the Sgr debris stream strongly points to a *spherical* mass potential for the Milky

Way to at least ~50 kpc. Our results here concur with and *strengthen* the similar arguments previously made by Ibata et al. (2001b) because even tighter coherence of the Sgr stream is demonstrated after properly removing Galactocentric parallax effects. A quantitative analysis of the halo flattening from these results is presented in Law et al. (2003).

Figure 7c, a projection of the $|Z_{GC}| > 11$ kpc portions of the tidal arms onto the Galactic plane, illustrates the tilt in the Sgr orbital plane. Figure 7d shows the variation in the width of the Sgr stream when projected onto the sky. As may be seen, the debris stream is most foreshortened and spans the largest angle when it is near us, in the general direction of the north and south Galactic poles. Figure 7d demonstrates how much of the high-latitude celestial sphere contains lines of sight that intercept the Sgr stream (especially accounting for the fact Fig. 7d does not display greater than 2 σ outliers from the Sgr midplane); particularly at the Galactic poles, Sgr debris is hard to avoid! Figure 12, discussed later, shows greater than 2 σ outliers from the Sgr plane and makes this point even more clearly. We review various proposed detections of Sgr debris in this context in §§ 8 and 9.

5.2.3. *Sagittarius Spherical Coordinate Systems*

Determining the Sgr orbital plane, as done in § 5.2.1, permits us to derive a more natural spherical coordinate system for the interpretation of Sgr tidal debris—one with the equator defined by the Sgr debris midplane. Two such systems (Table 2)—one heliocentric and one Galactocentric—are useful. In the first, Sgr latitudes, $B_{\odot}$, are defined by the Sgr debris *projected on the sky as viewed from the Sun*. We adopt a debris midplane (equator) corresponding to a pole (l, b) given by the $(l_{GC}, b_{GC}) = (273\overset{\circ}{.}8, -13\overset{\circ}{.}5)$ pole derived above. Sgr longitudes, $\Lambda_{\odot}$, are defined to increase in the direction of trailing Sgr debris, with the prime meridian, $\Lambda_{\odot} = 0°$, defined by the longitude of the center of the King profile fit to the main body of Sgr determined in the previous section. This first coordinate system is entirely observationally based, but, being Sun-centered, preserves Galactocentric parallax effects.

The second, *Galactocentric* spherical coordinate system—where the equator is defined by the Sgr plane in equation (8)—while immune from Galactocentric parallax effects, is, however, subject to scale and random errors in the determination of photometric parallaxes. We define a Galactocentric (Λ_{GC}, B_{GC}) system, with $\Lambda_{GC} = 0°$ taken as centered on Sgr, as before. Because the plane does not actually contain the Galactic center (it was not constrained to do so), we take as the center of the (Λ_{GC}, B_{GC}) system the point in the plane

---

[12] Equivalent side views of the Milky Way and Sgr with no restriction to less than 2 σ outliers are shown in Fig. 16 and show that the relative thinness of the distribution is not simply contrived by the present analysis.

TABLE 2
EULERIAN TRANSFORMATIONS TO THE SAGITTARIUS COORDINATE SYSTEMS

SYSTEM	EULER ANGLES			ROTATION CENTER		
	ϕ (deg)	θ (deg)	ψ[a] (deg)	X_{GC} (kpc)	Y_{GC} (kpc)	Z_{GC} (kpc)
$(\Lambda, B)_{\odot}$	183.8	76.5	194.1	0.0	0.0	0.0
$(\Lambda, B)_{GC}$	183.8	76.5	201.6	−8.51	−0.21	−0.05

[a] Adopted as $180\overset{\circ}{.}0$ for some figures in order to keep the intersection of the Sgr and Galactic planes horizontal.

closest to $(X_{GC}, Y_{GC}, Z_{GC}) = (-8.5, 0, 0)$ kpc, which is $(X_{GC}, Y_{GC}, Z_{GC}) = (-8.51, -0.22, -0.05)$ kpc.

Table 2 gives the Eulerian rotation angles (under the "x-convention"; see, e.g., Goldstein 1980), (ϕ, θ, ψ), and the Cartesian Galactic coordinates of the centers of rotation used to define the two Sgr (Λ, B) coordinate systems used here. Note that these systems as adopted are right-handed and therefore determined from the left-handed, Cartesian Galactic system after the translation $X_{GC} \rightarrow -X_{GC}$. For some illustrations presented here it is convenient and intuitive to leave the intersection of the Sgr and Galactic plane horizontal, and this is achieved by setting the third Euler angle rotation to $\psi = 180°$. This results in the following new Cartesian Sgr coordinate systems corresponding to each of the spherical coordinate systems derived above,

$$X_{Sgr,\odot} = d_\odot \cos(\Lambda_\odot + 14°11) \cos(B_\odot) ,$$

$$Y_{Sgr,\odot} = d_\odot \sin(\Lambda_\odot + 14°11) \cos(B_\odot) , \qquad (9)$$

$$Z_{Sgr,\odot} = d_\odot \sin(B_\odot) ,$$

where $d_\odot = (X_{Sgr,\odot}^2 + Y_{Sgr,\odot}^2 + Z_{Sgr,\odot}^2)^{0.5}$ is the distance of the star from the Sun, and a second system (distinct from the normal Galactic $[X_{GC}, Y_{GC}, Z_{GC}]$ coordinates used above),

$$X_{Sgr,GC} = d_{Sgr,GC} \cos(\Lambda_{GC} + 21°60) \cos(B_{GC}) ,$$

$$Y_{Sgr,GC} = d_{Sgr,GC} \sin(\Lambda_{GC} + 21°60) \cos(B_{GC}) , \quad (10)$$

$$Z_{Sgr,GC} = d_{Sgr,GC} \sin(B_{GC}) ,$$

where $d_{Sgr,GC} = (X_{Sgr,GC}^2 + Y_{Sgr,GC}^2 + Z_{Sgr,GC}^2)^{0.5}$ is the distance from the center of the (Λ_{GC}, B_{GC}) system as given above and in Table 2.[13]

Figure 7e makes use of the latter coordinate system to show a projection of Sgr perpendicular to the best-fitting Sgr plane. The canting of the Sgr major axis with respect to the best-fitting plane and in the direction of the normal to the Galactic plane can be seen. Indeed, the angle of this tilt is nearly identical to the angle between the Sgr major axis and the normal to the Galactic plane (see Fig. 7f), or a little more than about 6° in each case. This canting is the rationale for removing the Sgr center from our calculation of the best-fitting plane above. Figures 7e and 7f shows how the beginning of the Sgr tidal stream emanates from the main body more or less evenly to either side of the debris midplane, despite the tilt of main body of Sgr. Figures 7e and 7f provides a slight qualification to the usual assumption (e.g., Lynden-Bell 1982) that the major axes of satellite systems are aligned with the direction of orbital motion and should therefore point in the direction of their tidal tails. This observed canting may provide an additional constraint on dynamical models because torquing of the tidal elongation depends on the details of the noncircular satellite orbital trajectory with respect to the Galactic potential.

5.3. *No Magellanic Cloud M-Giant Streams*

No other strong GC3 peak appears in the M-giant candidate pole counts in agreement with the preliminary analysis

---

[13] David R. Law has written a suite of codes for converting between different Galactic and Sgr coordinate systems. These computer routines are available at http://www.astro.virginia.edu/~srm4n/Sgr.

of 2MASS M giants by Ibata et al. (2002a). This GC3 result only applies however, for that part of the halo within ~75 kpc, for streams with substantial extent above $|b| = 30°$, and for tracers obeying the other specific M-giant photometric criteria employed here (e.g., eq. [2]). However, this result is reconfirmed for *all* late-type giants (M giants and carbons) by our analysis of M-giant streams in Cartesian coordinates in §§ 7 and 8.3. In addition, no GC3 peak corresponds to tidal debris from the Magellanic Clouds, even though the Magellanic Clouds are copiously populated by such stars (e.g., Nikolaev & Weinberg 2000) and are, by far, the predominant reservoirs of late-type giants in the Galactic halo. Previous analysis of a sample of halo carbon stars by Ibata et al. (2001b) suggested the existence of a Magellanic carbon star stream. We note that while our GC3 analysis specifically leaves out the region around the Magellanic Clouds (excluding the zone $-25° > b > -53°$, $260° < l < 312°$) to avoid the interference of a large great circle band dominating Figure 6, any roughly coherent tidal streams extending more than about 25° from the Clouds should be apparent as a GC3 peak in that figure. Analysis of the distribution of 2MASS star counts by van der Marel (2001) shows the Large Magellanic Cloud to be elongated by Galactic tidal forces, but the lack of any GC3 peaks associated with the Magellanic Clouds suggests that any tidal forces on them either are not sufficient to create extended streams of extratidal stars, or at least that young, metal-rich populations are not presently participating in such streams.

The planar coherence of the Sgr debris and the implied sphericity of the Galactic potential suggests that other tidal streams in the outer Galaxy should also face little precessional smearing, remain spatially coherent for at least several gigayears, and therefore be evident as great circles on the sky. Ibata et al. (2002a) have argued that the lack of any other discovered M-giant GC3 streams means that the present accretion rate of luminous, low-mass satellites must be very low and that most of the luminous part of the Milky Way halo must have been in place more than 3 Gyr ago, before the accretion of Sgr. However, this conclusion applies only to systems sufficiently metal-rich to produce M giants. Most halo globular clusters and Galactic dSph galaxies contain few if any such stars because they are dominated by old, metal-poor populations (note, as just one example, the total absence of the four Sgr globular clusters in the M-giant distribution of the central part of Sgr shown in Fig. 4). Indeed, the Sgr center and the Magellanic Clouds are the only readily identifiable, *intact* stellar systems away from the Milky Way disk within the full-sky, 2MASS M-giant distribution explored here. Thus, the lack of other M-giant streams places no limit on the present accretion rate of older, more metal-poor systems.

6. ANALYSIS OF OBSERVED TIDAL FEATURES IN THE SAGITTARIUS PLANE

6.1. *Tidal Tails*

The celestial sphere projection of M giants in Figure 3 gives only a rudimentary sense of the relative distances of Sgr tidal features by their apparent brightness. Figure 8 shows the *planar* distribution of the dereddened K_s magnitudes of M-giant candidates with $(J-K_s)_0 \geq 1.0$ and $-10° \leq B_\odot \leq +10°$ as a function of Sgr longitude. Figure 9 presents the same distribution in a polar projection. Figures
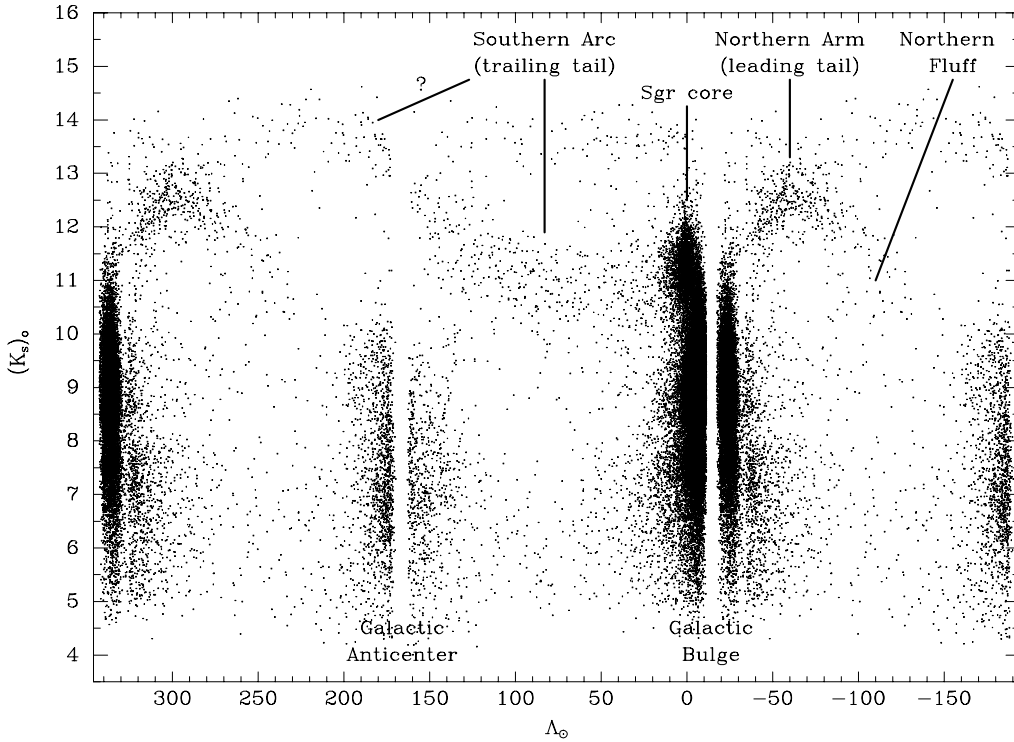
FIG. 8.—Dereddened K_s-band magnitudes for M-giant candidates with $(J-K_s)_0 > 1.00$ shown as a function of Sgr longitude, $\Lambda_\odot$, along the great circle in the sky defined by the Sgr debris (Sgr orbit). Only candidates within Sgr latitude range $-10° < B_\odot < +10°$ are shown. For clarity, we remove sources with $E(B-V) > 0.555$. The center of Sgr is at $(\Lambda_\odot, [K_s]_0) = (0°, 11.25 \text{ mag})$. Other features and possible features of the Sgr debris stream are indicated.
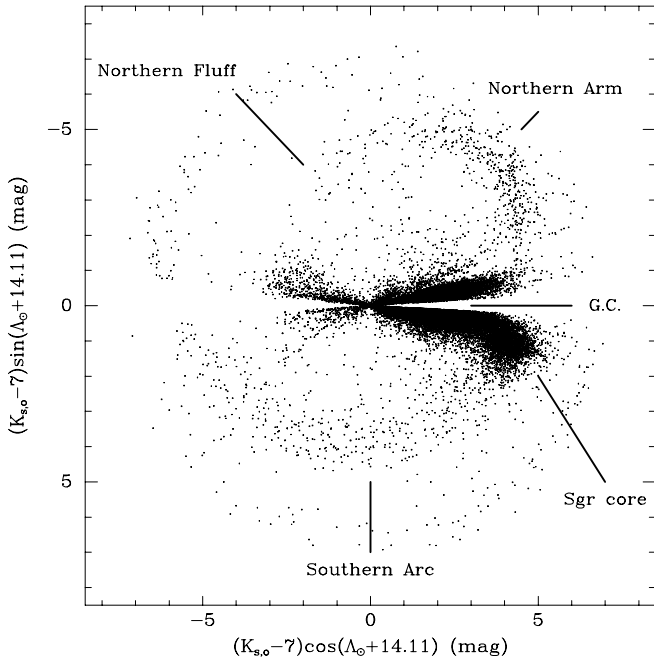

FIG. 9.—Same as Fig. 8, but shown in a cross-sectional plot of the Sgr orbital plane (i.e., the approximation of that plane given by the $[\Lambda_\odot, B_\odot]$ coordinate system), where $(K_s)_0$ magnitudes of M-giant candidates are shown radially (after subtraction of 7 mag). Stars with $(K_s)_0 < 7$ have been left out of the figure. The term $(\Lambda_\odot + 14°.11)$ places the Galactic plane horizontal across the center of the figure. The direction of $\Lambda_\odot = 0$ is toward the Sgr center (to the right and below the Galactic plane), and $\Lambda_\odot$ increases counterclockwise. This figure shows the same sample of stars as given in Fig. 8.

8 and 9 show directly observed quantities, so are free of interpretation. Both figures show the more complex character of the southern arc and northern arm, and give proof of their contiguous connection: While the two features are on average at different mean K_s magnitudes, projections of the magnitude-longitude trends through the zone of avoidance show that the two features meet at the Sgr center and that they represent the leading (northern arm) and counterpart trailing (southern arc) tidal tails.

In Figures 10 and 11 we present the M-giant planar distributions in terms of derived distances from the Sun and distances from the Galactic center (technically, the latter is the center of the GC system given in Table 2). The M-giant photometric parallaxes are derived from the absolute magnitude-color relation given in equation (5).

Figures 8–11 make clear the leading/trailing tail structure of the Sgr dwarf and the rosette nature of its orbit. Figure 11, which shows the distribution of stars projected onto the presumed Sgr orbital plane, gives a particularly clear impression of the rosette shape. We fit this distribution to a model of the Sgr dwarf in the Galactic potential in a subsequent contribution (Law et al. 2003), but as a general guide to understanding the overall structure of the tidal arms illustrated in Figure 11 we call attention to Ibata & Lewis (1998) model K6-a, shown in their Figure 3 (a model highlighted more clearly in Fig. 3 of Ibata et al. 2001b). Although shown in the slightly different (canted by about 13°.5) X_{GC}-Z_{GC} plane, the overall appearance of the Ibata & Lewis K6-a model illustration bears great resemblance to the M-giant distribution shown in Figure 11 (see also Fig. 14, particularly panel c). Another useful interpretive guide is Figure 8 of Helmi & White (2001), which shows one of their models
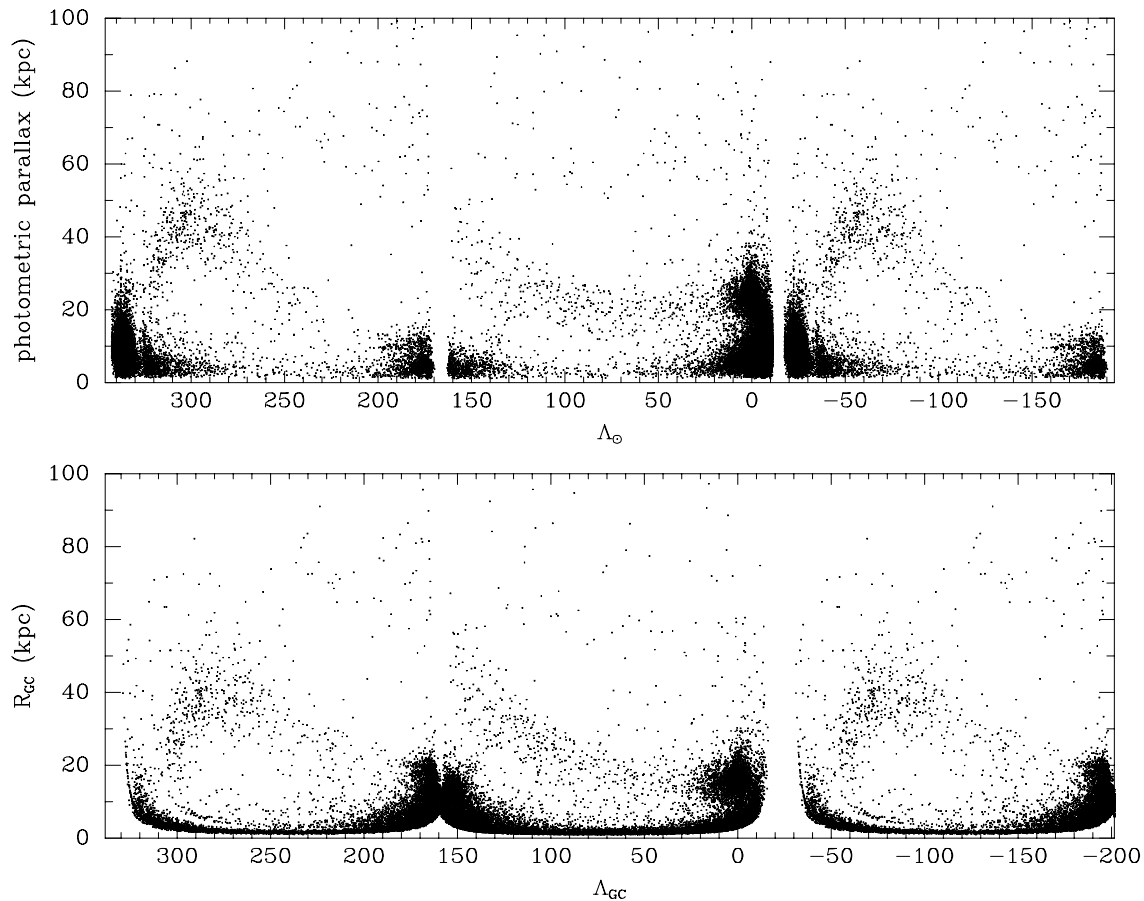
FIG. 10.—*Top:* Same as Fig. 8, but for photometric parallax distances (in kpc) after assigning each M-giant candidate an absolute magnitude according to its $J-K_s$ color. Stars within Sgr latitude range $-10° < B_\odot < +10°$ are shown. *Bottom:* The perspective from the Galactic center point of view. After calculation of photometric parallaxes, distances from the center of the best-fit plane (eq. [8]) are calculated. For this panel, a stellar sample with $(J-K_s)_0 > 1.00$ and $E(B-V) < 0.555$ is adopted, as in the top panel, but stars with $-10° < B_{GC} < +10°$ are shown. To remove additional contamination at large distances (where the adopted B_{GC} latitude range translates to a broad spatial range), we impose the additional constraint that stars lie within 7 kpc of the best-fit Sgr plane.

in a coordinate system similar to that shown in the top panel of Figure 10.

6.2. *Trailing Tidal Debris*

As may be seen in Figures 8 and 9, the center thread of the southern arc M giants varies by only about a magnitude across the southern Galactic hemisphere. The actual mean photometric distance of this trailing debris tail is (1) roughly 25 kpc where it attaches to the center of Sgr, (2) slightly less than 20 kpc when it achieves its closest distance to us near the south Galactic pole, and then (3) gets progressively more distant toward the Galactic anticenter (e.g., ∼40 kpc at $\Lambda_\odot \sim 160°$). The mean Galactocentric distance of the southern arc ranges from $R_{GC} = 16$ kpc at the Sgr center and a similar distance when it passes beneath the Galactic center ($\Lambda_{GC} \sim 70°$) to ∼50 kpc at the Galactic anticenter.

The disposition of this trailing tidal arm at longitudes even farther from the Sgr center is less clear. Inspection of Figures 8–11 (and particularly the bottom panel of Fig. 10) suggests that the trailing arm crosses the Galactic plane, since there appears to be a continuation of the sweeping southern arc north of the Galactic plane and an overdensity of points near $(\Lambda_\odot, K_s) \sim (185°, 13$–14$)$. Unfortunately, this is where our selection of M giants becomes both incomplete and noisy (see discussion of Fig. 15 below). A large

number of stars appear at $(K_s)_0 > 13.0$ at all longitudes, but their reality as M giants, much less Sgr M giants, must be considered highly uncertain and remains to be verified spectroscopically. We address the issue of the length of the tidal tails further in § 6.4 below.

6.3. *Leading Tidal Debris*

The northern arm can be seen (Figs. 8–11) to represent the leading tidal debris tail of Sgr. Figures 10 and 11 show that the approximate center of the locus of the leading tidal debris arm reaches a mean apogalacticon distance of about 40 kpc around $\Lambda_{GC} = 280°$ ($l \sim 350°, b \sim 45°$).

Figure 11 makes clear the relationship between the diffuse north Galactic cap (NGC) "fluff" and the northern arm: The diffuse NGC material apparently represents an extension of the northern arm, which together constitute one "northern loop" around the Galactic center and returning back toward the Galactic plane. The NGC material is more spread out on the celestial sphere simply because it is closer and foreshortened along the line of sight. Figures 8–10 show the looping northern arm spreading across the NGC, covering a large angular range when it gets to the smallest distances from us (e.g., Fig. 10, *top panel*). The top panel of Figure 10 gives the strongest impression that debris from the leading arm of Sgr orbits back toward the Galactic plane
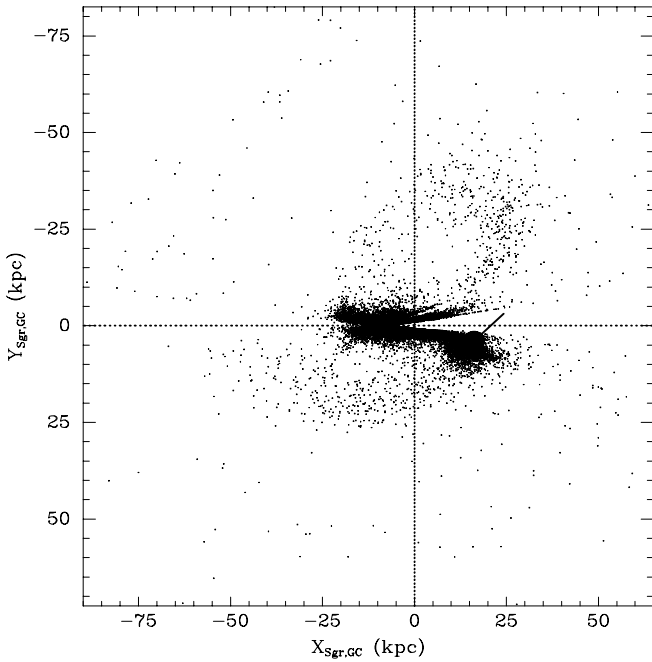
FIG. 11.—Similar to Fig. 9, but the radial dimension now shows distances from the Galactic center derived from the photometric parallaxes, and the plane shown is the best-fit plane from § 5.2 (the plane shown is slightly tilted from a traditional [X_{GC}, Z_{GC}] projection; see Table 2). The center of the coordinate system is actually given by (X_{GC}, Y_{GC}, Z_{GC}) = (−8.51, −0.21, −0.05) kpc, and the Sun lies near ($X_{Sgr,GC}$, $Y_{Sgr,GC}$) = (−8.5, 0) kpc (see § 5.2). The stellar sample is the same as that shown in the lower panel of Fig. 10. The nominal direction of motion of the main body of Sgr is shown by the angled line projecting from the Sgr center. The Sgr proper motion and radial velocity are from Ibata et al. (1997). The continuity of the northern arm and southern arc, and their association with the Sgr center, is evident in this projection, despite obscuration by the Galactic disk. The depth of Sgr features in this plot are artificially broadened by $\sigma_d/d \sim 0.2$ uncertainties along the line of sight from the Sun (see § 5.2).

near the solar circle: because no distance scaling problem can move stars *on the celestial sphere*, that material is seen to either side of $\Lambda_\odot = 256°$ (the direction closest to the north Galactic pole) points to the likelihood of Sgr material falling to either side of the solar circle.

6.4. *The Sagittarius Leading Arm Near the Solar Neighborhood*

In § 5.2 it has been found that the Sun lies within a kiloparsec of the Sgr orbital plane, a distance well within the width of the Sgr tidal debris stream; thus the actual proximity of Sgr debris to us depends on the length of the leading arm and where it crosses the Galactic plane on this side of the Galactic center if it is long enough to do so. For a variety of reasons, whether and where the northern tidal arm crosses the Galactic plane toward the southern hemisphere must still be considered uncertain, because the stars that look to be nearby parts of the leading arm in Figures 8–11 might also be contributions of M giants from the Galactic intermediate Population II/thick disk, bulge, or inner halo, or might even be other substructure. The following summary points suggest the *plausibility* of Sgr debris near the Sun, but further work is needed to confirm this scenario:

1. In the fit to the Sgr plane in § 5, we obtained an rms residual of nearly 2 kpc. While there is a ∼20% distance smearing imposed from the intrinsic spread about the

adopted color-magnitude relation, it is clear that Sgr debris girdles the Sgr orbital midplane with a total width of 4–8 kpc or more. This is supported by the fact that the southern arc (at a distance of about 20 kpc) is 10°–20° or more wide on the sky (e.g., Figs. 3, 7d, and 12). Simplistically assuming a cross-section for the tidal arms not too far from circular in shape would then yield a *depth* of the Sgr arms *within* the orbital plane (e.g., that projection shown in Fig. 11) of about the same order of magnitude. Thus, should the leading stream be long enough to reach the Galactic plane on this side of the Galactic center, and should it do so within several kiloparsecs from the Sun, then Sgr debris will pass through the solar neighborhood.

2. Although previous models (e.g., Ibata et al. 2001b; see, e.g., their Fig. 3) derive an orbit for Sgr similar to that traced by the rosette of debris seen here and predict current passage of leading-arm debris through the Galactic plane at a mean distance of ∼4 kpc outside the solar circle, our own best-fitting models to the present data set (Law et al. 2003) obtain a passage of the center of the leading Sgr within two kiloparsecs of the Sun.

3. Figures 10 and 11 show the presence of 15–30 kpc distant M giants stretching from $\Lambda_\odot = 225°$ to 280° or more. An even wider angular distribution at closer distances suggests the passage of leading-arm material both exterior *and* interior to the solar circle at these distances (the NGP is near $\Lambda_\odot = 256°$). Unfortunately, increased confusion between Sgr debris and disk, intermediate Population II/thick disk, inner halo, and bulge M giants in the inner Galaxy means that the exact disposition of the nearby Sgr debris requires spectroscopic weeding of Milky Way contaminants.

4. The tidal debris model shown by Ibata et al. (2001b, their Fig. 3) shows a southern extension of the downward moving northern debris that passes not only through the Galactic plane, but also through the trailing debris arm and to larger distances. Such a feature may be the origin of the slight excess of more distant stars (with $11.5 < K_s < 13$) in the predicted longitude range ($\Lambda_\odot \sim 15°$–65°). The lower right quadrant of Figure 14c (presented below), which matches the overall appearance of the Ibata et al. model, shows this apparent excess of more distant stars more clearly.

Radial velocities of both very bright and faint M-giant stars in each hemisphere would be particular useful for checking whether the above features are consistent with a vertical flow of Sgr stars through the nearby Galactic plane and onward, past the trailing debris arm. We discuss recent spectroscopic observations bearing on these subjects in another contribution.

6.5. *Density Variation Along the Tidal Arms*

Both the length of and density variation along the tidal debris arms of a disrupting satellite system are a function of the duration, strength, and overall nature of the interaction with the Milky Way (Johnston 1998). Figure 12 is an attempt to unwrap the Sgr tidal material into a ribbon around the sky to illustrate surface density variations in the Sgr tidal arms on the plane of the sky. The top panel shows the ribbon in celestial coordinates. Only stars lying within 7 kpc of the best-fit plane to the Sgr debris are shown. A less distorted projection is one in a Sgr coordinate system (Fig. 12, *bottom*). In our analysis of density variation with position we concentrate on the morphologically simpler, trailing
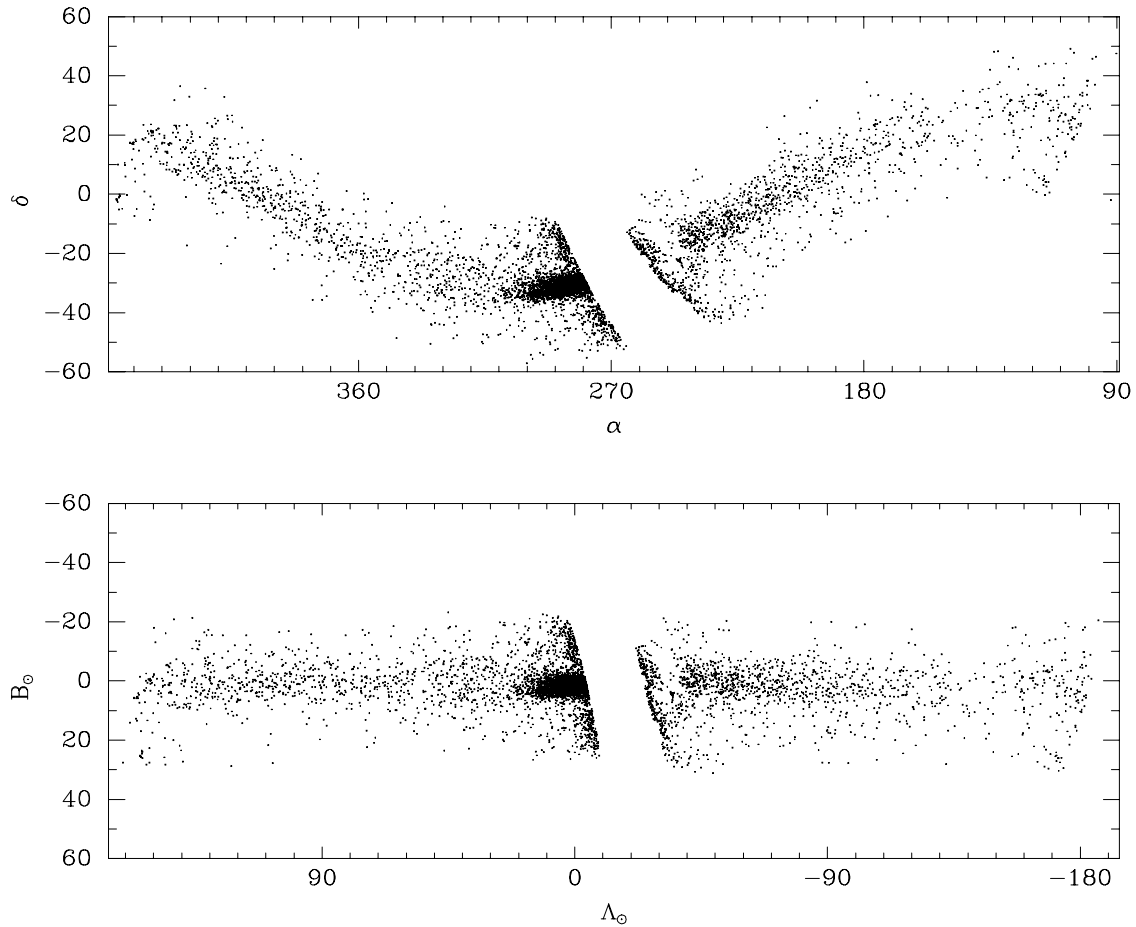
Fig. 12.—The $-7 < Z_{\mathrm{Sgr,GC}} < 7$ kpc sample explored in Fig. 13 shown in equatorial and Sgr coordinates

arm. Moreover, because of its nearly equal distance from us as a function of Sgr longitude, the southern arc of Sgr provides a facile means by which to measure density/mass-loss variations relatively free of the effects of foreshortening. Therefore, the natural longitude system to use is $\Lambda_{\odot}$, not Λ_{GC}. To remove the bulk of Galactic disk/bulge contamination, we show only stars more than 10 kpc from the Galactic center (assuming a Galactic center distance of 8.5 kpc), more than 15 kpc from us, and with $|b| > 10°$. To increase the signal-to-noise ratio of the tail density, we include bluer M giants by opening our selection criterion to $0.95 \leq (J-K_s)_0 \leq 1.10$.

In Figure 13 we show the numbers of these M giants as a function of $\Lambda_{\odot}$ position. Counts are shown for tallies within *slabs* of various thicknesses centered on the Sgr midplane. To isolate those stars in each slab associated specifically with the southern arc, we fit a quadratic function to the photometric parallax distances of all stars in the slab as a function of $\Lambda_{\odot}$ (with an iterative rejection of 2.5 σ outliers). For ± 3, ± 5, and ± 7 kpc wide slabs, the σ of the southern arc distances are 3.6, 3.7, and 3.9 kpc, respectively. This *depth spread* is larger than the ~ 2 kpc sigma *width spread* found in our fits of the best-fit plane to the Sgr debris, but the depth spread is of course affected by the artificial ($\sigma_d/d \sim 0.2$) spreading due to "standard candle" scatter (§ 5.2).

To determine a background level of non-Sgr "contaminants" in the southern arc, we count M-giant candidate stars in tidal-stream–like tubular volumes of the Galactic

halo, but in a direction that avoids Sgr, the Magellanic Clouds, and regions of large reddening. Through trial and error we found an acceptable orientation by rotating the slabs containing the southern arc tubular volumes $35°$ about the line of nodes represented by the intersection of Sgr and Galactic planes. In this orientation, the southern arc tubes now sample random halo volumes associated with the great circle pole $(l, b) = (272°, +23°)$. Although nearly as polar as the original Sgr plane (and therefore presumably sampling a similar background Galactic halo density law), this "background plane" suffers from the shortcoming that wider slabs centered on it become ever more contaminated by Sgr contributions near the Galactic plane. In one direction this includes parts of the Sgr center, but, because we are concerned here with assessing the density of the more diffuse parts of Sgr, it is less critical to obtain an accurate accounting of the background near the Sgr center (which has, in any case, been done more properly in the radial profile fits in § 4). Figure 13 includes the derived background counts for the ± 3 kpc wide slab as representative; the background is typically about 10% in the tail regions away from the Sgr center. Tests of various sized background slabs show that the background level away from the Sgr center is fairly constant, at 0.33 times the slab width per $5°$ longitude. This adopted background is subtracted in the density plots shown.

Both Figures 12 and 13 demonstrate that, for the most part, the trailing tidal arm of Sgr shows no substantial density variation with longitude, especially over the range
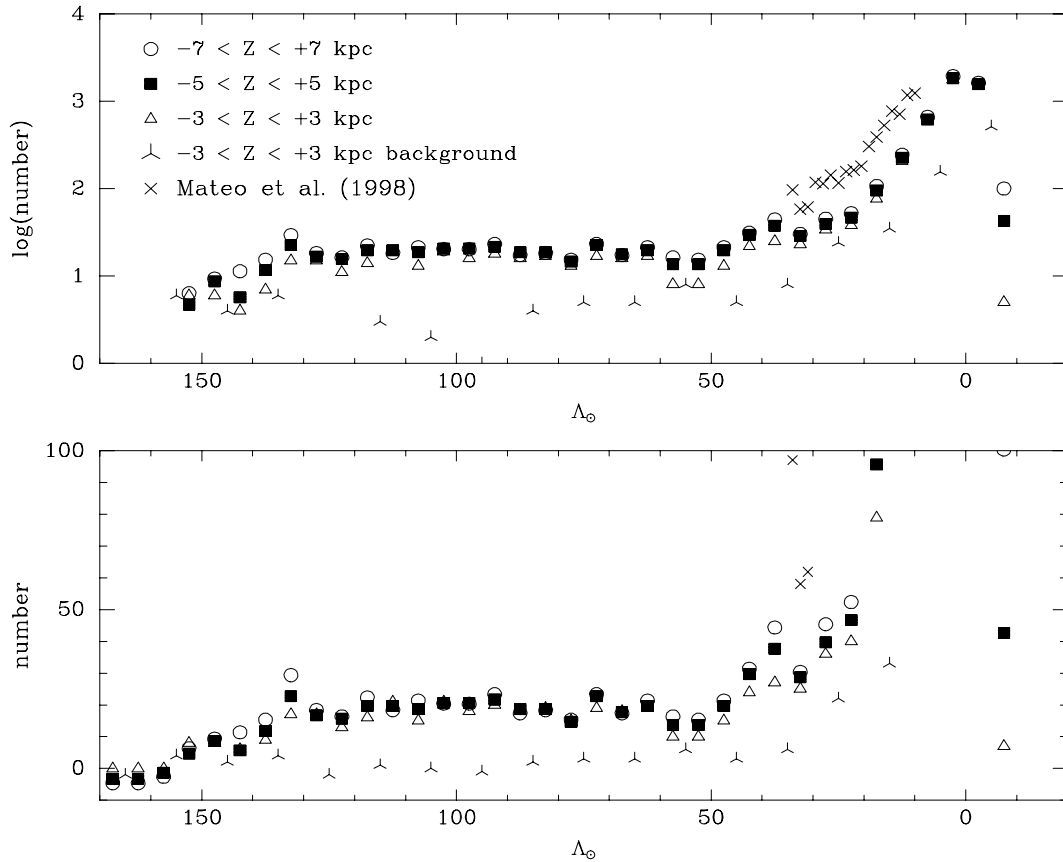
FIG. 13.—Background-subtracted counts (per $5°$ of longitude) of $0.95 \leq (J-K_s)_0 \leq 1.10$, trailing tail M giants as a function of longitude $\Lambda_\odot$. The open circles, filled squares, and open triangles show counts for different allowed ranges of distance, $Z = Z_{Sgr,GC}$, from the best-fitting Sgr midplane, whereas the three-pointed star shows counts in a $Z = \pm 3$ kpc range of distance from a " background " plane (see § 6.5). To improve statistics, the background points are shown for $10°$ longitude bins, rather than the $5°$ bins shown for the Sgr tail data.

$45° \lesssim \Lambda \lesssim \sim 140°$. Generally, the relative density variation along the Sgr tail is steadier than is observed (Odenkirchen et al. 2003) in the case of the tidal tails of Pal 5. The relatively steady Sgr tidal tail density suggests a more or less constant mass-loss rate for the timescale represented by this portion of the tail.

Nevertheless, some small variations in density do appear in Figures 12 and 13. The density decline at large $\Lambda_\odot$ is in part due to reddening and Galactic latitude limitations (note that the Galactic anticenter is near $\Lambda_\odot = 166°$). Figures 12 and 13 hint at a slightly higher density of M giants some $25°$–$50°$ in longitude downstream from the Sgr center. A smaller, less significant overabundance also appears at $\Lambda_\odot \sim 133°$. Figure 13 shows the more significant of these apparent overdensities as a " hump " in the tidal tail distribution for $25° < \Lambda_\odot < 50°$ (recall that the King limiting radius of Sgr along the major axis is $30°$, so this excess is distinct from the central King profile). An apparent widening in the tail at these longitudes is also suggested by Figure 12, as well as by the separation of the $z = \pm 3$ kpc points from the $z = \pm 5$ and ± 7 kpc points in Figure 13 at this longitude compared with other places along the trailing debris tail. We propose two possible explanations for the existence of this particular density feature:

1. Tidal tail caustics that correspond to the strongest phases of gravitational shocking during the orbit of the parent satellite have been seen in simulations of globular cluster disruption by Combes, Leon, & Meylan (1999). Although transient and made up of a constantly changing set of stars, these symmetric (leading and trailing) lumps are seen to persist in the cluster models for almost 1 Gyr in the Combes et al. models. For a Sgr-like system, dispersal within a few orbital times occurs because of the mixing of stars with a large range in energies and drift rates. Published Sgr orbits that approximately match our data (e.g., Fig. 3 in Ibata et al. 2001b) show Sgr to have passed through perigalacticon very recently (within ~ 0.1 Gyr), and an increased number of released stars might be expected from the associated gravitational shock (e.g., 1999b). If the " hump " in Figure 13 is related to a perigalacticon release event, then a symmetrically placed feature might be expected in the leading tail; unfortunately, this feature, if it exists, would lie close to the Galactic plane, where our data become more confused, although a larger density of stars at $-50° < \Lambda_\odot < -30°$ is not inconsistent with the data (see Fig. 12). That one major " hump " is seen in the trailing tail is more or less consistent with the dispersal timescale mentioned above. However, as discussed in § 4.3, it is possible that much more than just the hump in the tail may be associated with the last perigalacticon disruption event. A detailed assessment of the overall structure of the region where the Sgr King profile transitions into the tail and the relation of observed features to recent mass loss requires more careful

modeling, especially given the many nuances in the structural morphology of satellites that can be induced by tidal disruption (Johnston et al. 1999b; 2002a).

2. If, as is suggested by the Sgr disruption model of Ibata et al. (2001b), as well as the various pieces of evidence within the M-giant distribution discussed in § 6.4, the leading tidal arm penetrates back into the south Galactic hemisphere and crosses the trailing arm, we would expect an increased density of stars at about the longitudes where the excess density is observed. The presence of overlapping leading-arm debris could also lead to the observed widening of the apparent trailing arm at this point either through foreshortening or precessional displacement of the leading-arm material compared with the true trailing-arm stars. Radial velocities of stars in the hump should reveal a clear signal of this overlap. Early evidence from our M-giant radial velocity work suggest this may be the case (see also the discussion of overlapping Sgr tails in this part of the sky by Johnston et al. 1999b).

In Figure 13 we have shown for comparison the Sgr longitudinal profile over the range $10° < \Lambda_\odot < 34°$ obtained by Mateo et al. (1998) for main-sequence turnoff stars. The detailed shape of their profile is remarkably consistent with the 2MASS M-giant profile over the longitudinal range of overlap. However, because the main body of Sgr is canted somewhat with respect to the mean trend of the debris, and because Mateo et al. extrapolated their outer fields from the

direction of the major axis of the Sgr center, their outer fields progressively fall away from the center of the debris stream (see Figs. 12 and 7f, where the $\Lambda_\odot = 34°$ Mateo et al. point corresponds to a location about 12 kpc below the Sgr center).

6.6. *Length of, and Possible Population Variation along, the Tidal Arms*

The lengths of the Sgr tidal debris arms are of interest not only because they bear on the question of the duration of the mass-loss process but because of the issue of whether the leading tail is long enough to reach the solar neighborhood. As described earlier, uncertainty over the length of the leading tail is complicated by contamination by thick disk, bulge, and other M giants at low Galactic latitudes, and the possibility of tail overlap below the Galactic plane. It would be useful, therefore, if the length of the southern tail could serve as a guide. Section 6.2 offered evidence that the southern arc may extend to the northern hemisphere at the Galactic anticenter, but confidence in this result is limited by increased magnitude errors at large K_s, which makes selection of M giants both incomplete and more contaminated by "false positives." Figure 14 demonstrates the latter problem with planar distributions of giant star candidates binned by $(J-K_s)_0$ color.
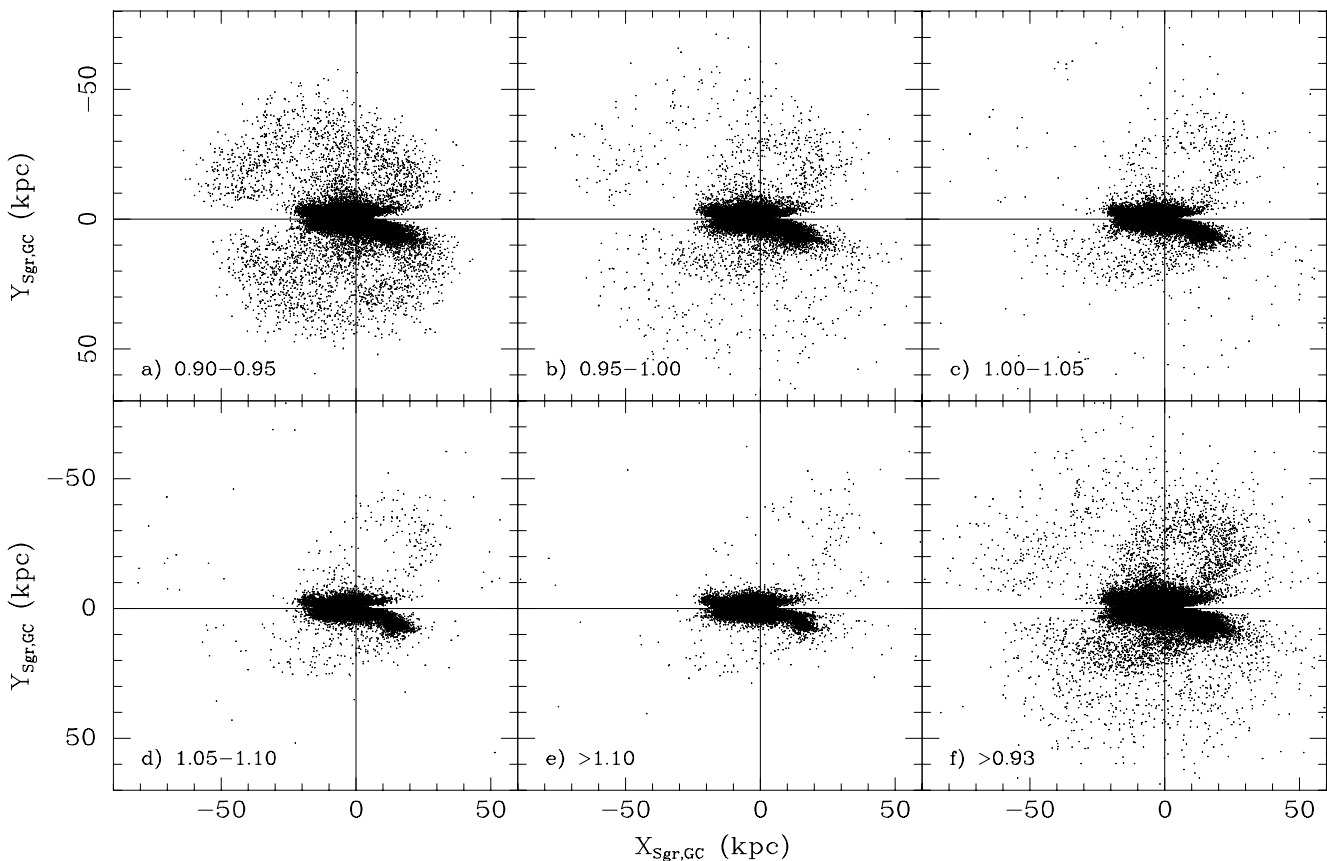

FIG. 14.—The $-7 < Z_{\mathrm{Sgr,GC}} < 7$ kpc late-type giant candidate sample shown by various $(J-K_s)_0$ color bins. All stars with $E(B-V) \geq 0.555$ have been removed from the sample. The solid lines mark the approximate location of the Galactic center. The apparent change in distances of Sgr debris features with $J-K_s$ color may reflect a change in the proportions of different age/metallicity populations among the M giants along the tidal arms compared with those in the Sgr center that were used to define the color-absolute magnitude relation for photometric parallaxes.
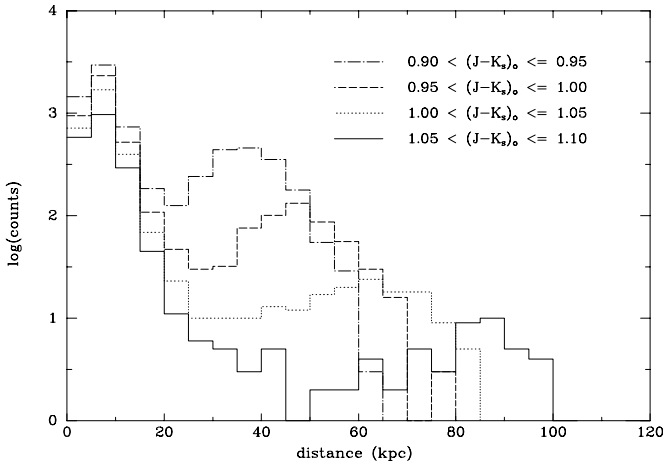
Fig. 15.—Star counts for various $(J-K_s)$ color bins as a function of radius in a wedge ($Y_{GC} > 0, Z_{GC} > 0, Z_{GC} > Y_{GC}$) more or less free of stars from Sgr and the Magellanic Clouds. All stars with $E(B-V) \geq 0.555$ have been removed from the sample.

TABLE 3
Color of the RGB Tip for Sgr Popula-
tions

Age (Gyr)	[Fe/H]	$(J-K_s)_{2MASS}$
10–11	−1.3	0.968
5....................	−0.7	1.035
0.5–3	−0.4	0.665–1.114

Notes.—RGB tip colors from Bertelli et al. 1994 with conversions from Bessell & Brett 1988 colors to 2MASS colors using transformations in Carpenter 2001.

Figure 14a shows the spatial distribution of stars in the color range $0.90 < (J-K_s)_0 \leq 0.95$, and quite evident is a "shell" of excess, presumably contaminating stars introduced at the nominal photometric distance limit (∼35 kpc) of stars of this color range. Since for the same apparent magnitude error limit redder giant candidates are projected to greater distances, we see how the shell of excess contaminants is larger in the $0.95 < (J-K_s)_0 \leq 1.00$ color bin shown in Figure 14b and expands outward with color until, for stars redder than $(J-K_s)_0 \sim 1.0$, the contaminating shell is outside the distance range shown. The distance progression of these "contamination shells" with $(J-K_s)_0$ color is illustrated in Figure 15, where we have shown star counts as a function of distance for four $(J-K_s)_0$ color bins within a cone selected to be more or less free of Sgr stars and the Magellanic Clouds—specifically $Y_{GC} > 0$, $Z_{GC} > 0$, and $Z_{GC} > Y_{GC}$, where the latter limit is used to avoid much of the Galactic disk; Figure 16 is a useful aid for orientation to

this wedge. The peak of the "contamination shell" for $0.90 < (J-K_s)_0 \leq 0.95$ is plainly visible at a distance of about 35 kpc, for example, and at 47 kpc for $0.95 < (J-K_s)_0 \leq 1.00$. Only for $(J-K_s)_0 > 1.05$ is the outer limit of the northern loop confidently free of significant contamination when viewed (as in Fig. 14) in projections of density within a slab of finite width (note that in contrast the counts shown in Fig. 15 are for a volume element increasing as the cube of the distance).

Convolved and competing with the above technical problem of determining the true length of the Sgr tidal arms is a second complication arising from stellar population considerations: M-type red giant stars occur only in metal-rich populations. While the Sgr center has ample numbers of sufficiently metal-enriched stars to explain a substantial M giant population there now, the Sgr metallicity gradient found by Alard (2001) and the clear age-metallicity relationship among the Sgr populations found by Layden & Sarajedini (2000) suggest that tidal debris that left the satellite at increasingly earlier times would be increasingly metal poor on average. Thus, one might expect a natural limit to the extent that the Sgr tidal tails *could* be traced with M giants, with that limit corresponding to the oldest possible tidal debris that can contain M giants.

In Table 3 we give the age-metallicity characteristics of the three primary Sgr populations identified by Layden &
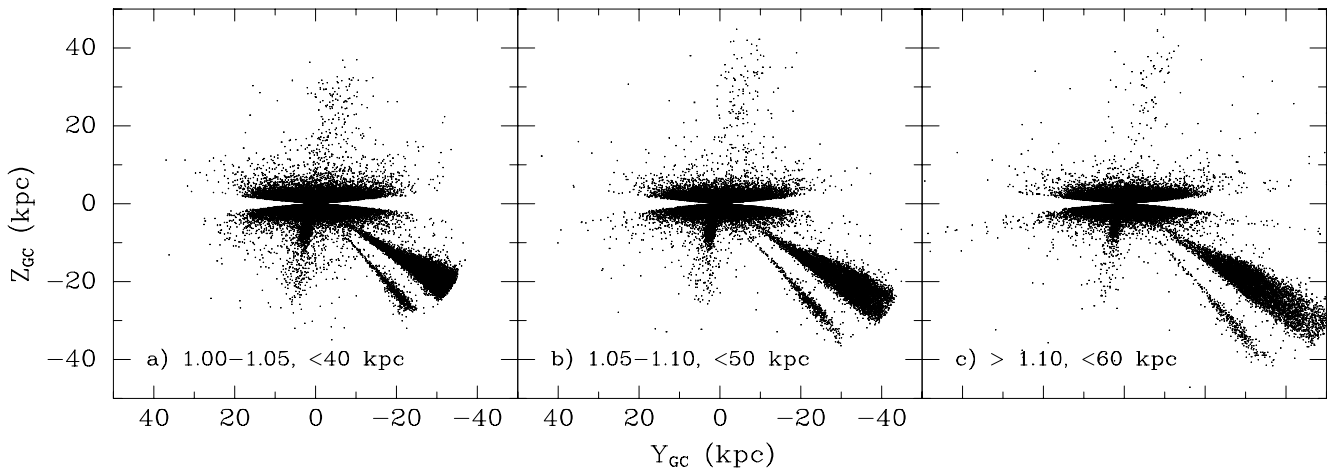

Fig. 16.—Views of the Milky Way distribution of 2MASS late-type giant candidates in projection on the Galactic YZ coordinate system. The panels show the distribution by various $(J-K_s)_0$ color bins. All stars with $E(B-V) \geq 0.555$ have been removed from the sample. In order to remove the noise of contamination at the magnitude limits of the survey, samples have been pruned of stars with photometric parallax distances more than 40, 50, and 60 kpc in the $(J-K_s)_0$ samples shown in (a), (b) and (c), respectively. Note that the top of the northern loop is slightly truncated by these distance limits. The "bowing" of the Sgr plane is due to the Galactocentric parallax effect described in § 5.2.

Sarajedini (2000). For each of these populations, we use the isochrones and other data in Bertelli et al. (1994) to determine the $(J-K_s)$ color of the RGB tip, accounting for the conversion to the 2MASS photometric system using the equations in Carpenter (2001). As may be seen, the most metal-poor population in the Sgr system is virtually invisible to the color-selected M-giant candidate sample shown in Figures 8–11 (recall the invisibility of the M54 globular cluster in Fig. 4). Thus, uncovering the distribution of these older detached giant star populations requires use of earlier giant stars, but doing so with 2MASS, as shown in Figure 14a, is complicated by the severe contamination at distances of particular interest. On the other hand, younger populations will have had less time to separate from the Sgr core. Therefore, the apparently decreasing length of both leading and trailing M-giant tidal tails as we map them with progressively cooler giant star tracers (Fig. 14) suggests *a mean stellar age/metallicity variation along the tidal tails*.[14]

The actual tidal release age of any particular part of the Sgr arms as deduced from the apparently youngest stars is an upper limit because (1) the steepness of the luminosity function means that the incidence of stars at the actual tip of the RGB is relative rare, so that any particular M giant is likely blueward of the RGB-tip color for its age/metallicity population (Table 3), and (2) presumably stars created from residual, bound gas in the core are not instantaneously released but must first somehow find themselves outside the tidal boundary (see § 4.3.4). Therefore, it is reasonable to suspect that the M-giant population explored in this paper is actually tracing only the very most recently lost stars (perhaps only the last several gigayears or so) from what may be a longer tidal interaction and net tidal arm length. Such youthful ages for the length of tails reported here are consistent with Sgr disruption models (e.g., Johnston et al. 1999b; Law et al. 2003).

Nevertheless, the highly tuned samples shown in Figures 14b–14d offer the strongest evidence that the trailing Sgr arm is at least long enough to presently lie across the Galactic plane in the northern Galactic hemisphere toward the Galactic anticenter. If so, then Sgr disruption models (e.g., Law et al. 2003) suggest that the corresponding leading arm can be long enough to reach the Galactic plane on this side of the Galactic center. Moreover, Figure 14c (in particular) offers tantalizing evidence that the *leading* Sgr arm may extend not only beyond the Galactic plane but beyond the trailing Sgr arm as well: The " spray " of stars in the lower right quadrant of the orbital plane is similar to the wrapped, leading-arm stars shown in the K6-a model of Ibata et al. 2001b (see their Fig. 3).

7. FROM SGR TO THE GALACTIC HALO

7.1. *Minimum Integrated Mass Loss Of Sgr*

The longitudinal profile in Figure 13 enables an estimate of the fractional mass of the Sgr system in its tidal arms under the assumption that the M giants provide a suitable and equitable tracer over the entire Sgr+tail system.

Presuming mass in the Sgr system to be symmetrically divided about its center (so that we only use southern hemisphere Sgr stars with $\Lambda > 0$ in our calculations), we find that the tails, defined as those Sgr stars lying outside the King profile (§ 4, Table 1), contain about 15% the number of stars within the King profile. This estimate is derived from the counts for stars within the $|Z_{Sgr,\odot}| = 5$ kpc slab in Figure 13.

Johnston et al. (1999b, 1999c) have given a formalism for calculating the mass-loss rate in a dwarf satellite based on a measured profile such as that shown in Figures 5 and 13. Using their formula (18), an orbital period of the Sgr system of 0.7 Gyr, and only the clearly visible tail from the King profile to $\Lambda_{\odot} = 155°$, we obtain a mass-loss rate for Sgr that is 17% of the mass interior to the King limiting radius per gigayear. A slightly different formulation by Johnston et al. (2002a) yields a mass-loss rate about 40% smaller. These order-of-magnitude estimates are consistent with the above empirically determined M-giant mass fraction in the Sgr tails if those tails correspond to mass lost over the last about 1.5–2 orbits; this is indeed the timescale suggested by matching tails reproduced by Sgr disruption models (e.g., Law et al. 2003).

As discussed above, because M giants trace only recently formed tidal debris, they permit only estimates of a *lower limit* to the net stellar mass lost by Sgr and the fractional contribution of Sgr debris to the Milky Way halo. Moreover, in this discussion we have ignored the issue of whether a sizeable fraction of the stars within the Sgr King profile represent stars that have become unbound in the most recent perigalacticon passage along the lines of the scenario envisaged in § 4.3.3. Thus, the mass-loss limit estimated above pertains primarily to stars detached prior to the recent perigalacticon.

7.2. *Sagittarius Stellar Contribution to the Milky Way Halo*

Figure 16 shows the distribution of 2MASS late-type giants projected onto the Galactic Y-Z plane. In this orientation, we see the Sgr orbital plane almost " edge-on " as the vertical spike spanning both hemispheres, as in Figure 7a. The panels illustrate the same color ranges as Figure 14c–14e; however, unlike the latter figures, in which the sample has been limited to stars in a 14 kpc–wide slab centered on the Sgr plane, Figure 16 shows the entire 2MASS sample, except for stars more reddened than $E(B-V) = 0.555$. In addition, to avoid substantial noise from projection of the faint magnitude " contamination shells " (§ 6.6), it is necessary to remove all sources with estimated photometric parallax distances larger than 40, 50, and 60 kpc, respectively, in Figures 16a, 16b, and 16c. These distance limits effectively remove the bulk of the faint-end contaminants (see Fig. 15), at the expense of slightly truncating the most distant parts of the northern loop. Figure 16 illustrates that, apart from the Magellanic Clouds, which are the sources of the large " finger of God " features[15] in the lower right of each panel, unbound Sgr debris appears to be the predominant source of late-type giant stars in the Milky Way halo.

---

[14] A tendency for the tidal arms to appear more tightly wrapped for bluer colors may further hint at a shift in the mean color-magnitude relation for M giants in the tails compared with the color-magnitude relations adopted from the Sgr center, in the sense that the tails contain more metal-poor (brighter) M giants than the center of Sgr.

[15] That the Magellanic Clouds are seen as " finger of God " spikes in Fig. 16 is attributable to the fact that the color–absolute magnitude relation that we have adopted is specifically tuned to the most metal-rich Sgr population, and is not necessarily a good description of the various Magellanic populations.

On the basis of the data in Figure 16 and assessing only the northern Galactic hemisphere to avoid the complication of the Magellenic Clouds, we estimate that Sgr debris represents more than about 75% of the high halo ($Z_{GC} > 13$ kpc) in the color ranges shown. The estimate rises to 80% or more if the high halo is defined by $Z_{GC} > 20$ kpc. These estimates are based on assuming that all stars within 5 kpc or so of the Sgr plane are indeed Sgr debris and so will be overestimated to the degree that there are nonrelated halo stars in that volume; however, based on the apparent mean density of stars away from that plane, this should be a minor effect (except in the case of chance coincidence of other M-giant substructure near the Sgr plane).[16] Of course, these calculations do not (1) include Sgr debris stars lopped off the top of the northern loop by the distance limits (which would increase the fractional Sgr contribution), (2) account for any residual contamination of the halo by false positives introduced by photometric errors, or (3) account for any possible increases in the number of M giants at larger radii than the limits shown or at Galactic latitudes lower that those analyzed. In addition, (4) our criterion for selecting M giants was guided specifically by the location of *Sgr*-type M giants in the NIR two-color diagram, although age-metallicity effects in the relevant parts of the two-color diagram are minor for these types of stars. Despite these minor uncertainties, that Sgr debris is the major contributor of the high-latitude halo M-giant population to 60 kpc seems a reasonable conclusion.

The dominance of Sgr in creating the Galactic halo M-giant population is reflected in the great circle cell counts analysis discussed in § 5. However, our results differ somewhat from those of Ibata et al. (2002a), whose analysis of the 2MASS early release data led them to conclude that Sgr debris represented only about 5% of the halo M-giant population. Although the two analyses use different selection criteria to isolate M-giant stars, we are uncertain exactly why they arrive at such substantially different limits on the M-giant contribution to the halo. It may be that the exclusion of disk giants based on a Galactic latitude limit, as done by Ibata et al., is not as restrictive as our Z_{GC} criterion, but a more likely contributor to the difference is our elimination of the excess background by the "contamination shell" (§ 6.6) in both the Cartesian and the GC3 analysis presented in § 5.

However, we are in agreement with Ibata et al. (2002a) that, apart from the presumably bound population of red stars in the Magellanic Cloud represented by the finger of God spikes, it would appear that the Clouds have *not* been a major contributor to the halo M-giant population.

These results pertain only to Sgr contribution to the halo of the latest type giant stars and say nothing about the net mass contributed to the halo, either in the form of dark matter or in stars of all spectral types. However, along these lines, we find interesting the result of Vivas et al. (2001; discussed below), in which almost every one of the RR Lyraes they find along the line of sight to the apogalacticon of the northern loop could conceivably be a part of Sgr tidal debris, possibly including even the nearby RR Lyraes, depending on the disposition of the Sgr debris near the Sun. In any case, that Vivas et al. find a "hole" in their RR Lyrae counts precisely at the distance of the interior of the northern loop is dramatic and suggests that even for such old stars

---

[16] The § 6.5 analysis of mean contamination in the general volume around the trailing tail found about a 10% effect.

Sgr may be a dominant contributor to at least the outer (>25 kpc) halo.

8. COMPARISON TO PREVIOUS SGR SEARCHES AND POTENTIAL IDENTIFICATIONS

Dinescu et al. (2002) have summarized the various searches for extended Sgr debris to date; their Figure 4 gives a representation of the placement of various detections and nondetections on the celestial sphere, along with a great circle for the Ibata et al. (1997) Sgr orbit, which reasonably approximates that which we have found here. Given our new understanding of the three-dimensional position of Sgr debris, it is worth reviewing the previous detections of Sgr debris in more detail here, and, in particular, taking into account the *distances* of the stars that constitute the various detections. A comparison with other surveys is especially useful (1) as a check on distance scales from the disparate tracers that have been used, (2) because we are now able to place almost all previous detections into a unified context, and (3) because comparisons with surveys of other Sgr tracers provide new insights into the Sgr disruption and debris trails. Figure 17, which repeats the M-giant distribution of Figure 10, provides our summary comparison of the detections by Sgr longitude and distance. Figure 17 includes only detections of extratidal Sgr material and excludes the numerous studies near the Sgr center.

8.1. *Connecting to the Sloan and QUEST Detections*

Perhaps the most striking visual impression of extended Sgr (and other potential) tidal debris in the halo has been that afforded by the SDSS. In several studies analyzing data from the first Sloan observations in a strip along the celestial equator, the presence of Sgr's extended tidal arms have made themselves known (e.g., Fig. 18a). Figure 18b shows a slice through the 2MASS M giants along the celestial equator, which mimics the region of the sky surveyed by the Sloan survey on the equator. While the latter survey covers a roughly 2°.5 wide strip along the equator, we opened the declination range of our comparison image to $-10° < \delta < +10°$ to increase the density of plotted points for our lower density population of M giants.

The first published results from Yanny et al. (2000), while only in two limited-angle wedges of the equatorial stripe, nevertheless showed excess star counts of A-type stars in several regions that can now be firmly identified with parts of the southern arc at $\Lambda_\odot \sim 104°$ and the far side of the northern loop at $\Lambda_\odot \sim 295°$. The heliocentric distances Yanny et al. (2000) infer for their two structures are 28 and 48 kpc, respectively. These distances generally agree with our results (Fig. 17). Although they do not comment on it, the Yanny et al. data also show an excess of stars less than 20 kpc away in the same direction of the sky (see, e.g., their Figs. 18 and 19), consistent with our finding of *closer* M-giant candidates at the same longitudes ($\Lambda_\odot \sim 295°$). Because of uncertainty over the mean distance of this nearby Yanny et al. clump, it is not represented in Figure 17.

A similar detection of two density enhancements toward the northern loop has been discovered in the study of RR Lyraes discovered in the Sloan equatorial strip by Ivezić et al. (2000), as well as in the QUEST RR Lyrae Survey (Vivas et al. 2001), which explores nearly the same region of
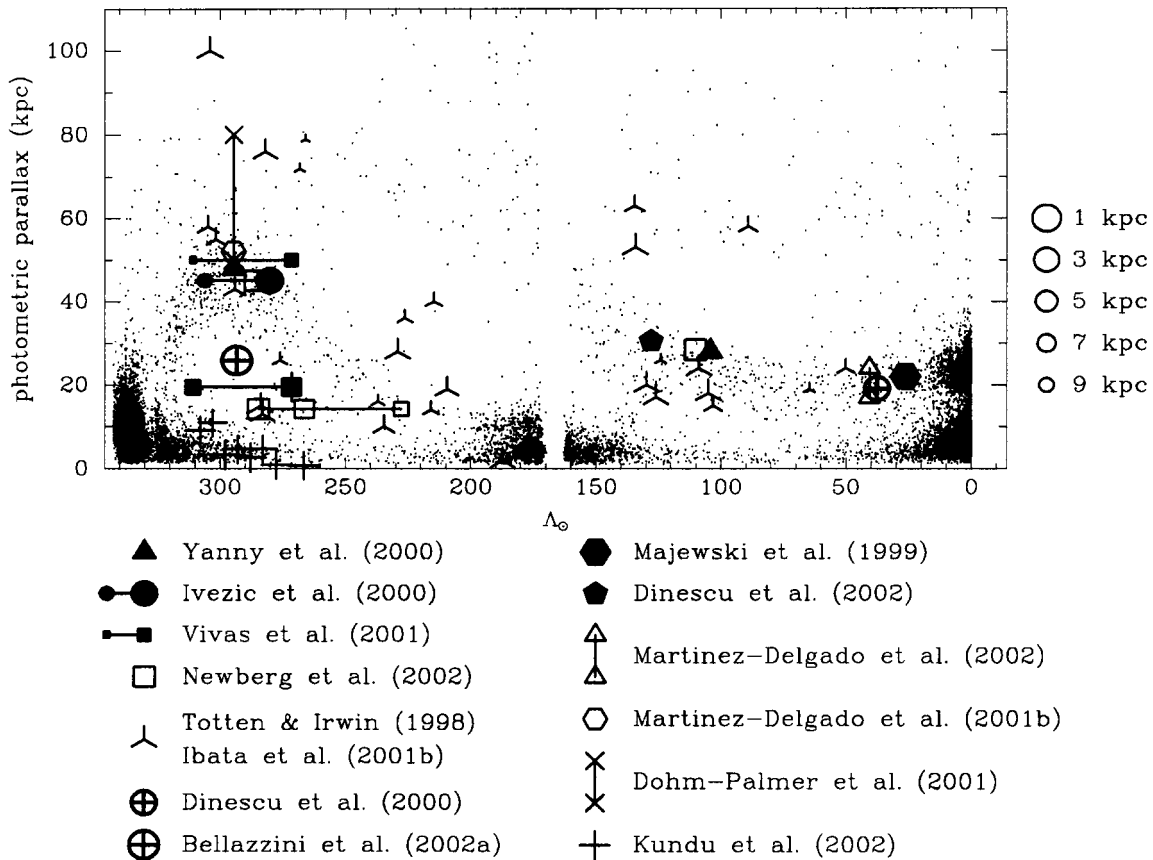
FIG. 17.—Summary of previous claims or suggestions of Sgr debris detections. Only detections near or outside the King limiting radius are shown. Filled symbols are used for detections based on horizontal branch stars. Open symbols denote detections making use of main-sequence stars. Crosslike symbols are detections based on red giant branch or asymptotic giant branch (i.e., carbon) stars. The clusters Pal 12 (Dinescu et al. 2000) and NGC 5634 (Bellazzini et al. 2002a) are shown by circled plus signs. In some cases the papers cited give either a range of distance, an uncertainty of distance, or a range of longitude for their Sgr detections. These ranges are indicated by solid lines connecting points. In each case, the symbols are sized to indicate relative proximity of the detection, at the cited distance, to the Λ_{GC} Sgr midplane (an approximate size scale is shown in the legend to the right). In the case when ranges of values are shown, the endpoint sizes correspond to the relative $Z_{Sgr,GC}$ distance at that point. The Martínez-Delgado et al. (2002) and Dinescu et al. (2000) symbols have both been shifted by 1° of longitude away from each other for clarity. To reproduce the Ibata et al. (2001b) carbon star sample, only Totten & Irwin (1998) carbon stars with $11 < R < 17$ and having radial velocities are used, and this sample is trimmed to only stars within 12 kpc of the Sgr plane. Obviously dusty carbon stars for which only an upper limit to distance has been given by Totten & Irwin (1998) have been left out.

sky ($13 < \alpha < 16$ hr). Both surveys comment primarily on an excess of RR Lyrae stars at 45 and 50 kpc, respectively, a feature that we can now confidently associate with the same expanse of the Sgr northern loop identified by the Newberg et al. (2002) and Martínez-Delgado et al. (2001b) surveys, and shown in the upper right quadrant of Figure 11. The distances of these more distant RR Lyraes are also in reasonably good agreement with the M-giant distribution presented here ($\Lambda_\odot \sim 270°$–$310°$, Fig. 17).

As with Yanny et al.'s A stars, both Ivezić et al. and Vivas et al. also have in their distance distribution of RR Lyrae stars a large number at distances that correspond to the less than 20 kpc M-giant candidates seen at $\Lambda \sim 295°$ in Figure 17. Figure 4 of Vivas et al. and especially the middle panel of Ivezić et al.'s (2000) Figure 8 are very similar in appearance to the distribution of stars one would obtain along the same line of sight in our Figure 11. Vivas et al. find that from 16–23 kpc there is a bona fide excess of stars over an R_{GC}^{-3} law, but they attribute the majority of this excess to be likely bound and unbound RR Lyrae stars from the tidally disrupted Pal 5 system, while Ivezić et al. apparently do not find an excess over a -2.7 power law. Clearly radial velocity data are needed to determine whether any of the less than 20

kpc M giants and RR Lyrae may be related to Sgr or other tidal debris interior to the solar circle (e.g., wrapped up leading-arm material as described in Johnston et al. [1999a] and Kundu et al. [1999]), or whether they are all part of the Galactic bulge, intermediate Population II/thick disk and/or inner halo.

Interior to their $\sim$45–50 kpc clumps, both RR Lyrae surveys also show a prominent "hole" in their distribution that appears to correspond to the interior of the northern loop. This is an interesting result, because Sgr disruption models (e.g., Ibata et al. 2001b; Law et al. 2003) predict that trailing-arm debris, if extended beyond the length limit revealed by M giants here, should eventually reach and cross through the northern loop hole. Indeed, the cluster NGC 5364, which lies right in the middle of the northern loop hole (see Fig. 17), is consistent with the position and velocity of such extended, wrapped Sgr trailing debris (Bellazzini et al. 2002a, 2003). If NGC 5634 is Sgr debris, one might expect to see a population of Sgr RR Lyraes along with it. Further work is needed to clarify this dilemma.

Our analysis (§ 7.2) for the fractional contribution of Sgr *M giants* to the halo pertains to a stellar species expected
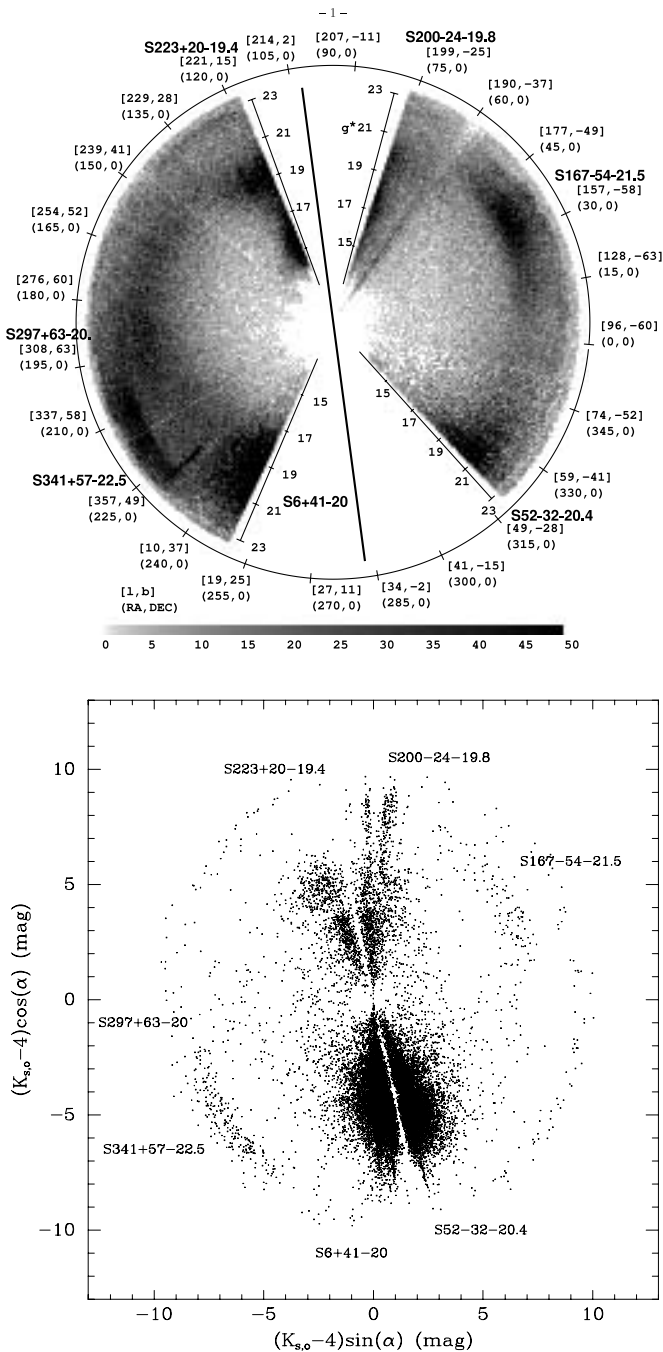
FIG. 18.—*Top:* Main-sequence turnoff stars from the SDS S equatorial slice by Newberg et al. (2002), reprinted by permission of Heidi Newberg. *Bottom:* Celestial equator slice of the 2MASS M giants for comparison to the SDSS (Newberg et al. 2002, Fig. 1). All stars in the M-giant sample within $10°$ of the celestial equator and having $1.00 < (J - K_s)_0 < 1.10$ are used in this rendition. We exclude stars with $|b| < 5°$. The azimuthal directions of features identified by Newberg et al. (2002) are indicated. Two spikes appearing at the very top of the figure are from inexact dereddening at this low latitude.

only for relatively metal-rich ($[Fe/H] \gtrsim -1$) populations— and it is not altogether too remarkable that the relatively minor fraction of halo stars that are that metal-rich could have come from a very small number of contributors like Sgr. However, the overall distribution of *RR Lyrae stars* in this part of the sky, including the contrast of near and far

clumps and the intervening hole, appears to match closely the distribution of the M giants. The RR Lyrae data suggests that the dominance of younger, more metal-rich populations traced by Sgr M giants in the halo extends to older, more metal-poor populations (at least for the outer halo and in this one direction of the sky).

The most extensive use of the SDSS for stream detections is that presented for presumed main-sequence turnoff stars in a nearly complete equatorial stripe by Newberg et al. (2002). Figure 18a here is a reproduction of their Figure 1; we include on Figure 18b the azimuthal locations of features pointed out and discussed by Newberg et al. It is clear that the strong Newberg et al. feature S167−54−21.5 is indeed the southern arc tidal arm of Sgr, and their feature S341+57−22.5 is the far side of the northern loop (as suggested by their own discussion of these features); the Sgr longitudes of these features are (see Fig. 10) $\Lambda_\odot \sim 110°$ and $\sim 286°$, respectively. But we can also make the connection of the more diffuse clumping S297+63−20.0, which Newberg et al. attribute tentatively as "a stream or other diffuse concentration of stars in the halo," as well as a lot of the similar-magnitude fluff contiguously connected to this feature from $\alpha \sim 150°$ to $\alpha \sim 210°$, to M giants tens of kiloparsecs above the Galactic plane that are in the heart of the descending, foreshortened northern loop near $\Lambda_\odot = 265°$ and stretching more generally from $\Lambda_\odot \sim 230°$ to $\Lambda_\odot \sim 285°$ (see Fig. 17). The consistency with the M-giant debris here is noteworthy, and the wide spread of the S297+63−20.0 feature elicits further interest into the question of precisely where the northern loop crosses the Galactic plane near the Sun.

Newberg et al. draw attention to several other features located at the low-$|b|$ edges of their survey wedges. For example their feature S223+20−19.4 is discussed in the context of a possible "newly discovered dwarf galaxy in the Galactic plane" at a distance of about 11 kpc, but they also admit the possibility that it is a metal-weak, disklike structure with large-scale height and scale length. Ibata et al. (2003) have suggested the possibility that the Sloan detection may be a perturbation of the disk, possibly the result of ancient warps. To aid interpretation of this feature, Helmi et al. (2003) discuss models of both old, shell-like and younger, more coherent tidal features. Yanny et al. (2003) have shown that the feature is likely to be a disrupted galaxy, based partly on the low-velocity dispersion of stars within it. Figure 18 gives the appearance of a distinct structure at the same position and at a corresponding distance modulus ($m - M \sim 15$) if we assume these are M-giant stars. This structure appears to span both sides of our zone of avoidance (although predominantly situated north of the Galactic plane in this slice through the Galaxy), with an overdensity of stars that also corresponds more or less to the Newberg et al. S200−24−19.8 structure.[17] This feature shows up in Figure 10 as the ~ 8–15 kpc distant, oblong-shaped feature spanning $\Lambda_\odot \sim 150°$–$200°$ in the top panel and the $R_{GC} \sim 12$–22 kpc feature spanning $\Lambda_{GC} \sim 140°$–$180°$ in the bottom panel. It is unlikely that the 2MASS feature is from improper dereddening, since the S223+20 structure extends to reasonably high latitudes ($b > 20°$). Figures 10 and 18 supports the reality of the

---

[17] The apparent overdensity in the 2MASS M-giant sample corresponding to the S200−24−19.8 structure shows more clearly when bluer M giants are included in the analysis.

Sloan find, and in two contributions (Rocha-Pinto et al. 2003; Crane et al. 2003) this 2MASS feature is explored further, with the conclusion that it is a new tidal tail system unrelated, but analogous, to that of the Sgr dwarf.

8.2. *Other Searches for Distant Sgr Debris*

The M-giant results have already been compared with those of Mateo et al. (1998) in Figure 13 and § 6.5. Near the Mateo et al. strip of fields, and slightly closer to the center of the Sgr tidal debris stream, is the possible detection of Sgr red clump stars in the ASA 184 field ($[l, b] = [11°, -40°]$) by Majewski et al. (1999a). The distance modulus with reddening of these stars at $\Lambda_\odot \sim 26°$ is projected to be $(m - M - A)_V = 16.8$, which is 22 kpc assuming $A_V = 0.15$; this distance is in agreement with the M-giant distribution in Figure 10. Majewski et al.'s nondetections in the other three fields they studied—SA 184, SA 107, and ASA 107—can be understood by comparison with the Sgr debris streams as delineated by M giants: SA 184 and SA 107 are off the Sgr orbital plane (these fields were used as control fields for ASA 184 and ASA 107 by Majewski et al.). The fourth field they studied, ASA 107, however, *does* lie $[(l, b) = (353°, +41°)]$ in the thick of the northern loop at $\Lambda_\odot = 300°$ (which is why it was originally selected for study). Unfortunately, the mean distance of the loop at this point, i.e., ~45 kpc, translates to an expected red clump magnitude of $V \sim 19.5$, which was just beyond the limit of their study.[18] This point has been made previously by Martínez-Delgado et al. (2003).

Another Kapteyn selected area previously suspected to contain Sgr debris is SA 71 $[(l, b) = (167°, -35°)]$. Dinescu et al. (2002) report an excess of $B-V \leq 1.1$ stars for $18 < V < 20$, and most prominently in the range $18 < V < 19$. These stars also appear to have distinct proper motions consistent with the Sgr orbit. SA 71 lies near the main Sgr debris stream toward the Galactic anticenter ($\Lambda_\odot \sim 128°$), where the M giants are centered at about 28 kpc distance. By assuming that their excess population corresponds to the Sgr horizontal branch/red clump, Dinescu et al. derive a distance for their potential Sgr debris of 29–32 kpc, in good agreement with the M giants. Dinescu et al. explore three other selected areas—SA 29, SA 45, and SA 118—and find no similar Sgr-like detection. As these authors point out, SA 29 and SA 45 are considerably off the primary Sgr orbit. However, in their Figure 3 the field SA 118 is shown to be nearly similarly displaced from the Ibata et al. (1997) Sgr orbit as SA 71. Our ability to pinpoint more precisely the path of the Sgr debris allows us to determine that, in fact, SA 71 is much closer to the primary debris great circle than is SA 118; this could explain their Sgr debris nondetection in SA 118.

Martínez-Delgado et al. (2002) have identified potential main-sequence Sgr stars in deep BR imaging near the globular cluster Pal 12, previously identified by Dinescu et al. (2000) as a likely Sgr globular cluster. Martínez-Delgado et al. estimate the distance of these stars as 17–24 kpc, depending on assumptions about the expected absolute magnitudes of the stars. At this longitude ($\Lambda_\odot \sim 40°$), we find the mean M-giant distance to be about 19 kpc, which is also the same distance as Pal 12, and this is consistent with the Martínez-Delgado results. In a similar, deep CMD search in a field in the SDSS equatorial strip, Martínez-Delgado et al. (2001b) also find a signal that they tentatively associate with horthern hemisphere Sgr dwarf material. The distance to the feature, which they propose is "the Sagittarius stream or traces of a new nearby dwarf galaxy," is 51 ± 12 kpc ($R_{GC} = 46 \pm 12$ kpc). Their identified stellar population indeed corresponds to the distant part of the northern loop at $\Lambda_\odot = 295°$ and is only slightly farther than other detections in this part of the sky, including our own. The lack of detection of the near side of the northern loop by both Majewski et al. (1999a) and Martínez-Delgado et al. (2001b) relates to the bright-end magnitude limits in both surveys.

Finally, two searches for giant stars have recently published possible detections of Sgr debris in the northern hemisphere. Dohm-Palmer et al. (2001) have found four giant stars with similar velocities and distance in fields near the Sgr midplane near $\Lambda \sim 295°$. At least some of these stars, at a typical distance of 50 kpc and a moderate positive velocity, are a plausible Sgr northern loop detection consistent with the M-giant distribution. Finally, Kundu et al. (2002) have found a position-velocity sequence of eight giant stars with unusually large negative velocities as part of a large K-giant survey. These stars lie very near the Sgr midplane and may correspond to the very near side of the northern loop (see Fig. 17).

We may summarize the comparisons discussed to this point as almost uniform in agreement with regard to both the locations of Sgr debris in position on the sky *and* with respect to distance (despite the disparate methods for identifying and gauging the Sgr debris).

8.3. *Carbon Stars*

Carbon stars have also been associated with the Sgr plane. The large-area APM Survey (Totten & Irwin 1988) revealed dozens of carbons stars having positions and radial velocities consistent with the Sgr tidal tails and which Ibata et al. (2001a, 2001b) used to define a Sgr orbital plane and a debris model that generally resembles the distributions of 2MASS M giants. However, the carbon star luminosities adopted in these studies yield photometric parallax distances that are, on average, ~35% larger than the M-giant distance scale (which has been shown to agree with numerous other studies; Fig. 17), even when very dusty N-type stars are ignored.[19]

Calibration of the carbon star distance scale has been historically complex, being complicated by variability, obscuring dust shells and metallicity effects. While Totten, Irwin, & Whitelock (2000) have demonstrated good agreement between infrared, JK-based distance estimates and an assumed R-band carbon star absolute magnitude of $M_R = -3.5$, Demers, Dallaire, & Battinelli (2002) have noted a metallicity trend whereby the $[Fe/H] = -1.4$

---

[18] Interestingly, there is an excess of stars at this magnitude visible in the Fig. 4 of Majewski et al. (1999a), but the excess was deemed as not statistically significant by those authors.

[19] The assertion of an overestimated distance scale assumes that the carbon stars near the Sgr plane shown in Fig. 17 are predominantly Sgr debris. Totten & Irwin (1998) have mentioned that CH-type carbon stars "are likely to be somewhat fainter intrinsically than N-type stars and hence closer than estimated..."
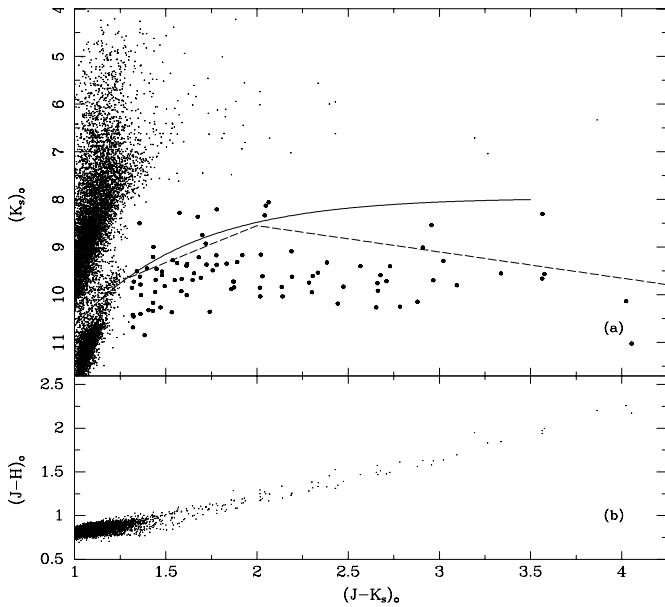
FIG. 19.—CMD of stars within 5° of the Sgr center (Table 1) and highlighting the carbon star population. The solid line is the mean carbon star color-magnitude relation from Totten et al. (2000) derived as a fit to the NIR photometry of a sample of carbon stars from Milky Way satellite galaxies, converted to 2MASS colors (Carpenter 2000) and shifted to the Sgr distance modulus ($m - M = 16.9$). The dashed line shows the approximate ridge line for LMC carbon stars in Weinberg & Nikolaev (2001), shifted 1.65 mag brighter to account for the distance modulus difference between Sgr and the LMC. Points used in the various fits discussed in the text are marked with larger points. Stars in this plot also obey the following dereddened color criteria: $(J-H) > 0.40(J-K_s) + 0.25$ and $(J-H) < 0.561(J-K_s) + 0.36$.

carbon stars in Fornax are 0.25 mag fainter in K_s absolute magnitude than $[Fe/H] \sim -0.5$ LMC carbon stars.[20]

The 2MASS database makes possible a new attempt to calibrate the Sgr carbon star color-magnitude relation and apply it to self-consistent photometry of presumed carbon stars in the Sgr tidal tails. Figure 19 highlights 95 extreme-colored ($[J-K_s]_0 > 1.3$) stars within 5° of the Sgr center that lie in a well-defined carbon star locus extending from the Sgr red and asymptotic giant branches. Stars with $(K_s)_0 < 8$ are most likely foreground carbon stars associated with the Galactic bulge. Although it contains several times more carbon stars, this Sgr carbon star sequence is consistent with the Sgr carbon star locus of Whitelock et al. (1999). However, both the present and the Whitelock et al. sequences fall below the carbon star loci determined for Milky Way satellites (Totten et al. 2000) and the LMC (Weinberg &

Nikolaev 2001) when these loci are adjusted for the distance to the Sgr core. The mean $(K_s)_0$ of the highlighted points in Figure 19 is 9.59 ± 0.06 mag. In the color range $1.3 < (J-K_s)_0 < 2.0$, the Sgr carbon locus is 0.39 ± 0.07 mag fainter than the Weinberg & Nikolaev LMC locus, while for $(J-K_s)_0 \geq 2.0$ the Sgr locus is 0.64 ± 0.10 mag underluminous.

Even were these vagaries in the mean calibration of the absolute magnitude color relation worked out, the spatial distribution of 2MASS-selected carbon stars (Fig. 20) provides a poor estimate of Sgr morphology relative to M giants because (1) Sgr carbon stars are much less populous [30 times less numerous than $0.95 \leq (J-K_s)_0 < 1.10$ M-giant candidates in the same area of the Sgr center], (2) carbon stars have a larger intrinsic scatter in their color-magnitude relation (an rms of 0.59 mag in the Fig. 19 carbon sample compared with 0.46 mag for the Fig. 1c M giants), and (3) a substantial number of carbon stars are long period variables. 2MASS in particular provides mainly single-epoch observations of a carbon star sample that likely contain a substantial fraction of $\Delta K > 0.4$ Mira, as well as lower amplitude, variable stars (Whitelock et al. 1999).

Figure 20 shows the orbital plane distribution of Galactic carbon stars [selected as sources with $(J-K_s)_0 \geq 1.3$], with absolute magnitudes derived from (a) the Weinberg & Nikolaev (2001) loci dimmed by 0.5 mag and (b) by adopting a simple $M_{K_s} = (9.59 - 16.90) = -7.31$ for all stars.[21] Comparison of Figures 20a and 20b shows that the northern loop is actually better defined and more similar to the M-giant distribution when the constant, $M_{K_s} = -7.31$ color-absolute magnitude relation is adopted than if one were to calibrate from the color-magnitude relation derived from other Milky Way satellites. A "finger of God" effect for the Sgr center is a result of intrinsic spread in the color-magnitude relation (Fig. 19) and source variability. About five or six dozen high-latitude carbon stars lie near the Sgr plane but only loosely trace the M-giant tidal arms (compare Figs. 20 and 11).

To give some impression of the relative contribution of carbon stars to the Galactic halo from the Sgr dwarf, we show in Figure 20c the Galactic Y_{GC}-Z_{GC} distribution of all stars with $(J-K_s)_0 \geq 1.3$. This figure should be compared with the corresponding M-giant panels in Figure 16. For clarity a constraint of $(K_s)_0 < 11.75$ is imposed (without this criterion the distribution is significantly noisier, likely due to a "contamination shell" problem as found for the M giants in § 6.6). Outside the quadrant containing the Magellanic Clouds, Sgr appears to have been the predominant source of high-latitude, $R_{GC} \lesssim 75$ kpc halo field carbon stars.

8.4. Globular Clusters

It is presently known that four globular clusters with positions near the Sgr center, NGC 6715 (M54), Terzan 7, Terzan 8, and Arp 2, are associated with the dwarf galaxy: these

---

[20] Kunkel, Demers, & Irwin (1997) also find a median $R = 15.2$ mag for more than 400 carbons in the LMC periphery, which, with an LMC distance modulus of 18.55, yields an M_R closer to -3.35 for these carbon stars. Totten et al. (2000) note a "vertical scatter about the fitted (color-magnitude) curve [that] covers a range of $\sim \pm 0.5$ mag, with occasional more extreme outliers that in the main are probably caused by variable stars." Their data also reveal something of a population gradient in that the bright, blue CH-type LMC carbons of Hartwick & Cowley (1988), which have been argued (Suntzeff et al. 1993) to be a very young (0.1 Gyr) AGB population, lie well above their fit color-magnitude relation, while the more "normal" LMC carbons as well as a number of other dSph and SMC carbons create much of the vertical scatter 0.5 mag or more *fainter* than the fit. This trend echoes the Demers et al. (2002) conclusion regarding likely metallicity effects on carbon star luminosities.

[21] In contrast to previous plots presented here for M giants (e.g., those shown Fig. 14) that only included stars within a *linear* distance from the Λ_{GC} plane, Fig. 20 shows stars with *angular* ($|B_\odot| < 10°$) separations from the Sgr plane; with the larger uncertainty in the carbon star photometric parallaxes, we risk losing Sgr carbons with a linear constraint on distance from the Sgr plane.
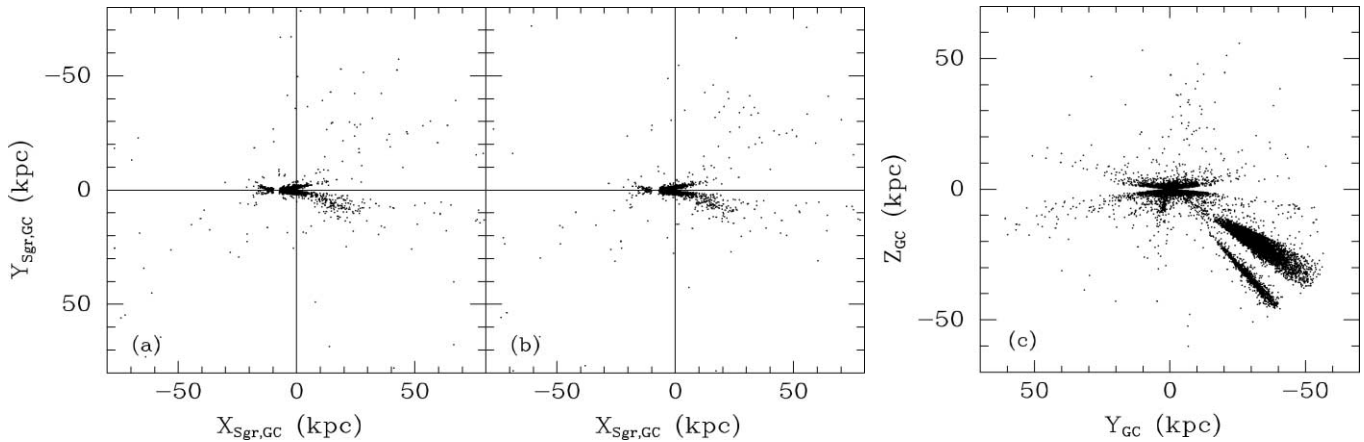
Fig. 20.—Planar distribution of all carbon star candidates within $|B| = 10°$ of the $\Lambda_\odot$ plane and having $(J-K_s)_0 \geq 1.3$. (a) Distribution after adopting the Weinberg & Nikolaev (2001) LMC color-magnitude ridge lines, adjusted to the distance modulus of Sgr and then dimmed an additional 0.5 mag. (b) Distribution after assuming all carbon stars have $M_{K_s} = -7.31$. In both panels, a large number of stars—likely contaminants—have projected photometric parallax distances beyond the bounds of the region shown. A small hole in the distribution near the Sun is from carbon stars incompleteness at the bright end of the catalog used here. (c) Nearly edge-on view of carbon star sample with distances as in (b). In this panel all carbon star candidates with $(J-K_s)_0 \geq 1.3$ are shown, but, for clarity, the sample has been limited to $(K_s)_0 < 11.75$.

globular clusters have similar distances and radial velocities to the main body of Sgr (Ibata et al. 1995). A fifth cluster that lies in the heart of the southern arc (Fig. 17), Pal 12, has been shown to have orbital characteristics that make it a reasonably good candidate for association with Sgr (Dinescu et al. 2000; see also Martínez-Delgado et al. 2002). Several studies of the Galactic globular cluster population have sought additional possible cluster members of the Sgr debris streams, with a number of additional candidates proposed (Irwin 1999; Dinescu et al. 2001; Palma et al. 2002; Bellazzini et al. 2002a, 2003). The recent analysis by Bellazzini et al. (2003), in particular, makes a strong case for several additional Sgr clusters. Because, as Bellazzini et al. (2003) have shown, precise knowledge of the Sgr orbit is of great use to sorting out interesting candidates, we defer an analysis of connections of the Sgr debris streams and globular clusters to a companion contribution containing velocity data, as well as our best-fit model to the M-giant data.

9. DENSITY OF NEARBY SGR STELLAR DEBRIS

In § 6.4 we discussed the proximity of the Sgr northern arm to the solar neighborhood. In § 6.6 we argued that the southern srm seemed to be at least 180° long, sweeping into the northern hemisphere; if so, then models of the Sgr disruption (e.g., Law et al. 2003) show that the northern loop is long enough to cross the Galactic plane on this side of the Galactic center. In Figures 14c and 14d we find evidence that the leading arm may even cross the *trailing* arm in the southern hemisphere. And in § 8 and Figure 17 we showed apparently confirmatory evidence from other surveys that Sgr debris is approaching the solar neighborhood from the NGC. How might the suggested local presence of debris from the Sgr dwarf spheroidal have impacted previous studies of the Galactic halo, many of which have been conducted with halo stars relatively near the Sun in potentially "Sgr-contaminated" regions of the Galaxy? The question turns on the relative density of leading Sgr arm debris passing through/near the solar neighborhood.

We can estimate the local density of Sgr stars by extrapolating the M-giant density just above the Galactic plane and converting that density to other spectral types (colors) via an adopted luminosity function. This is most straightforward for evolved stars, where the luminosity function can be derived directly from 2MASS observations of the Sgr center—for example, the background-subtracted Sgr CMD shown in Figure 1c. To eliminate residual, unsubtracted contamination from non-Sgr stars and isolate the Sgr RGB we apply the following criterion:

$$K_s > -7.22(J - K_s) + 17.64 . \qquad (11)$$

This selection effectively separates the Sgr RGB from the residual contributions of the Galactic bulge population several magnitudes brighter (see Fig. 1c). The resulting luminosity function so calculated is shown in Figure 21a. The Figure 1c CMD begins to "run out" beyond $(K_s)_0 = 14.3$.

The color function for evolved stars corresponding to the luminosity function is shown in Figure 21b. From the slope of the RGB, the $(K_s)_0 = 14.3$ mag limit means that the color function is complete only for RGB stars redder than $(J-K_s)_0 \sim 0.80$—roughly spectral types later than K3.

The ratios of stars of different spectral types can be computed by comparing counts by colors. Bessell & Brett (1988; see also Bessell et al. 1991) have given approximate colors for stars by spectral type and luminosity class. Obviously metallicity effects are important, but for a rough calculation the corresponding 2MASS color for the Bessell & Brett types is simplistically adopted. Accordingly, the 2MASS color of a type M0 III star is $(J-K_s)_0 \sim 0.98$ (Carpenter 2001). Table 4 presents the Figure 1c counts for evolved Sgr stars as determined by the color functions presented in Figure 21b. Roughly, for every Sgr M giant we expect three stars of type K3 III–M0 III, and more than seven K giants of any type (a substantially conservative lower limit due to the incompleteness of the early K-type giant counts because of the magnitude limit of the Fig. 1 sample).

We now extrapolate the M-giant density in the Sgr leading tidal arm to the solar neighborhood by counting the
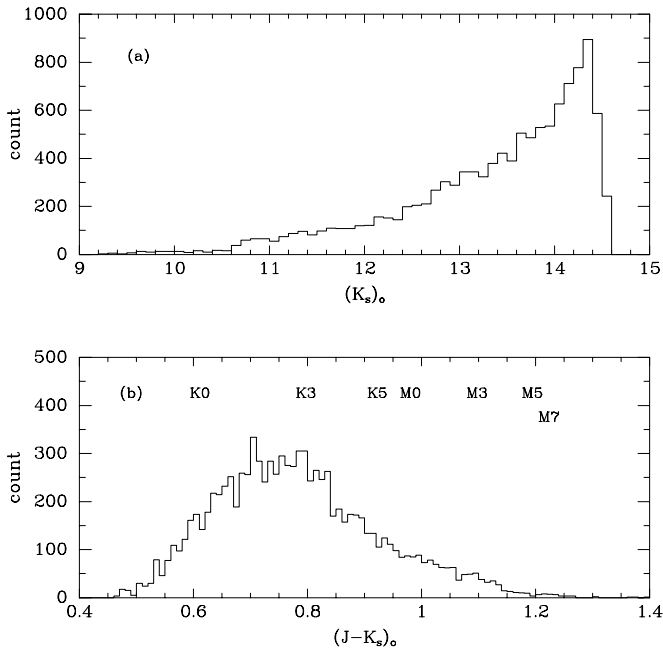
FIG. 21.—(a) Luminosity function for Sgr RGB stars shown in Fig. 1c isolated by the relation $(K_s)_0 > -7.22(J-K_s)_0 + 17.64$. (b) Color function for stars with $(K_s)_0 < 14.3$. The color function becomes incomplete for RGB stars bluer than $(J-K_s)\sim0.80$. Approximate colors (ignoring metallicity effects) for spectral types for luminosity class III objects from Bessell & Brett (1988) are indicated (converted to the 2MASS system using Carpenter 2001).

TABLE 4

RELATIVE COUNTS OF STARS IN THE SGR CENTER BY SPECTRAL TYPE AND COLOR

Spectral Type	Adopted $(J-K_s)_0$ Range	Counts
>M0 III	>0.980	1000
K3 III–M0 III	0.797–0.980	3009
K0 III–K3 III...............	0.611–0.797	>4678

NOTES.—Color definitions from Bessell & Brett 1988 translated to 2MASS system using Carpenter 2001.

number of M-giant stars $[0.98 \le (J-K_s)_0 < 1.30]$ in a 5 kpc radius cylinder centered on the Sun and whose axis is roughly perpendicular to the Galactic plane.[22] To avoid disk contamination and primarily sample the nearby Sgr leading arm, only stars with $-30 < Y_{\mathrm{Sgr,GC}} < -9$ kpc are tallied; 70 are found, which results in an M-giant density of about 0.042 kpc^{-3}. Under the assumption that all of these stars are leading-arm Sgr stars, and using Table 4, this implies a density of 0.17 kpc^{-3} for nearby Sgr giant stars of spectral type later than K3. Because the M : K giant ratio decreases with age/metallicity, and given the evidence for possible age/metallicity/giant color variations depicted in Figure 14, the above K-giant density is a lower limit.[23] This density is comparable to the density of a velocity clump of nine, mostly metal-poor ([Fe/H] < −1) red giants having *Hipparcos* proper motions and radial velocities and located within 2.5 kpc of the Sun, discussed by Helmi et al. (1999). These authors postulate that this clump, which has a velocity perpendicular to the plane consistent with that expected for nearby Sgr debris (roughly 225 km s^{-1} downward), came from a progenitor system that "probably resembled the Fornax and Sagittarius dwarf spheroidal galaxies" and that may have contributed 12% of all metal-poor halo stars outside the solar circle (a number that may be 3 times smaller according to a reanalysis by Chiba & Beers 2000). These nine stars are distributed all over the sky with no obvious

[22] The actual cylinder used is centered on $[X, Z]_{\mathrm{Sgr,GC}} = [-8.5, 0]$ kpc and parallel to the $Y_{\mathrm{Sgr,GC}}$ axis in Fig. 11.
[23] For example, Majewski et al. (2002b) stress how the *observed* age distribution of bound populations in a steadily disintegrating stellar system is more heavily weighted toward younger populations and does not accurately reflect the balance of populations to be found in tidal debris from that stellar system.

spatial structure within the 2.5 kpc radius volume, as might be expected for a large stream passing near the Sun. Together, the aforementioned properties of this clump of giant stars are enticingly consistent with Sgr leading arm debris in the solar neighborhood; however, the derived (by both Helmi et al. and Chiba & Beers) L_Z angular momentum for this clump is apparently too large, and the apogalacticon for its progenitor system is too small, compared with expectations for the nearly polar Sgr orbit that would have produced the M-giant tidal arms observed here. Both inconsistencies depend to some extent on the adopted Galactic rotation curve (mass profile) and local standard of rest velocity and should be readdressed with a Galactic model that self-consistently explains the Sgr debris stream in all directions.

The halo luminosity function is poorly constrained for giant stars. Reid & Majewski (1993; see their Fig. 5) have compiled numerous estimates of the halo luminosity function and derive a mean "globular cluster" luminosity function to represent the halo. Adopting this function for the local halo produces a density of later than K3 halo giants [assuming $M_V(\mathrm{K3\ III}) \sim 0.0$] of order 45 kpc^{-3}, a number that is about a factor of 2 higher than Morrison's (1993) estimate (taking into account the fainter absolute magnitude limit in her study) and so perhaps represents an upper limit. To the extent that the true local halo giant density is thus described, one might therefore conclude that if the Sgr leading arms is in the solar neighborhood, it contributes only of order 0.4%–0.8% of the *local* evolved halo stars and would not likely have significantly impacted studies (e.g., Yoss, Nesse, & Hartkopf 1992; Morrison et al. 1993) of nearby "halo giants." However, it may well have affected more distant halo giant samples, e.g., that by Ratnatunga & Freeman (1989) of stars in the south Galactic Pole field SA 141, a sample for which they noted a particularly small velocity dispersion and which contains stars of the approximate velocity expected for the trailing Sgr tail in this general direction. Assuming an effective vertical halo scale height of 3.5 kpc (Reid & Majewski 1993) and the local halo giant density from above, Sgr dominates the halo K-giant density by 5–6 scale heights, or 17–20 kpc above the plane—distances comparable to those probed by the SA 141 survey.

Because of some uncertainty in the actual stellar densities of the local halo population(s), it is difficult to assess accurately the relative impact of Sgr debris on studies of Galactic structure. We may, however, more directly calculate the actual number of Sgr stars contributing to a particular survey. Here we focus on the magnitude limited survey of stars at the NGP by Majewski (1992), for which a relatively complete radial velocity and proper motion analysis of stars (mainly F–K dwarfs) to $V \sim 19$ is described in Majewski et al. (1994, 1996). To estimate the number of such stars that

could have been contributed by Sgr, we integrate the 15 Gyr old (the precise age adopted has little affect on the analysis) theoretical luminosity function for a cluster with metal abundance $Z = 4 \times 10^{-3}$ by Silvestri et al. (1998); this luminosity function was found to give a good match to observationally derived RGB and main-sequence luminosity functions for the globular cluster 47 Tucanae by those authors. Taking into account the volume completeness limits of the Majewski (1992) survey as a function of (M_V), we integrate the Silvestri et al. luminosity function from the main-sequence turnoff at $M_V = 3.4$ to $M_V = 8.0$ and scale this number by the ratio of the Sgr later than K III giant density above to the integral of the luminosity function for $M_V \leq 0$ (assumed to represent the luminosity of K III giants). The result leads to an estimate that some 5–10 Sgr dwarfs should be present in the subsample of Majewski (1992) dwarfs discussed by Majewski et al. (1996). It is interesting, therefore, that the halo sample in that survey is constituted by three phase space clumps with of order this number of stars each, and two of the clumps (as well as the net average of all halo stars in the survey) show a net negative radial velocity, as expected for Sgr debris at the north Galactic pole. A more detailed assessment of the particular energy and momentum distribution of those phase space clumps in the context of Sgr models that accommodate nearby debris flow is warranted, but clearly the several recent findings of excess numbers of stars with a downward motion from the NGP—for example, from the Majewski et al. survey of dwarf stars and the Kinman, Suntzeff, & Kraft (1994; Kinman et al. 1996) studies of horizontal branch stars—offer tantalizing possibilities of earlier detections of the leading Sgr arm near the Sun.

10. EPILOGUE

The 2MASS database has been used to make the first all-sky map of the M-giant populations of the Sagittarius dwarf spheroidal galaxy system. The present discussion provides the first relatively reddening-free description and analysis of the central regions of the dwarf, as well as extensive new information on the extended tail structure of tidally stripped stars. The latter is particularly useful for placing all previous studies of the Sgr system into a well-defined context and places the most stringent constraints yet on models of the disruption of Sgr in the Galactic potential. We have concentrated on an empirical description of the Sgr system and resisted extensive interpretation via disruption model-fitting here for the following reasons: (1) The degree to which a simple *empirical* description of the 2MASS results nonetheless advances our understanding of the Sgr system is manifest. (2) Published model fitting to previously extant data (especially the works by Helmi & White 2001; Ibata et al. 2001b; Ibata & Lewis 1998 to which we have frequently referred) provide a sufficiently accurate match to the spatial distributions described here that a general sense of the Sgr orbit and destruction are in hand, while further refinements will benefit from the addition of kinematics (see Law et al. 2003). (3) A survey to obtain the velocities of stars in the extended Sgr tidal arms is underway, and first results for hundreds of M giants will be included in future contributions. A Sgr system accurately characterized both spatially and kinematically will become a powerful fiducial against which to delineate the structure and dynamics of the Milky Way and its halo.

The primary results from this paper may be summarized as follows:

1. 2MASS provides a facile means by which to explore the Sgr dwarf galaxy and its tidal tail system, because that system contains a prominent population of M-giant stars (Fig. 1) and such stars are readily identifiable using JHK_s infrared photometry (Fig. 2; § 2).

2. When an M-giant selection is applied to aperture photometry from the magnitude error-limited 2MASS point source catalog, the center of the Sgr dwarf and both its leading and trailing tidal tails are among the most prominent, high-latitude features observed in the sky (e.g., Fig. 3; § 3).

3. The central parts of the Sgr system, as traced by 2MASS M giants, exhibit a smooth distribution resembling a dwarf spheroidal galaxy, although one of high ellitpicity ($\epsilon > 0.6$) and large extent (Fig. 4, § 4). As with other dSph galaxies, radial profile fits to the center of Sgr (with the ends of the semimajor axis excised to minimize the contribution from the tidal tails) can be described by a King profile, albeit one of very large core (224′) and limiting (30°) semimajor radii (Fig. 5; Table 1; § 4.1). A power law+core (PLC) fit to the radial profile is also provided, although like the King function fit, this functional form cannot provide a good match to the radial profile transition to the tidal tails. However, by comparison with the extragalactic population of dwarf ellipticals, the extreme ellipticity of these Sgr fits in the direction of the tidal streams suggests the significant presence of sizeable tidally stripped population and implies that these functional fits do not represent the gravitationally bound dwarf.

4. Two departures of the observed radial profile (Fig. 5) from the King (and PLC) fits are the presence of a central cusp (§ 4.2.1) and a break to the tidal tails (§ 4.2.2). The approximately half-degree radius central cusp is coincident with the location of the globular cluster M54; however, because that cluster is typically characterized as an old, metal-poor system, it cannot be contributing M giants to the central excess of these stars above the flat part of the King profile. The connection between M54 and the concentration of stellar populations of a variety of ages at its location (Layden & Sarajedini 2000) is still unclear, although one hypothesis (§ 4.3.3) is that the nucleated center of Sgr may correspond to the residual bound core of a dramatically disrupting Sgr system. The outer break in the Sgr radial profile to an $\sim r^{-2}$ declining population resembles breaks seen in the outer parts of the radial profiles of other dSph galaxies and which have been interpreted as possible extratidal debris; in the case of the Sgr system this is now established definitely to be the case.

5. The integrated brightness of Sgr is found to be $V_0 = 3.63$, with the cusp adding a few more hundredths of a magnitude of light. If the distance modulus to Sgr is taken as 16.9, we find that the center of the Sgr system edges out Fornax as the brightest of the dSph galaxies, with an absolute magnitude of $M_V = -13.27$. These results appear to be consistent with the similarity of the Fornax globular cluster specific frequency to that of the Sgr progenitor (§ 4.3.2).

6. When the observed King parameters of the radial profile and the Sgr central velocity dispersion are combined in the usual King (1966) methodology, we estimate the mass of Sgr to be $5 \times 10^8 \, M_\odot$ and obtain a total $M/L_V = 25 \, M_\odot / L_\odot$ (§ 4.3.2). However, since even this mass is substantially

below that needed for a system to withstand the Galactic tidal force over scales of the observed King limiting radius, we argue (§ 4.3.3) that the true mass, tidal radius, and bound fraction of the observed central Sgr system must be substantially smaller than suggested by the King profile, and that Sgr is presently undergoing a major mass-loss event—perhaps almost complete disruption—induced by tidal shocking from the last perigalacticon passage. A much smaller radius for the bound Sgr core would help to resolve the timing problem (" M-giant conundrum ") posed by the presence of relatively recently formed stars (M giants) spread along tidal tails of comparable age (§ 4.3.4).

7. The tidal tails of the Sgr system span both Galactic hemispheres (§§ 7 and 8.3, Figs. 3 and 8–11) but show relatively little evidence for precession (Figs. 6, 7, and 13). Given the 13° tilt of the Sgr orbital plane, an almost spherical halo potential is implied (§ 5.2.2). In § 5.2 we provide fits to the debris (orbital) plane and define Sgr coordinate systems based on that plane that are useful for interpreting the Sgr tidal system. The trailing arm is followed for at least 150° from the Sgr center to the Galactic anticenter, and perhaps farther, into the north Galactic hemisphere (§ 6.2; Figs. 8–11). For a large fraction of this extent, the density of the trailing debris and its distance from the Sun are more or less constant. The leading arm makes a northern loop with mean apogalacticon ∼40 kpc (§ 6.3; Figs. 8–11) and a path that takes it to the north Galactic cap, from where it arcs back down toward the Galactic disk.

8. We find ourselves at an unusual time in Galactic history: For less than 2% of the Sun's orbit around the Galaxy are we as close to the path of the leading-arm debris as we are now. If the leading arm is long enough to reach the Galactic plane on this side of the Milky Way, we should expect to find Sgr stars in or near the solar neighborhood (§§ 6.4). The implications of this possibility for studies of the Galactic structure near the Sun are discussed in § 9; while the density of Sgr stars would be swamped by those of other stellar populations locally, Sgr would dominate the halo tens of kiloparsecs above the disk. Several previous surveys of halo stars might contain Sgr representation. Analysis of all M giants in our sample indeed reveal Sgr to be the prominent contributor of such stars to the high halo (§§ 5.1 and 7.2 and Figs. 6 and 16). A similar conclusion holds for carbon stars (§ 8.3 and Fig. 20). No evidence for extended M-giant tidal tails from the Magellanic Clouds are seen (§ 5.3).

9. The relatively constant density of the Sgr trailing arm over a great part of its extent (Figs. 12 and 13) implies a relatively constant mass-loss rate over the last several Sgr orbits, excluding the possible last major disruption event (§ 6.5). Some evidence for stellar population variations along the arms is suggested by the changing color of M giants with position (§ 6.6). It is likely that older tracer stars will map the arms to even greater length than is possible with M giants. The number of stars in the tidal arms is at least 15% that within the King limiting radius (§ 7.1).

10. Good correspondence is found between the location and distances of M-giant tidal debris and nearly all previous identifications of Sgr debris (§ 8 and Figs. 17 and 18). However, Sgr carbon stars are found to be subluminous compared with carbon stars in other Galactic satellites (§ 8.3 and Fig. 19), requiring adjustment of the previous Sgr carbon star distance scale. In any case, the carbon stars provide a much less clear picture of the Sgr system than is offered by the 2MASS M giants (Fig. 20).

REFERENCES

Alard, C. 1996, ApJ, 458, L17
———. 2001, A&A, 377, 389
Alcock, C., et al. 1997, ApJ, 474, 217
Amendt, P., & Cuddeford, P. 1994, ApJ, 435, 93
Aparicio, A., Carrera, R., & Martínez-Delgado, D. 2001, AJ, 122, 2524
Bassino, L. P., & Muzzio, J. C. 1995, Observatory, 115, 256
Bellazzini, M., Ferraro, F. R., & Buonanno, R. 1999a, MNRAS, 304, 633
———. 1999b, MNRAS, 307, 619
Bellazzini, M., Ferraro, F. R., & Ibata, R. 2002a, AJ, 124, 915
———. 2003, AJ, 125, 188
Bellazzini, M., Ferraro, F. R., Origlia, L., Pancino, E., Monaco, L., & Oliva, E. 2002b, AJ, 124, 3222
Bertelli, G., Bressan, A., Chiosi, C., Fagotto, F., & Nasi, E. 1994, A&AS, 106, 275
Bessell, M. S., & Brett, J. M. 1988, PASP, 100, 1134
Bessell, M. S., Brett, J. M., Scholz, M., & Wood, P. R. 1991, A&AS, 89, 335
Binney, J., May, A., & Ostriker, J. P. 1987, MNRAS, 226, 149
Binney, J., & Tremaine, S. 1987, Galactic Dynamics (Princeton: Princeton Univ. Press)
Bonifacio, P., Pasquini, L., Molaro, P., & Marconi, G. 1999, Ap&SS, 265, 541
Bullock, J. S., Kravtsov, A. V., & Weinberg, D. H. 2001, ApJ, 548, 33

Burkert, A. 1997, ApJ, 474, L99
Burton, W. B., & Lockman, F. J. 1999, A&A, 349, 7
Caldwell, N., Armandroff, T. E., Seitzer, P., & Da Costa, G. S. 1992, AJ, 103, 840
Carpenter, J. M. 2001, AJ, 121, 2851
Chiba, M., & Beers, T. C. 2000, AJ, 119, 2843
Cole, A. A. 2001, ApJ, 559, L17
Combes, F., Leon, S., & Meylan, G. 1999, A&A, 352, 149
Crane, J. D., Majewski, S. R., Rocha-Pinto, H. J., Frinchaboy, P. F., Skrutskie, M. F., & Law, D. R. 2003, ApJ, 594, L119
Cseresnjes, P. 2001, A&A, 375, 909
Cseresnjes, P., Alard, C., & Guibert, J. 2000, A&A, 357, 871
Da Costa, G. S., & Armandroff, T. E. 1995, AJ, 109, 2533
Da Costa, G. S., Armandroff, T. E., Caldwell, N., & Seitzer, P. 1996, AJ, 112, 2576
Demers, S., Dallaire, M., & Battinelli, P. 2002, AJ, 123, 3428
Dinescu, D. I., Majewski, S. R., Girard, T. M., & Cudworth, K. M. 2000, AJ, 120, 1892
———. 2001, AJ, 122, 1916
Dinescu, D. I., et al. 2002, ApJ, 575, L67
Dohm-Palmer, R. C., et al. 2001, ApJ, 555, L37
Dubinski, J. 1994, ApJ, 431, 617

Dubinski, J., & Carlberg, R. G. 1991, ApJ, 378, 496
Edelsohn, D. J., & Elmegreen, B. G. 1997, MNRAS, 290, 7
Eggen, O. J. Lynden-Bell, D., & Sandage, A. R. 1962, ApJ, 136, 748
Elias, J. H., Frogel, J. A., Matthews, K., & Neugebauer, G. 1982, AJ, 87, 1029
Font, A. S., Navarro, J. F., Stadel, J., & Quinn, T. 2001, ApJ, 563, L1
Freeman, K. C. 1993, in ASP Conf. Ser. 48, The Globular Cluster-Galaxy Connection, ed. G. H. Smith & J. P. Brodie (San Francisco: ASP), 608
Frenk, C. S., White, S. D. M., Davis, M., & Efstathiou, G. 1988, ApJ, 327, 507
Gilmore, G., Wyse, R. F. G., & Norris, J. E. 2002, ApJ, 574, L39
Glass, I. S. 1975, MNRAS, 171, 19P
Goldstein, H. 1980, Classical Mechanics (2d ed.; Reading: Addison-Wesley), 143
Gómez-Flechoso, M. A. 1998, Ap&SS, 263, 155
Gómez-Flechoso, M. A., Fux, R., & Martinet, L. 1999, A&A, 347, 77
Gómez-Flechoso, M. A., & Martínez-Delgado, D. 2003, ApJ, 586, L123
Harbeck, D., et al. 2001, AJ, 122, 3092
Hartwick, F. D. A., & Cowley, A. P. 1988, ApJ, 334, 135
Hayashi, E., Navarro, J. F., Taylor, J. E., Stadel, J., & Quinn, T., 2003, ApJ, 584, 541
Helmi, A., Navarro, J. F., Meza, A., Steinmetz, M., & Eke, V. R. 2003, ApJ, 592, L25
Helmi, A., & White, S. D. M. 2001, MNRAS, 323, 529
Helmi, A., White, S. D. M., de Zeeuw, P. T., & Zhao, H. 1999, Nature, 402, 53
Hurley-Keller, D., Mateo, M., & Grebel, E. K. 1999, ApJ, 523, L25
Ibata, R. A. 1999, in IAU Symp. 186, Galaxy Interactions at Low and High Redshift, ed. J. Barnes & D. B. Sanders (Dordrecht: Kluwer), 39
Ibata, R. A., Gilmore, G., & Irwin, M. J. 1994, Nature, 370, 194
———. 1995, MNRAS, 277, 781
Ibata, R., Irwin, M. J., Lewis, G. F., Ferguson, A. M. N., & Tanvir, N. 2003, MNRAS, 340, L21
Ibata, R., Irwin, M., Lewis, G. F., & Stolte, A. 2001a, ApJ, 547, L133
Ibata, R., & Lewis, G. F. 1998, ApJ, 500, 575
Ibata, R. A., Lewis, G. F., Irwin, M. J., & Cambrésy, L. 2002a, MNRAS, 332, 921
Ibata, R. A., Lewis, G. F., Irwin, M. J., & Quinn, T. 2002b, MNRAS, 332, 915
Ibata, R., Lewis, G. F., Irwin, M., Totten, E., & Quinn, T. 2001b, ApJ, 551, 294
Ibata, R. A., Wyse, R. F. G., Gilmore, G., Irwin, M. J., & Suntzeff, N. B. 1997, AJ, 113, 634
Irwin, M. 1999, in IAU Symp. 192, The Stellar Content of Local Group Galaxies, ed. P. Whitelock & R. Cannon (San Francisco: ASP), 409
Irwin, M., & Hatzidimitriou, D. 1995, MNRAS, 277, 1354
Ivezić, Ž., et al. 2000, AJ, 120, 963
Jiang, I., & Binney, J. 2000, MNRAS, 314, 468
Johnston, K. V. 1998, ApJ, 495, 297
Johnston, K. V., Choi, P. I., & Guhathakurta, P. 2002a, AJ, 124, 127
Johnston, K. V., Hernquist, L., & Bolte, M. 1996, ApJ, 465, 278
Johnston, K. V., Majewski, S. R., Siegel, M. H., Reid, I. N., & Kunkel, W. E. 1999a, AJ, 118, 1719
Johnston, K. V., Sackett, P. D., & Bullock, J. S. 2001, ApJ, 557, 137
Johnston, K. V., Sigurdsson, S., & Hernquist, L. 1999b, MNRAS, 302, 771
Johnston, K. V., Spergel, D. N., & Haydn, C. 2002b, ApJ, 570, 656
Johnston, K. V., Spergel, D. N., & Hernquist, L. 1995, ApJ, 451, 598
Johnston, K. V., Zhao, H., Spergel, D. N., & Hernquist, L. 1999c, ApJ, 512, L109
King, I. 1962, AJ, 67, 471
———. 1966, AJ, 71, 64
Kinman, T. D., Pier, J. R., Suntzeff, N. B., Harmer, D. L., Valdes, F., Hanson, R. B., Klemola, A. R., & Kraft, R. P. 1996, AJ, 111, 1164
Kinman, T. D., Suntzeff, N. B., & Kraft, R. P. 1994, AJ, 108, 1722
Klessen, R. S., & Kroupa, P. 1998, ApJ, 498, 143
Kleyna, J. T., Geller, M. J., Kenyon, S. J., Kurtz, M. J., & Thorstensen, J. R. 1998, AJ, 115, 2359
Kleyna, J., Wilkinson, M. I., Evans, N. W., Gilmore, G., & Frayn, C. 2002, MNRAS, 330, 792
Klypin, A., Kravtsov, A. V., Valenzuela, O., & Prada, F. 1999, ApJ, 522, 82
Kocevski, D. D., & Kuhn, J. R. 2000, AAS Meeting, 197, 3002
Koribalski, B., Johnston, S., & Otrupcek, R. 1994, MNRAS, 270, L43
Kroupa, P. 1997, NewA, 2, 139
Kuhn, J. R., & Miller, R. H. 1989, ApJ, 341, L41
Kuhn, J. R., Smith, H. A., & Hawley, S. L. 1996, ApJ, 469, L93
Kundu, A., et al. 2002, ApJ, 576, L125
Kunkel, W. E., Irwin, M. J., & Demers, S. 1997, A&AS, 122, 463
Law, D. R., Majewski, S. R., Johnston, K. V., & Skrutski, M. F. 2003, in ASP Conf. Ser., Satellites and Tidal Streams, ed. F. Prada, D. Martínez-Delgado, & T. Mahoney (San Francisco: ASP), in press (astro-ph/0309577)
Layden, A. C., & Sarajedini, A. 2000, AJ, 119, 1760
Lee, T. A. 1970, ApJ, 162, 217
Light, R. M. 1988, Ph.D. thesis, Yale Univ.
Lynden-Bell, D. 1982, Observatory, 102, 202
Majewski, S. R. 1992, ApJS, 78, 87

Majewski, S. R. 1993, ARA&A, 31, 575
———. 2003, in ASP Conf. Ser. Vol., New Horizons in Globular Cluster Astronomy, ed. G. Piotto, G. Meylann, S. G. Djorgovski, & M. Riello (San Francisco: ASP), 447
Majewski, S. R., Munn, J. A., & Hawley, S. L. 1994, ApJ, 427, L37
———. 1996, ApJ, 459, L73
Majewski, S. R., Ostheimer, J. C., Patterson, R. J., Kunkel, W. E., Johnston, K. V., & Geisler, D. 2000, AJ, 119, 760
Majewski, S. R., Siegel, M. H., Kunkel, W. E., Reid, I. N., Johnston, K. V., Thompson, I. B., Landolt, A. U., & Palma, C. 1999a, AJ, 118, 1709
Majewski, S. R., Siegel, M. H., Patterson, R. J., & Rood, R. T. 1999b, ApJ, 520, L33
Majewski, S. R., et al. 2002a, in The Shapes of Galaxies and their Dark Halos, ed. P. Natarajan (River Edge: World Scientific), 214
———. 2002b, in ASP Conf. Ser. Vol. 285, Modes of Star Formation and the Origin of Field Populations, ed. E. K. Grebel & W. Brandner (San Francisco: ASP), 199
Marconi, G., Buonanno, R., Castellani, M., Iannicola, G., Molaro, P., Pasquini, L., & Pulone, L. 1998, A&A, 330, 453
Martínez-Delgado, D., Alonso-García, J., Aparicio, A., & Gómez-Flechoso, M. A. 2001a, ApJ, 549, L63
Martínez-Delgado, D., Aparicio, A., Gómez-Flechoso, M. A., & Carrera, R. 2001b, ApJ, 549, L199
Martínez-Delgado, D., Gómez-Flechoso, M. A., & Aparicio, A. 2001c, in ASP Conf. Ser. 274, Observed HR Diagrams and Stellar Evolution, ed. T. Lejeune & J. Fernandes (San Francisco: ASP), 352 (M01), 468
Martínez-Delgado, D., Gómez-Flechoso, M. A., Aparicio, A., & Carrera, R. 2003, ApJ, in press (astro-ph/0308009)
Martínez-Delgado, D., Zinn, R., Carrera, R., & Gallart, C. 2002, ApJ, 573, L19
Mateo, M. L. 1998, ARA&A, 36, 435
Mateo, M., Olszewski, E. W., & Morrison, H. L. 1998, ApJ, 508, L55
Mateo, M., Udalski, A., Szymanski, M., Kaluzny, J., Kubiak, M., & Krzeminski, W. 1995, AJ, 109, 588
Mayer, L., Governato, F., Colpi, M., Moore, B., Quinn, T., Wadsley, J., Stadel, J., & Lake, G. 2001, ApJ, 559, 754
Mayer, L., Moore, B., Quinn, T., Governato, F., & Stadel, J. 2002, MNRAS, 336, 119
Merrifield, M. R. 2002, in The Shapes of Galaxies and their Dark Halos, ed. P. Natarajan (Singapore: World Scientific), 170
Moore, B., Ghigna, S., Governato, F., Lake, G., Quinn, T., Stadel, J., & Tozzi, P. 1999, ApJ, 524, L19
Morrison, H. L. 1993, AJ, 106, 578
Mould, J. R. 1976, A&A, 48, 443
Murali, C., & Dubinski, J. 1999, AJ, 118, 911
Navarro, J. F., Frenk, C. S., & White S. D. M. 1996, ApJ, 462, 563
———. 1997, ApJ, 490, 493
Newberg, H. J., et al. 2002, ApJ, 569, 245
Nikolaev, S., & Weinberg, M. D. 2000, ApJ, 542, 804
Odenkirchen, M., et al. 2001a, ApJ, 548, L165
———. 2001b, AJ, 122, 2538
———. 2003, AJ, 126, 2385
Olling, R. P. 1997, Dark Matter in Astro- and Particle Physics, ed. H. V. Klapdor-Kleingrothaus & Y. Ramachers (Singapore: World Scientific), 44
Ostheimer, J. C. 2003, Ph.D. thesis, Univ. Virginia
Palma, C., Majewski, S. R., & Johnston, K. V. 2002, ApJ, 564, 736
Palma, C., Majewski, S. R., Siegel, M. S., Patterson, R. J., Ostheimer, J. C., & Link, R. 2003, AJ, 125, 1352
Peñarrubia, J., Boily, C. M., Just, A., & Kroupa, P. 2000, Astron. Gesellschaft Abstr. Ser. 17, Abstracts of Contributed Talks and Posters presented at the Annual Scientific Meeting of the Astronomische Gesellschaft at Bremen, 50
Pryor, C. 1996, in ASP Conf. Ser. 92, Formation of the Galactic Halo . . . Inside and Out, ed. H. L. Morrison & A. Sarajedini (San Francisco: ASP), 424
Ratnatunga, K. U., & Freeman, K. C. 1989, ApJ, 339, 126
Reid, N., & Majewski, S. R. 1993, ApJ, 409, 635
Richstone, D. O., & Tremaine, S. 1986, AJ, 92, 72
Robin, A. C., Reylé, C., & Crézé, M. 2000, A&A, 359, 103
Rocha-Pinto, H. J., Majewski, S. R., Skrutskie, M. F., & Crane, J. D. 2003, ApJ, 594, L115
Rockosi, C. M., et al. 2002, AJ, 124, 349
Sackett, P. D., & Pogge, R. W. 1995, AIP Conf. Proc. 336, Dark Matter, ed. S. S. Holt & C. L. Bennett (New York: AIP), 141
Sackett, P. D., Rix, H., Jarvis, B. J., & Freeman, K. C. 1994, ApJ, 436, 629
Samurović, S., Ćirković, M. M., & Milošević-Zdjelar, V. 1999, MNRAS, 309, 63
Sarajedini, A., & Layden, A. C. 1995, AJ, 109, 1086
Schlegel, D. J., Finkbeiner, D. P., & Davis, M. 1998, ApJ, 500, 525
Searle, L., & Zinn, R. 1978, ApJ, 225, 357
Siegel, M. H., Majewski, S. R., Reid, I. N., & Thompson, I. 2002, ApJ, 578, 151
Silvestri, F., Ventura, P., D'Antona, F., & Mazzitelli, I. 1998, ApJ, 509, 192
Sparke, L. S. 2002, The Shapes of Galaxies and Their Dark Matter Halos, ed. P. Natarajan (Singapore: World Scientific), 178

Steinmetz, M., & Muller, E. 1995, MNRAS, 276, 549
Sung, E., Han, C., Ryden, B. S., Patterson, R. J., Chun, M., Kim, H., Lee, W., & Kim, D. 1998, ApJ, 505, 199
Suntzeff, N. B., Phillips, M. M., Elias, J. H., Cowley, A. P., Hartwick, F. D. A., & Bouchet, P. 1993, PASP, 105, 350
Totten, E. J., & Irwin, M. J. 1998, MNRAS, 294, 1
Totten, E. J., Irwin, M. J., & Whitelock, P. A. 2000, MNRAS, 314, 630
Trager, S. C., Djorgovski, S., & King, I. R. 1995, AJ, 109, 218
Tremaine, S. 1993, in AIP Conf. Proc. 278, Back to the Galaxy, ed. S. S. Holt & F. Verter (New York: AIP), 599
Unavane, M., Wyse, R. F. G., & Gilmore, G. 1996, MNRAS, 278, 727
van der Marel, R. P. 1991, MNRAS, 248, 515
———. 2001, AJ, 122, 1827
Velázquez, H., & White, S. D. M. 1995, MNRAS, 275, L23
Vivas, A. K., et al. 2001, ApJ, 554, L33
von Hoerner, S. 1957, ApJ, 125, 451

Walcher, J., Fried, J. W., Burkert, A., &., & Klessen, R. S. 2003, A&A, 406, 847
Warren, M. S., Quinn, P. J., Salmon, J. K., & Zurek, W. H. 1992, ApJ, 399, 405
Weinberg, M. D. 2000, ApJ, 532, 922
Weinberg, M. D., & Nikolaev, S. 2001, ApJ, 548, 712
Westfall, K. B., Ostheimer, J. C., Frinchaboy, P. M., Patterson, R. J., Majewski, S. R., & Kunkel, W. E. 2000, BAAS, 33, 718
Whitelock, P., Menzies, J., Irwin, M., & Feast, M. 1999, in IAU Symp. 192, The Stellar Content of Local Group Galaxies, ed. P. Whitelock & R. Cannon (San Francisco: ASP), 136
Yanny, B., et al. 2000, ApJ, 540, 825
———. 2003, ApJ, 588, 824 (Y03)
Yoss, K. M., Neese, C. L., & Hartkopf, W. I. 1987, AJ, 94, 1600
Zhao, H. 1998, ApJ, 500, L149
Zinnecker, H., Keable, C. J., Dunlop, J. S., Cannon, R. D., & Griffiths, W. K. 1988, in IAU Symp. 126, Globular Cluster Systems in Galaxies, ed. J. E. Grindlay & A. G. D. Phillip (Dordrecht: Kluwer), 603